Copyright
by
Matthew Alex Memberg
2002

A Design Procedure for Intermediate External Diaphragms on Curved Steel Trapezoidal Box Girder Bridges

by

Matthew Alex Memberg, B.S.C.E.

Thesis

Presented to the Faculty of the Graduate School of

The University of Texas at Austin

in Partial Fulfillment

of the Requirements

for the Degree of

Master of Science in Engineering

The University of Texas at Austin

August 2002

A Design Procedure for Intermediate External Diaphragms on Curved Steel Trapezoidal Box Girder Bridges

Approved by
Supervising Committee:

Joseph A. Yura

Karl H. Frank

For Nana, Grandma, and Grandpa

Acknowledgements

First of all, I thank my parents for all of their love and support. I would not have been able to come to Austin without their help. Thank you to my brother Larry for all of your help along the way – both in school and in life. We came out to Austin together and can look back at the past two years with a lot of pride. Thank you to all my friends and family, especially my grandfather, whose advice has kept me motivated since I started Georgia Tech in September 1995.

I must express my gratitude to the UT structural engineering faculty for having faith in me and offering me a Graduate Research Assistantship. I feel very fortunate to have been given the incredible opportunity to come to Austin. Thank you for taking a chance on me; I will never forget what the University has done for me. Thank you very much to TxDOT for sponsoring my GRA position and allotting the money to UT for research. Thank you to John Holt from the Bridge Design Division, the research coordinator for this project, for answering of all my questions and for all of your advice and concern.

Thank you to everyone on my project team for all of your help, assistance, and guidance: Dr. Yura, Dr. Frank, Brian Chen, Ben Cheplak, and Cem Topkaya. Dr. Yura, thank you for all that you have taught me about how think as an engineer and solve a real engineering problem. I consider it a great honor and a real pleasure to have worked with you.

I have sincere appreciation for the four lab technicians: Ray Madonna (who retired in August 2001), Blake Stasney, Dennis Fillip, and Mike Bell. I

have learned so much from each of you about how to work with tools and how to work in a laboratory environment. I really enjoyed the friendly working atmosphere at Ferguson. Thanks especially to Ray for all of your help with the wiring for the data acquisition system and for showing me the right way to do things. I thank the Ferguson staff for all of the help in taking care of the business related aspects of the research project and for making sure that all of my school bills were always paid on time.

A huge thanks goes to Bill West, the project superintendent at I-35 & US290 for JD Abrams, for making my life a whole lot easier by allowing us to use his equipment, have full access to the site, and even changing the work schedule and closing traffic lanes for us. Bill, thanks for making me laugh with all those outrageous one-liners.

Special thanks go to all of the students who helped me with various tasks at the bridge site, sometimes in extreme heat or during the overnight hours: Joe Fleishman, Alex Whittington, Amy Eskridge, my brother Larry, Alfredo Castro, and Mauricio Posada. Thank you to the TxDOT dumptruck drivers and supervisors for your help with the live load test on bridge K. Also, thank you to Sgt. Detlefsen of DPS for lending the truck scales.

Most of all, I thank all of my friends and fellow students from the UT structural engineering graduate program. Thank you for all of your help and friendship; it made all of the hard work worthwhile. I am honored to have been your colleague and your friend. I wish you all the best in the future.

August 2002

Abstract

A Design Procedure for Intermediate External Diaphragms on Curved Steel Trapezoidal Box Girder Bridges

Matthew Alex Memberg, M.S.E.

The University of Texas at Austin, 2002

Supervisor: Joseph A. Yura

Steel trapezoidal box girders are well-suited for curved bridges due to their high torsional rigidity. This bridge type features one or more steel trapezoidal girders with a cast-in-place concrete roadway slab. Once the slab is in place, the section becomes fully closed, and the stiffness and strength of the bridge cross-section significantly increases. Temporary intermediate external cross-frames, or diaphragms, are typically installed during the construction phase to limit rotations and twisting distortions in the girders in order to maintain alignment. It is important to optimize the number of intermediate external diaphragms due to their added cost for design, fabrication, installation, and removal.

A method for the design of intermediate external diaphragms is presented herein. The design procedure was developed through an investigation of torsion in curved girders and the effect of torsion on twin-trapezoidal box girder bridge systems. The design procedure was evaluated by comparing results with data from a highway bridge in Austin, Texas, that was completed in summer 2001. Two external diaphragms on the bridge were monitored during the concrete deck pours and during a live load test after the deck had hardened.

Table of Contents

Table of Contents viii

List of Tables xii

List of Figures xiii

CHAPTER 1 Introduction 1

1.1 Background 1

1.2 Bridge Studied 2

1.3 Scope 8

1.4 Introduction to Problem 9

CHAPTER 2 Torsion in Curved Girders 11

2.1 Torsion in Closed Sections 11

2.2 Quasi-Closed Trapezoidal Sections 11

2.3 Curved Girders Analyzed as Straight Girders 12

2.3.1 Justification 12

2.3.2 Induced Torques 13

2.4 Girder Torsional Constant 16

2.5 Angle of Twist Formulas 18

2.6 Effect of Torsion on Girders 21

2.7 Role of External Diaphragms in Resisting Rotations 23

CHAPTER 3 Modeling of the Bridge Deck 24
3.1 Standard Bridge Cross Section 24
3.2 Deck Analytical Model 25
3.3 Slab Support Displacement 26
3.3.1 Support Displacement Analogy 26
3.3.2 Support Displacement Moment Cases 26
3.4 Other Slab Loads 30
CHAPTER 4 Design Procedure for Intermediate External Diaphragms 32
4.1 Current Design Methods & Codes 32
4.2 Design Concept 33
4.3 Design for Construction Phase 34
4.3.1 Girder Properties 34
4.3.2 Rotation Due to Dead Loads 35
4.3.3 Required Number of Intermediate Diaphragms 36
4.3.4 Standard Diaphragm 38
4.4 Check Bridge in Service 41
4.4.1 Rotation due to Live Loads 41
4.4.2 Slab Moments 45
4.4.3 Capacity of Slab 47
4.4.4 Intermediate Diaphragms for In-Service Bridge 48

4.5 Limitations of Design Procedure 49
CHAPTER 5 Design Example 50
5.1 Design Problem 50
5.2 Design for Construction Phase 52
5.2.1 Girder Properties 52
5.2.2 Loading Condition 56
5.2.3 Required Number of Intermediate Diaphragms 57
5.2.4 Axial Forces for Design Diaphragm 58
5.3 Check Bridge in Service 62
5.3.1 Girder Properties 62
5.3.2 Loading Condition 63
5.3.3 Slab Moments 67
5.3.4 Capacity of Slab 71
5.3.5 Intermediate Diaphragms for In-Service Bridge 72
5.4 Design Summary 75
CHAPTER 6 Evaluation and Comparison of Design Method with Bridge K 76
6.1 Introduction 76
6.2 Data Acquisition System 76
6.2.1 Description 76
6.2.2 Overview of Diaphragm Instrumentation on Bridge K 78
6.3 Bridge K Concrete Pours 80
6.3.1 Description 80

6.3.2 Field Results for Diaphragms for Concrete Pours 81
6.3.3 Expected Forces in Diaphragms 84
6.3.4 Expected Girder Rotation 94
6.4 Bridge K Live Load Test 96
6.4.1 Description 96
6.4.2 Field Results for Diaphragms for Live Load Test 98
6.4.3 Expected Forces in Diaphragms 101
6.4.4 Expected Girder Rotation 113
6.5 Summary 116
CHAPTER 7 Summary and Conclusions 117
7.1 Summary 117
7.2 Design Procedure 117
7.3 Evaluation of Design Procedure 120
APPENDIX A Slab Moment Cases 121
APPENDIX B Bridge K Concrete Pour Data 127
APPENDIX C Bridge K Live Load Test Data 133
References 148
Vita 150

List of Tables

Table 5.1 Intermediate External Diaphragms for Example Bridge 75

Table 6.1 Bridge K Pouring Schedule 81

Table 6.2 Changes in Axial Force in Diaphragm #11 During Concrete Pours 83

Table 6.3 Changes in Axial Force in Diaphragm #18 During Concrete Pours 83

Table 6.4 Changes in Axial Force (kips) due to K Concrete Pours 91

Table 6.5 Locations of Instrumented Diaphragms 105

Table 6.6 Axial Force in Diaphragms During Live Load Test 110

Table 6.7 Axial Force in Diaphragms During Live Load Test 111

Table C.1 Axial Forces in Diaphragm #11 During K Live Load Test 139

Table C.2 Axial Forces in Diaphragm #18 During K Live Load Test 140

Table C.3 Axial Forces in Diaphragm #11 During K Live Load Test 146

Table C.4 Axial Forces in Diaphragm #18 During K Live Load Test 147

List of Figures

Figure 1.1 Cross-section of Trapezoidal Box Girder System 1

Figure 1.2 Site Location 3

Figure 1.3 Bridge K Dimensions 4

Figure 1.4 K Girder Dimensions 6

Figure 1.5 Cross-Section During Construction 6

Figure 1.6 Bridge K during Construction (at 17K Looking South) 7

Figure 1.7 Aerial view of Completed Bridge K (Looking North) 8

Figure 1.8 Cross-Section without Intermediate External Diaphragms 10

Figure 2.1 Equivalent Plate Method 12

Figure 2.2 Plan View of Curved Girder 13

Figure 2.3 Plan View of Curved Member Showing Center of Curvature 14

Figure 2.4 Induced Torsional Loads on Curved Girders 15

Figure 2.5 Idealized Girder Cross-Section 16

Figure 2.6 Angle of Twist Formulas 19

Figure 2.7 Girder Rotation 21

Figure 2.8 Equal and Opposite Displacement of Top Flanges 22

Figure 2.9 Differential Displacement in Slab (Exaggerated) 23

Figure 3.1 Typical Cross Section 24

Figure 3.2 Slab Analytical Model 25

Figure 3.3 One Girder Rotating 27

Figure 3.4 Both Girders Rotating w/ Antisymmetry 28
Figure 3.5 Both Girders Rotating in Opposite Directions (Symmetric) 29
Figure 3.6 Other Slab Loads 31
Figure 4.1 Maximum Allowable Rotation in Girders Before Deck is Poured 37
Figure 4.2 K-frame Configuation 39
Figure 4.3 Torque Acting on Intermediate Diaphragm 40
Figure 4.4 Antisymmetric Rotation due to In-Service Loads 41
Figure 4.5 Loading Case Corresponding to Largest Actual Rotation 44
Figure 4.6 Typical Moment Envelope in Slab with Small Girder Rotations 46
Figure 4.7 Typical Moment Envelope in Slab with Large Girder Rotations 46
Figure 4.8 Roadway Slab Design Strip 47
Figure 5.1 Example Bridge 50
Figure 5.2 Example Girder Cross-Section 51
Figure 5.3 Example Bridge Cross-Section 51
Figure 5.4 Span 1 Properties 53
Figure 5.5 Span 2 Properties 54
Figure 5.6 Span 3 Properties 55
Figure 5.7 Critical Diaphragm for Span 2 59
Figure 5.8 Critical Diaphragm for Span 3 60
Figure 5.9 Dimensions of Typical Diaphragm 60
Figure 5.10 Design Forces 61
Figure 5.11 Truck Train Lane Loading 63

Figure 5.12 Span 1 Slab Moments 68
Figure 5.13 Span 2 Slab Moments 69
Figure 5.14 Span 3 Slab Moments 70
Figure 5.15 Cross-Section of Slab Design Strip 71
Figure 5.16 Span 2 Slab Moments (2nd Pass) 74
Figure 6.1 Instrumented Locations on Bridge K 77
Figure 6.2 Member Numbering System 78
Figure 6.3 External Diaphragm #11 -- Looking South 79
Figure 6.4 Bridge K Pouring Sequence 80
Figure 6.5 Member Numbering System 83
Figure 6.6 Diaphragm #11-5 During K Concrete Pours 84
Figure 6.7 Plan View of Bridge K Span 18 85
Figure 6.8 Total Dead Load on Bridge K Span 18 86
Figure 6.9 Torque at Intermediate External Diaphragms in Span 18 86
Figure 6.10 Torque from Each Girder on Diaphragm #11 87
Figure 6.11 Torque from Each Girder on Diaphragm #18 87
Figure 6.12 Expected Forces in Diaphragm #11 from Worst Case 89
Figure 6.13 Expected Forces in Diaphragm #18 from Worst Case 90
Figure 6.14 Forces Transferred to Top Chord 92
Figure 6.15 Top Chord in Diaphragm #11 During K Pours 4 & 5 93
Figure 6.16 Top Chord in Diaphragm #18 During K Pour 3 94
Figure 6.17 Torque at Mid-Span 95

Figure 6.18 Live Load Test Truck Positions for Bridge K 96
Figure 6.19 Truck Positioning During K Live Load Test 97
Figure 6.20 External Diaphragms In Place for K Live Load Test 98
Figure 6.21 Temperature Correction for Diaphragm #18-2 100
Figure 6.22 Axial Force in Diaphragm #18-5 During K Live Load Test 101
Figure 6.23 Live Load Test Setup on Bridge K (Outer Run) 103
Figure 6.24 Live Load Test Setup on Bridge K (Inner Run) 104
Figure 6.25 Concentrated Load from Dumptrucks 104
Figure 6.26 Torques Transferred to Diaphragms 105
Figure 6.27 Expected Forces in Diaphragm #11 (Outer Run) 106
Figure 6.28 Expected Forces in Diaphragm #11 (Inner Run) 107
Figure 6.29 Expected Forces in Diaphragm #18 (Outer Run) 108
Figure 6.30 Expected Forces in Diaphragm #18 (Inner Run) 109
Figure 6.31 Axial Forces due to Deflection of Outer Girder 112
Figure 6.32 Axial Forces due to Deflection of Inner Girder 113
Figure A.1 Case 1 121
Figure A.2 Case 2 123
Figure A.3 Case 3 124
Figure A.4 Case 4 125
Figure A.5 Case 5 126
Figure B.1 Diaphragm #11-1 During K Concrete Pours 127
Figure B.2 Diaphragm #11-2 During K Concrete Pours 128

Figure B.3 Diaphragm #11-3 During K Concrete Pours 128
Figure B.4 Diaphragm #11-4 During K Concrete Pours 129
Figure B.5 Diaphragm #11-5 During K Concrete Pours 129
Figure B.6 Diaphragm #18-1 During K Concrete Pours 130
Figure B.7 Diaphragm #18-2 During K Concrete Pours 130
Figure B.8 Diaphragm #18-3 During K Concrete Pours 131
Figure B.9 Diaphragm #18-4 During K Concrete Pours 131
Figure B.10 Diaphragm #18-5 During K Concrete Pours 132
Figure C.1 Diaphragm #11-1 During K Live Load Test (Outer) 133
Figure C.2 Diaphragm #11-2 During K Live Load Test (Outer) 134
Figure C.3 Diaphragm #11-3 During K Live Load Test (Outer) 134
Figure C.4 Diaphragm #11-4 During K Live Load Test (Outer) 135
Figure C.5 Diaphragm #11-5 During K Live Load Test (Outer) 135
Figure C.6 Diaphragm #18-1 During K Live Load Test (Outer) 136
Figure C.7 Diaphragm #18-2 During K Live Load Test (Outer) 136
Figure C.8 Diaphragm #18-3 During K Live Load Test (Outer) 137
Figure C.9 Diaphragm #18-4 During K Live Load Test (Outer) 137
Figure C.10 Diaphragm #18-5 During K Live Load Test (Outer) 138
Figure C.11 Diaphragm #11-1 During K Live Load Test (Inner) 141
Figure C.12 Diaphragm #11-2 During K Live Load Test (Inner) 141
Figure C.13 Diaphragm #11-3 During K Live Load Test (Inner) 142
Figure C.14 Diaphragm #11-4 During K Live Load Test (Inner) 142

Figure C.15 Diaphragm #11-5 During K Live Load Test (Inner)..... 143

Figure C.16 Diaphragm #18-1 During K Live Load Test (Inner)..... 143

Figure C.17 Diaphragm #18-2 During K Live Load Test (Inner)..... 144

Figure C.18 Diaphragm #18-3 During K Live Load Test (Inner)..... 144

Figure C.19 Diaphragm #18-4 During K Live Load Test (Inner)..... 145

Figure C.20 Diaphragm #18-5 During K Live Load Test (Inner)..... 145

CHAPTER 1
Introduction

1.1 BACKGROUND

A popular choice for superstructure types for curved bridges is the steel trapezoidal box girder system. Trapezoidal box girders are well-suited for curved bridges because of their high torsional rigidity. This bridge type features one or more steel trapezoidal girders with a cast-in-place concrete roadway slab. Shear studs fastened to the top flanges of the girders create composite action between the girders and the slab. This significantly increases the stiffness and strength of the bridge cross-section. Refer to Figure 1.1 for a schematic of a typical twin-girder bridge cross-section.

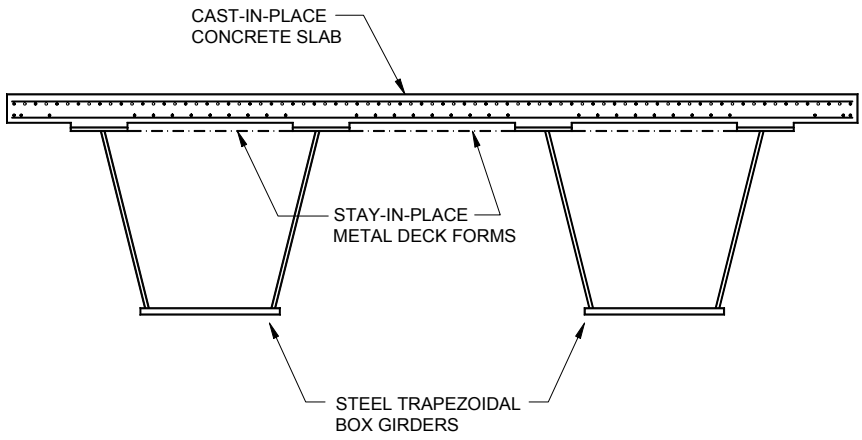

Figure 1.1 Cross-section of Trapezoidal Box Girder System

(John Holt, Texas Department of Transportation, 1998)

Although the trapezoidal girders are extremely rigid in the completed bridge, the top flanges of each girder require bracing during the construction phase. These top lateral braces, which are usually WT sections, form a "quasi-closed" section and are designed to resist torsion. These members also provide additional area at the location of the top flanges of the girders so that they will resist a portion of the girder bending moment; this area is usually ignored in design (Helwig & Fan, 1999).

Internal cross-frames, or diaphragms, are spaced evenly throughout the girder to control distortions in the cross-section and to provide lateral stability. Additionally, in multi-girder bridges, temporary external diaphragms can be installed during the construction phase between two girders to limit rotations and twisting distortions in the girders in order to maintain alignment. These temporary cross-frames are removed once the concrete deck has hardened sufficiently. The performance of intermediate external diaphragms in a twin-girder bridge was investigated during this study.

1.2 BRIDGE STUDIED

The bridge studied was located at the interchange of Interstate 35 (IH-35) and Texas Ranch Road 2222 / US 290 in Austin, Texas. A map of the area is shown in Figure 1.2. This interchange opened in September 2001. There are four bridges at the interchange; each consisting of steel trapezoidal girder systems for the curved central spans and straight concrete U-shaped girder systems for the approach spans. The bridges were designed by the Texas Department of Transportation (TxDOT) Design Division in Austin. The steel fabricator was Trinity Industries, Inc. in Houston, and the contractor for the project was Austin-based J.D. Abrams, Inc.

Bridge K, which connects southbound IH-35 to eastbound US 290, was studied for this project. The steel portion of Bridge K has three spans with a radius of curvature of approximately 575 feet at the centerline of the cross-section. The curved portion of the bridge is symmetric; end spans 17 and 19 are of equal length. Figure 1.3 shows the bridge in plan view.

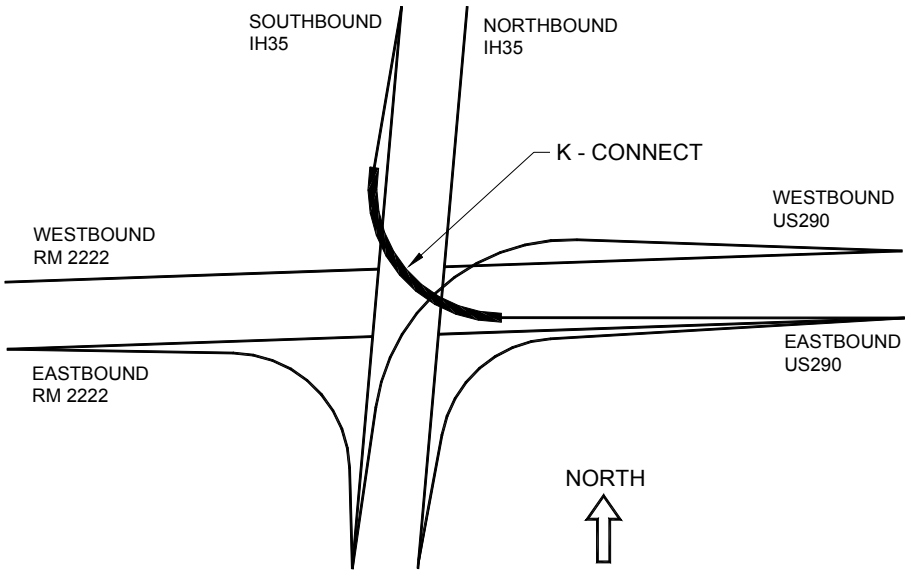

Figure 1.2 Site Location

(Cheplak, 2001)

The locations of the internal diaphragms, top lateral bracing, and external diaphragms are also shown in Figure 1.3. The internal diaphragms are spaced approximately every 16 feet. The location of an internal diaphragm is also known as a panel point. The external diaphragms, made up of L5x5x$^{1}/_{2}$ members were placed at every other panel point. WT8x33.5 members were used for all top lateral bracing. Solid plates with stiffeners are used as internal diaphragms at the end piers, and plates with access holes and stiffeners are located at the intermediate piers.

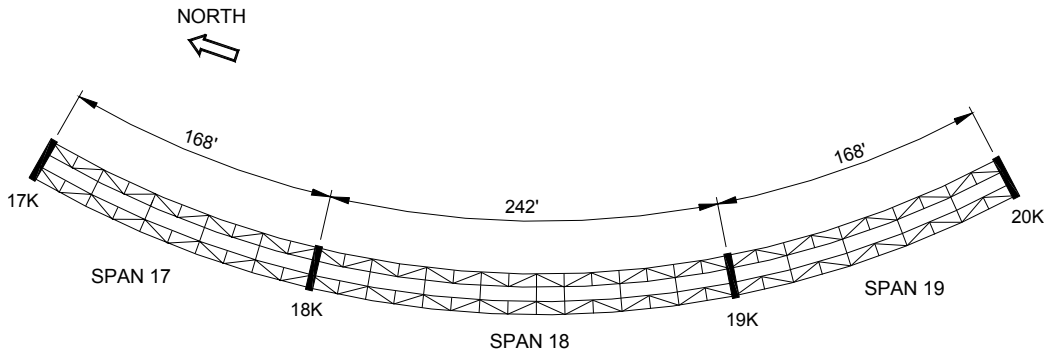

Figure 1.3 Bridge K Dimensions

(Cheplak 2001)

Figure 1.4 shows the dimensions of the girder cross-section. The dashed line in between the top flanges is because the girder is quasi-closed; there is a WT diagonal brace within each panel and not a solid plate. This concept is explained further in Chapter 2.

Figure 1.5 shows the bridge configuration at an external diaphragm location during the construction phase. Two external diaphragms were instrumented and monitored throughout the concrete deck pours to determine the change in axial forces of the cross frame members due to the weight of the concrete. These diaphragms remained in place for a live load test, which was conducted approximately three months after the pours were completed. Figure 1.6 shows an overall view of Bridge K during construction, and Figure 1.7 is photo of the completed bridge from the contractor's website (http://www.jdabrams.com).

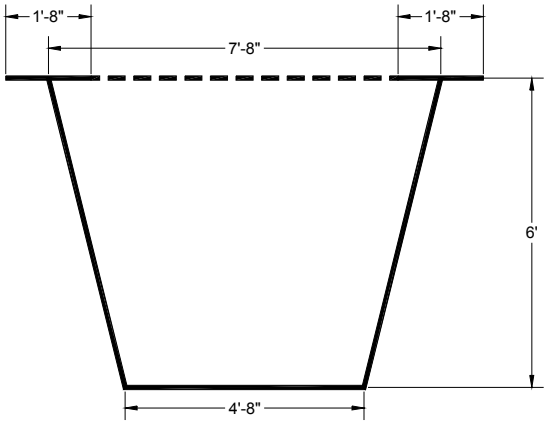

Figure 1.4 K Girder Dimensions

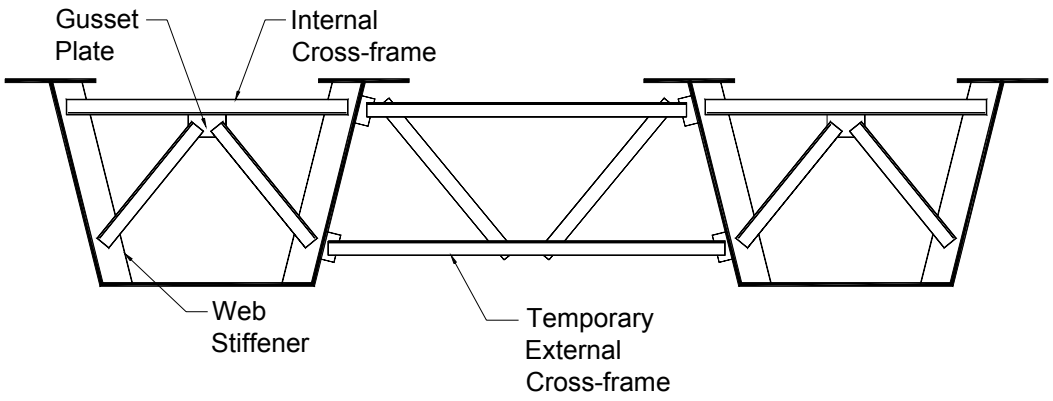

Figure 1.5 Cross-Section During Construction

(Cheplak, 2001)

Figure 1.6 Bridge K during Construction (at 17K Looking South)

(Cheplak, 2001)

In addition to the two external diaphragms that were instrumented on Bridge K, a total of eight top flange lateral braces and six individual girder cross sections were also instrumented to measure forces and stresses, respectively. Temperatures were also monitored at two separate locations inside the outer girder. That data are presented elsewhere (Cheplak et al 2002). The research was in conjunction with work done by Brian Chen and Cem Topkaya, Ph.D. candidates at the University of Texas at Austin (UT), and Ben Cheplak, UT M.S.E. 2001.

Figure 1.7 Aerial view of Completed Bridge K (Looking North)

(http://www.jdbrams.com, 2001)

1.3 SCOPE

This research was undertaken in order to understand the behavior of curved steel trapezoidal box girders and was sponsored by TxDOT. The research concentrated on top flange lateral braces and temporary intermediate external diaphragms because limited information is currently available on these topics. The work presented herein focused on the behavior of the temporary intermediate external diaphragms.

The aim of the research was to provide design guidelines for intermediate external diaphragms, as such guidelines presently do not exist. It is important to optimize the number of external diaphragms due to their added cost for design,

fabrication, installation and removal. Not all curved steel trapezoidal box girder bridges require intermediate external diaphragms; some have been successfully built with external diaphragms only at the piers (Helwig & Fan, 1999).

A general description of torsion in curved girders is given in Chapter 2 and an investigation of the effect of torsion on twin-trapezoidal girder bridge systems is presented in Chapter 3. This information was used to develop a design method for placing external diaphragms in curved trapezoidal box girder bridges (Chapter 4). The effectiveness of the design method in predicting the forces in the external diaphragm members was studied for both the construction phase and in-service loading of Bridge K (Chapter 6).

1.4 INTRODUCTION TO PROBLEM

The existence of torsional loads introduces challenges to the design of curved bridges. In steel trapezoidal girder bridges, torsional loads resulting from bridge curvature can cause the girders to undergo considerable rotations. In multi-girder bridges, the effect of torsion can be mitigated by installing intermediate external diaphragms at evenly-spaced intervals along the span. Currently, there are no design recommendations for establishing the need for and the design of intermediate external diaphragms in curved steel trapezoidal box girder bridges.

While the trapezoidal girders have high torsional resistance when closed, they are less stiff in both flexure and torsion during the construction phase due to only partial top flange bracing. As a result, the girder rotations and displacements are greater during the construction phase than in the completed bridge. Intermediate external diaphragms are used to effectively tie the box girders together until the slab is in place; box girders that are tied together have greater

stiffness and strength than separate girders with no interaction. Installing intermediate external diaphragms therefore reduces the girder rotations and displacements, resulting in less differential rotation in adjacent girders. The diaphragms help to maintain plane sections by forcing each girder to go through the same rotation at each individual diaphragm location.

Figure 1.8 shows a schematic of a cross-section of a twin-girder bridge without intermediate external diaphragms. The slab in between the two girders undergoes deformations due to the displacement of the top flanges of each girder. Depending on the amount of rotation of the girders, there may be undesirable stresses in the slab. If the girders are sufficiently stiff with respect to torsion, then they are able to resist the torsional loads without requiring intermediate external diaphragms.

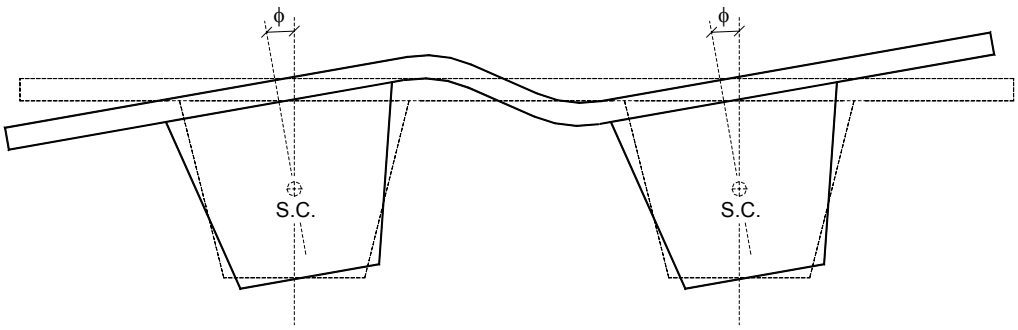

Figure 1.8 Cross-Section without Intermediate External Diaphragms

In order to understand the design problem, it is necessary to have an understanding of angle of twist (ϕ) and the moments that are induced in the bridge roadway slab by the individual girder rotations. In Chapter 2, equations are presented for calculating ϕ; and in chapter 3, explanations of the moments in the slab caused by differential movement and other loads are provided. The design procedure in Chapter 4 combines the information from Chapters 2 and 3.

CHAPTER 2
Torsion in Curved Girders

2.1 TORSION IN CLOSED SECTIONS

There are two types of torsion that act on cross-sections: Saint-Venant torsion and warping torsion. Saint-Venant torsion is the result of shear flow around the cross-section, while warping torsion is the result of bending deformation in the cross-section. In closed sections, warping torsion can be neglected (Kolbrunner & Basler, 1969). Furthermore, the internal diaphragms that are evenly spaced along the steel trapezoidal box girders resist any distortion of the cross-section. Therefore, the only torsion necessary to consider in these girders is Saint-Venant torsion.

2.2 QUASI-CLOSED TRAPEZOIDAL SECTIONS

Without the top flange bracing, the steel trapezoidal curved girders are open sections and have limited torsional resistance. The top laterals that are installed effectively close the section and increase its torsional stiffness significantly. The top laterals stretch across the top of the trapezoidal girder diagonally from one panel point to the next and can be analyzed as a fictitious plate with an equivalent thickness. With the imaginary plate on top of the girder, the section is considered closed for analytical purposes. The contribution to the equivalent thickness of the metal deck that is used to form the bottom of the concrete slab is not considered.

This method is known as the Equivalent Plate Method (Kolbrunner & Basler, 1969) and is recommended by many bridge design guides. The method is illustrated in Figure 2.1 for the top flange bracing pattern that is present in the IH-35/US290 interchange. The Figure shows a top view of the steel girder.

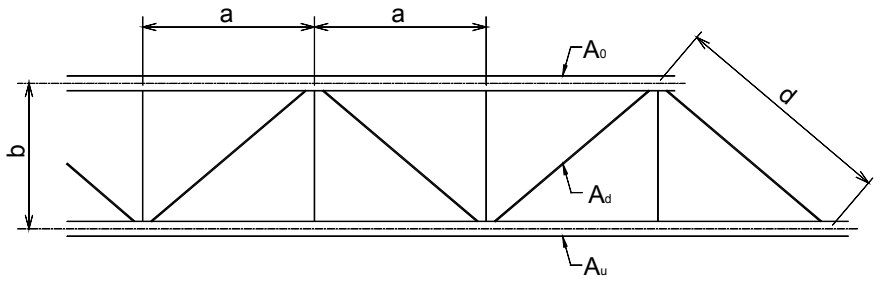

$$\textit{Effective plate thickness: } t^* = \left(\frac{E}{G}\right)\frac{ab}{\frac{d^3}{A_d} + \frac{a^3}{3}\left(\frac{1}{A_0} + \frac{1}{A_u}\right)} \qquad \textbf{(2-1)}$$

A_0, A_d, & A_u are cross-sectional areas

E is the elastic modulus, G is the shear modulus

Figure 2.1 Equivalent Plate Method

(Kolbrunner & Basler, 1969)

2.3 CURVED GIRDERS ANALYZED AS STRAIGHT GIRDERS

2.3.1 Justification

It is difficult to calculate exact moments and stresses for curved girders. The analysis requires sophisticated computer analysis programs that are only

available to researchers; furthermore, these analyses cannot be practically applied to bridge design. An approximate method is necessary.

One approximate method is to analyze the girder as if it were straight. Tung and Fountain (1970) demonstrated that this approximation is acceptable for girders that have subtended angles per span of up to 40° and are restrained from rotating at the ends. Since the radius is relatively large, it is assumed that the effect of curvature on the bending behavior of a curved girder is negligible. The bending moment of the girder can be determined by neglecting the curvature and using traditional beam theory for straight girders (Helwig & Fan, 2000).

2.3.2 Induced Torques

Although calculations for bending can be treated as if the girder were straight with the same length, the same cannot be assumed for torsion. Because the girder is curved, loads produce a twisting effect on the member which must be taken into consideration for design. This twisting effect can be best explained by examining a physical representation of a curved girder, as shown in Figure 2.2.

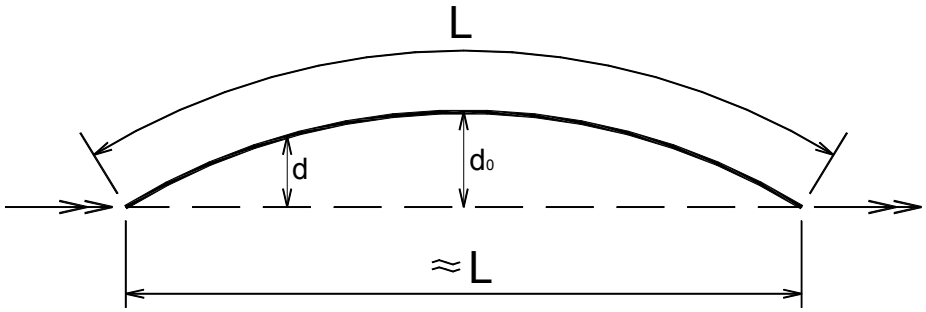

Figure 2.2 Plan View of Curved Girder

In Figure 2.2, a straight dashed line connects the two ends of a curved girder, called the chord. The straight perpendicular distance from any point on this line to the curved girder is d. The maximum d occurs at the center of the arc, where it is denoted d_0. d_0 is calculated using the radius of curvature (R) and subtended angle (α) of the girder (see Figure 2.3). Note that the girder is symmetric about the centerline.

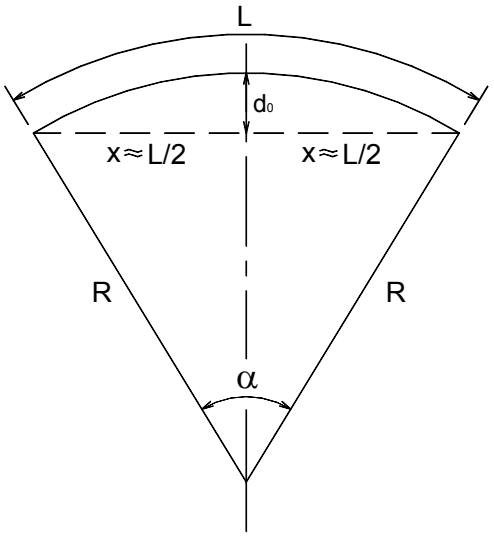

$$d_0 = R\left[1 - \sin\left(90° - \frac{\alpha}{2}\right)\right] \qquad \textbf{(2-2)}$$

Figure 2.3 Plan View of Curved Member Showing Center of Curvature

Assuming no eccentric loads, the applied torque at any point along the girder is a equivalent to the load at that point multiplied by d at that point. If the girder were straight, d would equal zero at every point along the member; therefore, there would be no torsion on the girder.

The torsional loads that result from the curvature of the girder must be applied on the straightened member that is used for design. Because of symmetry, half of this torque goes to one end support, and half goes to the other end support. The end supports must be able to withstand these torques, or the girder will rigidly rotate about the chord line.

A point load placed on a curved girder induces a torque equal to P x d. If the load is applied at mid-span, then the torque is equal to P x d_0. A uniformly distributed load on a curved girder induces a parabolic torque distribution. The torque at any point is calculated by multiplying the value of the distributed load w by d at that point, where d is defined as a parabolic function. Figure 2.4 shows how the torsion due to curvature is applied to a straight girder of equal length.

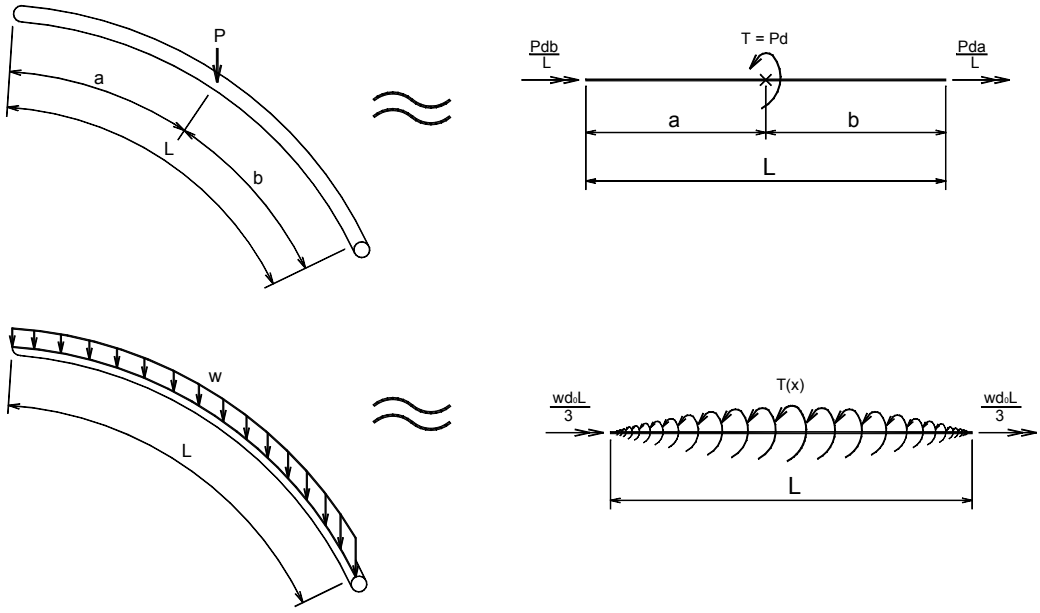

Applied torque at any point (k-ft/ft): $T(x) = \frac{4wd_0}{L}x - \frac{4wd_0}{L^2}x^2$

$$\left\{0 \le x \le \frac{L}{2}\right\} \quad \textit{symmetric} \qquad \textbf{(2-3)}$$

Figure 2.4 Induced Torsional Loads on Curved Girders

2.4 GIRDER TORSIONAL CONSTANT

The torsional stiffness of the girder can be quantified by the torsional constant, J. Steel trapezoidal girders, which are made up of steel plates that are welded together, can be analyzed as thin-walled sections because of the large aspect ratios of the plates. The formula for J for thin-walled shapes is a function of the area enclosed by the section and the ratios of length-to-thickness of all sides of the cross-section. This formula is presented in Figure 2.5.

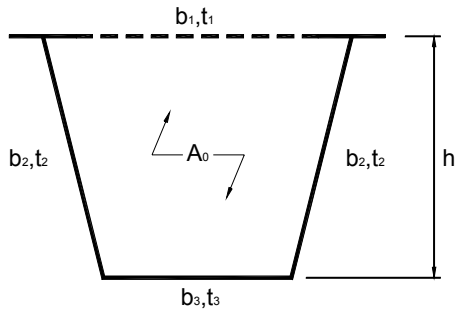

$$\textit{Area enclosed by section: } A_0 = \frac{1}{2}(b_1 + b_3)h \qquad \textbf{(2-4)}$$

$$\textit{Girder Torsional Constant: } J = \frac{4A_0^2}{\sum(b_i / t_i)} \qquad \textbf{(2-5)}$$

Figure 2.5 Idealized Girder Cross-Section

(Kolbrunner & Basler, 1969)

Equation 2-5 can be applied to any closed or quasi-closed trapezoidal box girder section. Because the trapezoidal girder is assumed to be a thin-walled section, the dimensions shown are measured from the centerline of each member.

J must be calculated for both the construction and in-service phases of the girder. The only aspect of the cross-section that changes with the addition of the slab is the length-to-thickness ratio of the equivalent top plate (b_1/t_1 in Figure 2.5). The values calculated for J will be used in the appropriate formulas for angle of twist to determine the amount of rotation expected in the girders.

The equivalent thickness of the top flange, which is calculated using the Equivalent Plate Method, has a significant impact on the girder torsional stiffness (J). Generally, if the equivalent thickness is small, J is small. As the equivalent thickness increases, J increases as well. Prior to the placement of the concrete slab, the contribution of the idealized top plate to the girder torsional stiffness is small. Typically, the equivalent top plate during the construction phase is five to 10 percent as thick as the web plates and bottom flange plates.

For bridge K, the equivalent top flange thickness is 0.04 inches, which is approximately five per cent of the thickness of both the web plates and the bottom flange plate. J for the quasi-closed girder is approximately 40,000 in^4. If the fictional top plate had the same thickness as the web plate, then J would be increased by over six times. With the concrete deck in place, the equivalent top plate thickness increases to approximately 1.4 inches, and J increases to approximately eight times the J from the construction phase. In contrast, J for the open girder (girder cross-section minus the top laterals) is approximately 25 in^4.

2.5 ANGLE OF TWIST FORMULAS

Four common torsional loadings that a bridge span will experience due to either eccentric loads or bridge curvature are: a singular applied torque, a uniformly distributed torque, a parabolic torque distribution, and a half-parabolic torque distribution. Formulas for angle of twist (ϕ) at any point along the member for these four loadings are presented within this section and are shown in Figure 2.6. In cases where more than one torsional loading type exists, the principle of superposition shall be used; elasticity of the girder is assumed.

(a) Concentrated Torque

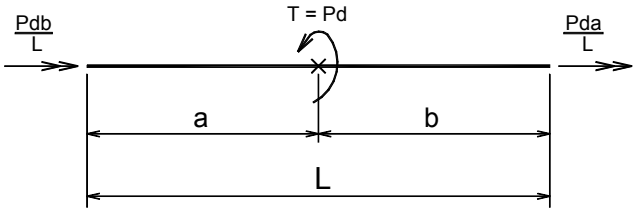

$$\phi(x) = \frac{Pdbx}{GJL} \qquad \{x < a\} \qquad \textbf{(2-6)}$$

$$\phi(x) = \frac{Pda(L-x)}{GJL} \qquad \{x \geq a\} \qquad \textbf{(2-7)}$$

$$\phi_{\max} = \phi(a) = \frac{Pdab}{GJL} \qquad \{x = a\} \qquad \textbf{(2-8)}$$

(b) Uniformly Distributed Torque

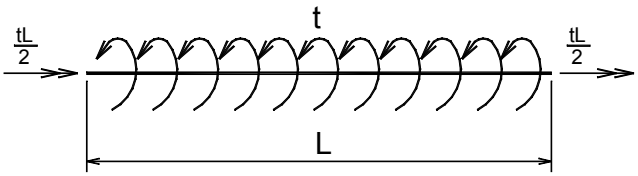

$$\phi(x) = \frac{tx}{2GJ}\left(L - x\right) \qquad \textbf{(2-9)}$$

$$\phi_{\max} = \phi\left(\frac{L}{2}\right) = \frac{tL^2}{8GJ} \qquad \textbf{(2-10)}$$

Figure 2.6 Angle of Twist Formulas

(c) Parabolic Torque Distribution

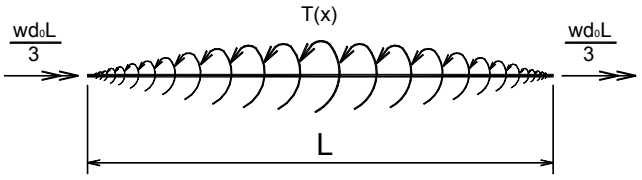

$$\phi(x) = \frac{wd_0 x}{3GJ}\left[\frac{2x^3}{L^2} - \frac{8x^2}{3L} + L\right] \qquad \left\{0 \le x \le \frac{L}{2}\right\} \ \textit{symmetric} \qquad \textbf{(2-11)}$$

$$\phi_{\max} = \phi\left(\frac{L}{2}\right) = \frac{7wd_0L^2}{72GJ} \qquad \textbf{(2-12)}$$

(d) Half-Parabolic Torque Distribution

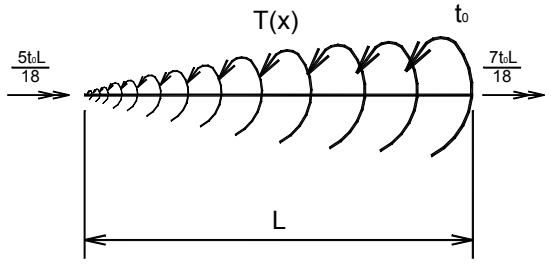

$$\phi(x) = \frac{t_0 x}{9GJ}\left[\frac{3x^3}{2L^2} - \frac{4x^2}{L} + \frac{5L}{2}\right] \qquad \textbf{(2-13)}$$

$$\phi_{\max} = \phi(0.533L) = \frac{0.0942t_0L^2}{GJ} \qquad \textbf{(2-14)}$$

Figure 2.6 Angle of Twist Formulas (continued)

2.6 EFFECT OF TORSION ON GIRDERS

Curved bridges experience significant torsional loads due to the bridge curvature. Dead loads, such as self-weight of the steel girders, which would normally create no torsion in straight bridges, induce large torsional moments in curved girders. In addition, torques can also be caused by eccentric loads on the bridge deck.

The torsional loads on the bridge cause each steel girder to rotate through an angle of ϕ radians about its shear center, as illustrated in Figure 2.7. For symmetrical girders, the shear center falls on the centerline of the girder. Steel trapezoidal girders are closed sections, so the shear center must be inside the enclosed area of the girder. If the girder is not symmetric, the shear center must be located.

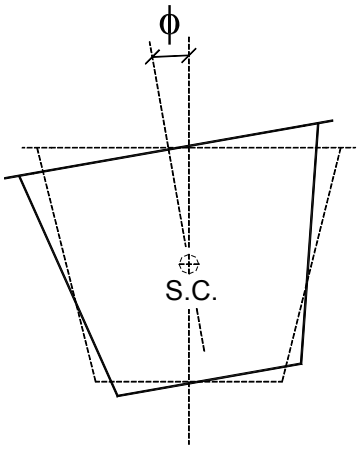

Figure 2.7 Girder Rotation

Rotations in the girder will cause the top flanges to displace vertically in opposite directions. For symmetric girders rotating through small angles and without distortion, the displacements are equal and can be calculated using this simple approximation:

$$\Delta = x_r \phi \qquad \textbf{(2-15)}$$

where x_r is the distance from the centerline of the girder to the intersection of the top flange and web, and Δ is measured from the top flange-web intersection working point (see Figure 2.8). This expression is valid for small rotations only. In fact, the rotations that the girder actually experiences in its final state are usually less than 1° (0.0175 rad). Additionally, with this simple formula, the vertical position of the shear center has no effect.

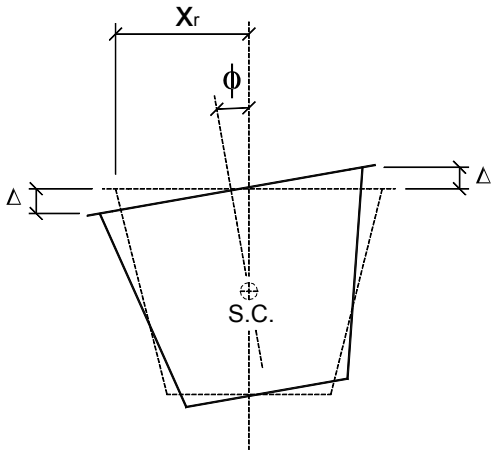

Figure 2.8 Equal and Opposite Displacement of Top Flanges

In multi-girder bridges, rotation in adjacent girders results in a differential displacement between the top flanges of the two girders. This differential

displacement can create significant bending moments in the slab. Once the magnitude of the moments reach the bending strength, the portion of the slab in between the two girders becomes ineffective in helping to resist loads on the structure. Figure 2.9 provides an exaggerated view of how the slab is affected by the differential displacement in the girders.

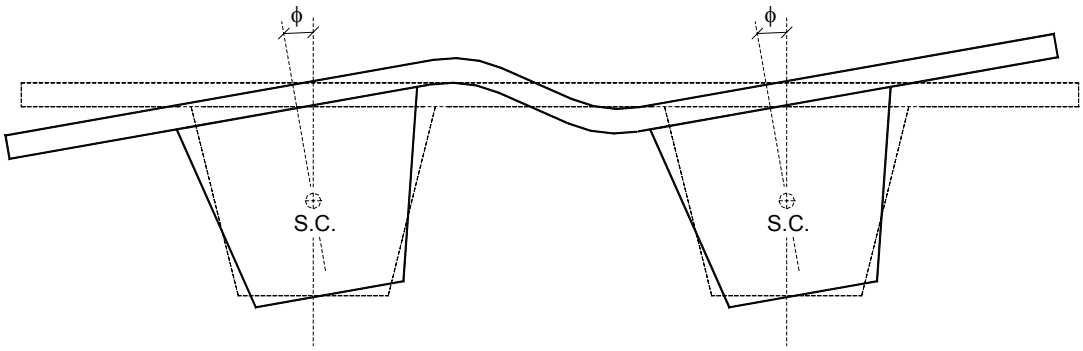

Figure 2.9 Differential Displacement in Slab (Exaggerated)

2.7 ROLE OF EXTERNAL DIAPHRAGMS IN RESISTING ROTATIONS

Curved girders loaded merely with self-weight will undergo rotations due to bridge curvature. Adding external diaphragms in between adjacent girders reduces the rotation by introducing restoring torques to counteract the individual twisting of each girder. The external diaphragms force the girders back into alignment at each diaphragm location and help to maintain plane sections by tying adjacent girders together. At these diaphragm locations, the entire bridge cross-section rotates together, and the relative angle of twist between adjacent girders is zero.

CHAPTER 3
Modeling of the Bridge Deck

3.1 STANDARD BRIDGE CROSS SECTION

The typical cross section of a bridge with two steel trapezoidal girders and a concrete roadway slab is shown in Figure 3.1. The two girders are identical in size, and they are equidistant from the centerline of the cross section. L_1 represents the nominal top width of the girder, and L_2 represents the nominal distance between the two girders. The nominal length of the overhang is labeled c. All of the dimensions shown in the figure are measured from the top flange-web intersections and are not clear distances.

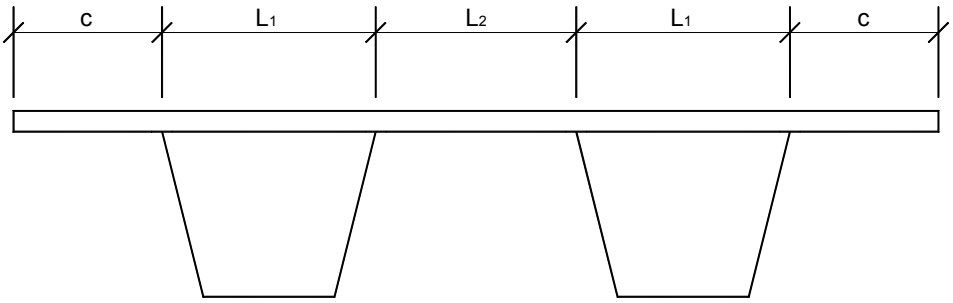

Figure 3.1 Typical Cross Section

L_2 is not the same as the effective span length S as defined in the American Association of State Highway Transportation Officials (AASHTO) *Standard Specifications for Highway Bridges (1996)* Section 3.24.1. Here, S is

the effective span length for which flexural reinforcement in the slab must be designed. In the case of external diaphragm design, S is not applicable.

3.2 DECK ANALYTICAL MODEL

A 1-ft strip of the cross-section is modeled as a beam on four simple supports with the height equal to the slab thickness. The four supports are located at the top flange-web intersections, representing where the slab actually rests upon the girders. Moments are assumed not to vary vertically through the slab, and the stiffness (EI) is assumed to be constant along the length.

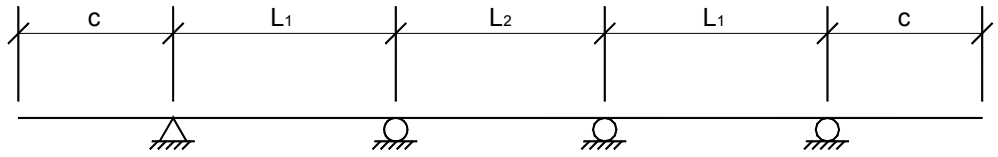

Figure 3.2 Slab Analytical Model

The reasoning for simple supports and not fixed or spring supports is that the restraining effect of the slab is not taken into account. In actuality, the slab will help to restrict the girder rotations, which will result in lower deformations, but that is beyond the scope of this study. When the slab cracks, it will no longer be able to contribute to helping restrict the girder rotations. Not considering this restraining effect is the conservative view.

3.3 SLAB SUPPORT DISPLACEMENT

3.3.1 Support Displacement Analogy

The differential displacements of the top flanges caused by girder rotations are analogous to imposing support displacements on the slab. Current design practices for slabs do not take these moments into account. In addition, there are moments caused by the self-weight of the concrete and by a design wheel load (as provided for by AASHTO Sec. 3.24.3),

3.3.2 Support Displacement Moment Cases

There are three possibilities of support displacement moments: only one girder rotating (See Figure 3.3); both girders rotating in the same direction (See Figure 3.4); or both girders rotating in opposite directions (See Figure 3.5). In the case that both girders do not experience the same differential displacement, the case of only girder rotating can be solved for each girder and then superimposed to produce the slab moment diagram.

Equations for the moments in the slab that are caused by the support displacements can be solved for in terms of Δ, L_1, L_2, and c so that they can be applicable to any symmetric twin steel trapezoidal bridge configuration. Expressions for each case for reactions and moment at any point along the member can be found in the Appendix.

3.3.2.1 Only One Girder Rotating

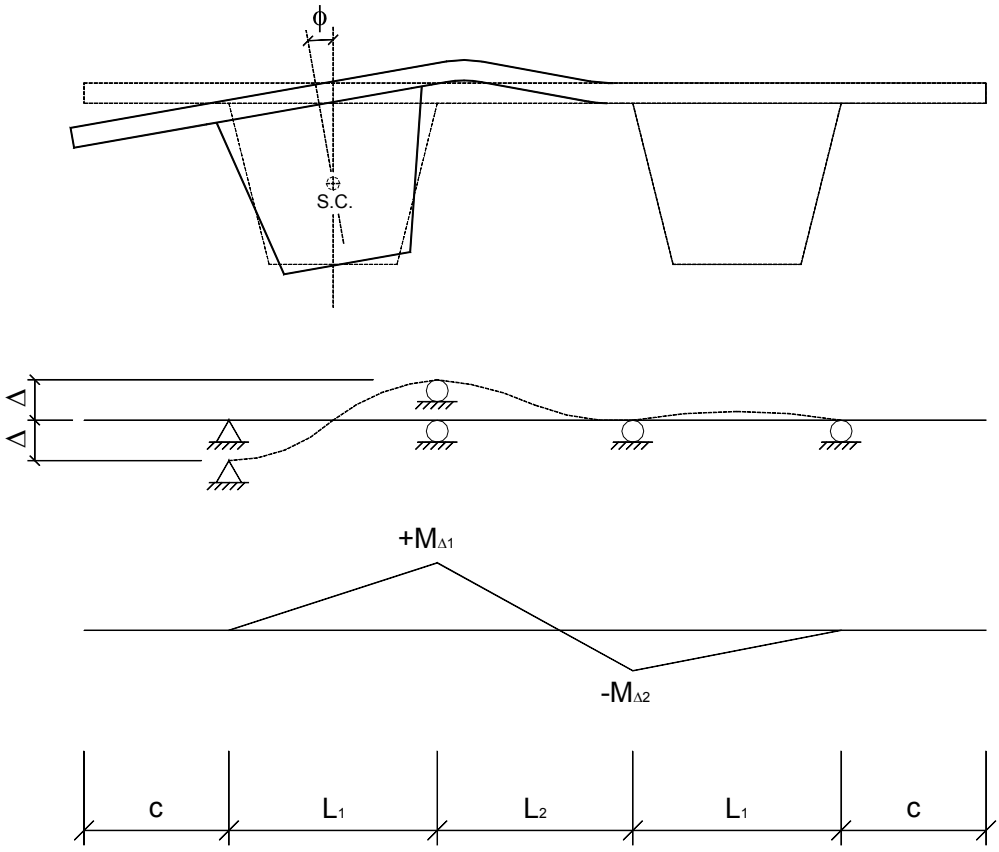

Figure 3.3 One Girder Rotating

3.3.2.2 Both Girders Rotating in the Same Direction

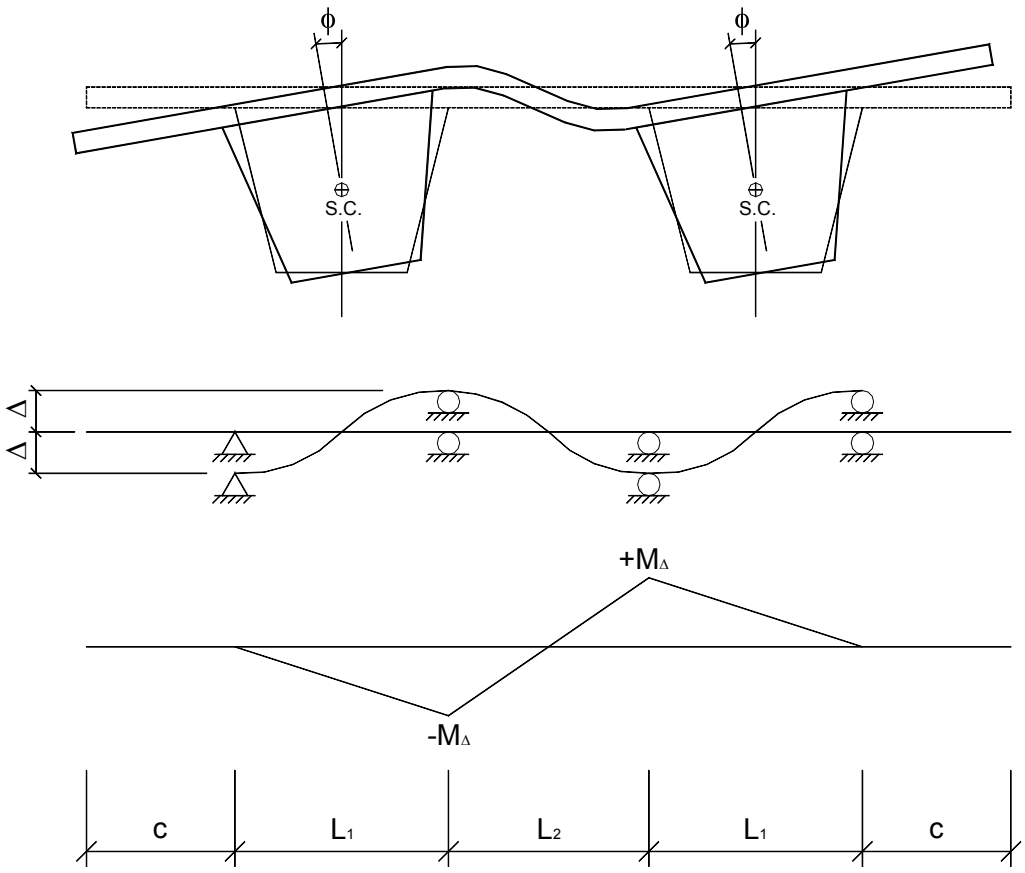

Figure 3.4 Both Girders Rotating w/ Antisymmetry

3.3.2.3 Both Girders Rotating in Opposite Directions

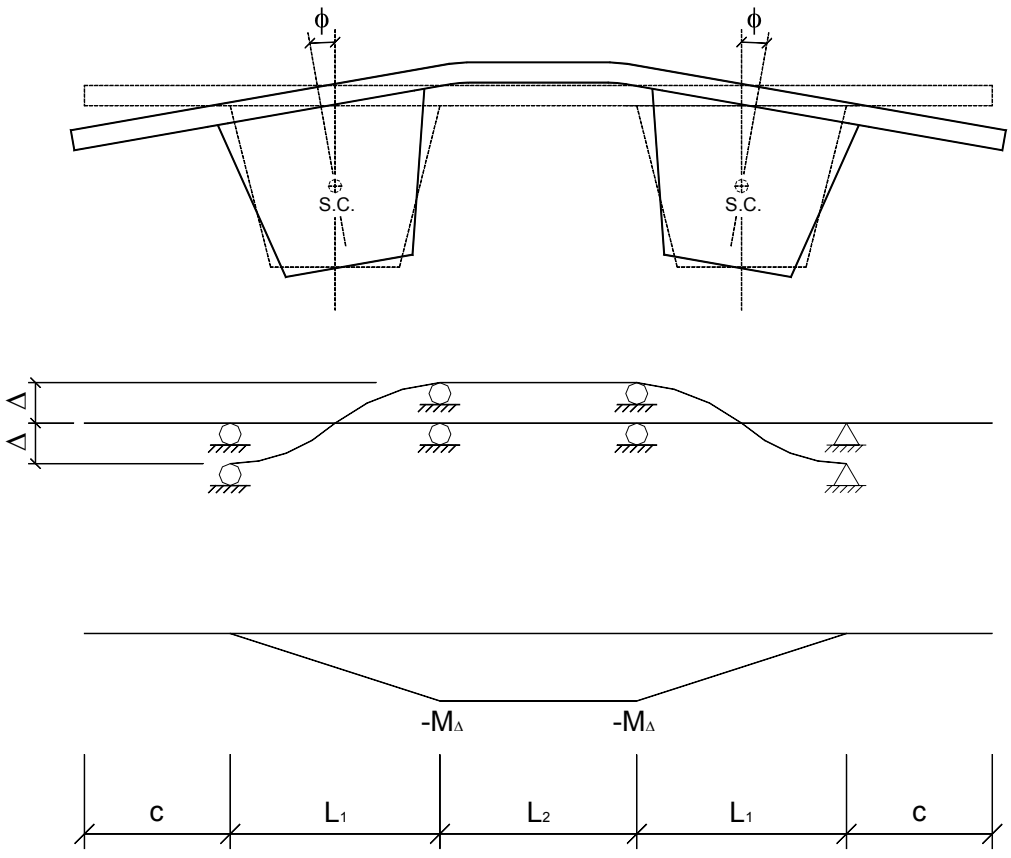

Figure 3.5 Both Girders Rotating in Opposite Directions (Symmetric)

3.4 OTHER SLAB LOADS

In the AASHTO *Standard Specifications for Highway Bridges*, the design wheel load (P) is the main loading for which the slab is designed for flexure. Slab rotations/support displacements are not considered. An AASHTO formula (Equation 3-15 for HS-20 loading and Equation 3-16 for HS-15 loading) reduces the design wheel load by a built-in distribution factor (E) and assumes that the bending moment is constant per foot width of slab. The bending moment calculated is then used to design the required slab flexural reinforcement.

The distributed design wheel load must be considered when checking the slab for adequacy from local bending effects. It has a maximum impact on the slab when placed at the center (i.e. the center of the beam with length L_2). With little or no slab support displacements, the wheel load is the dominating load case, but with significant girder rotations, its influence on the slab moment diagram is diminished greatly.

The dead load moments in the slab are minimal but must still be considered in the slab design. They are combined with the bending moment due to the distributed design wheel load from the AASHTO formula for flexural design. Both loading cases are illustrated in Figure 3.6. Expressions for reactions and moments at any point along the member can be found in the Appendix.

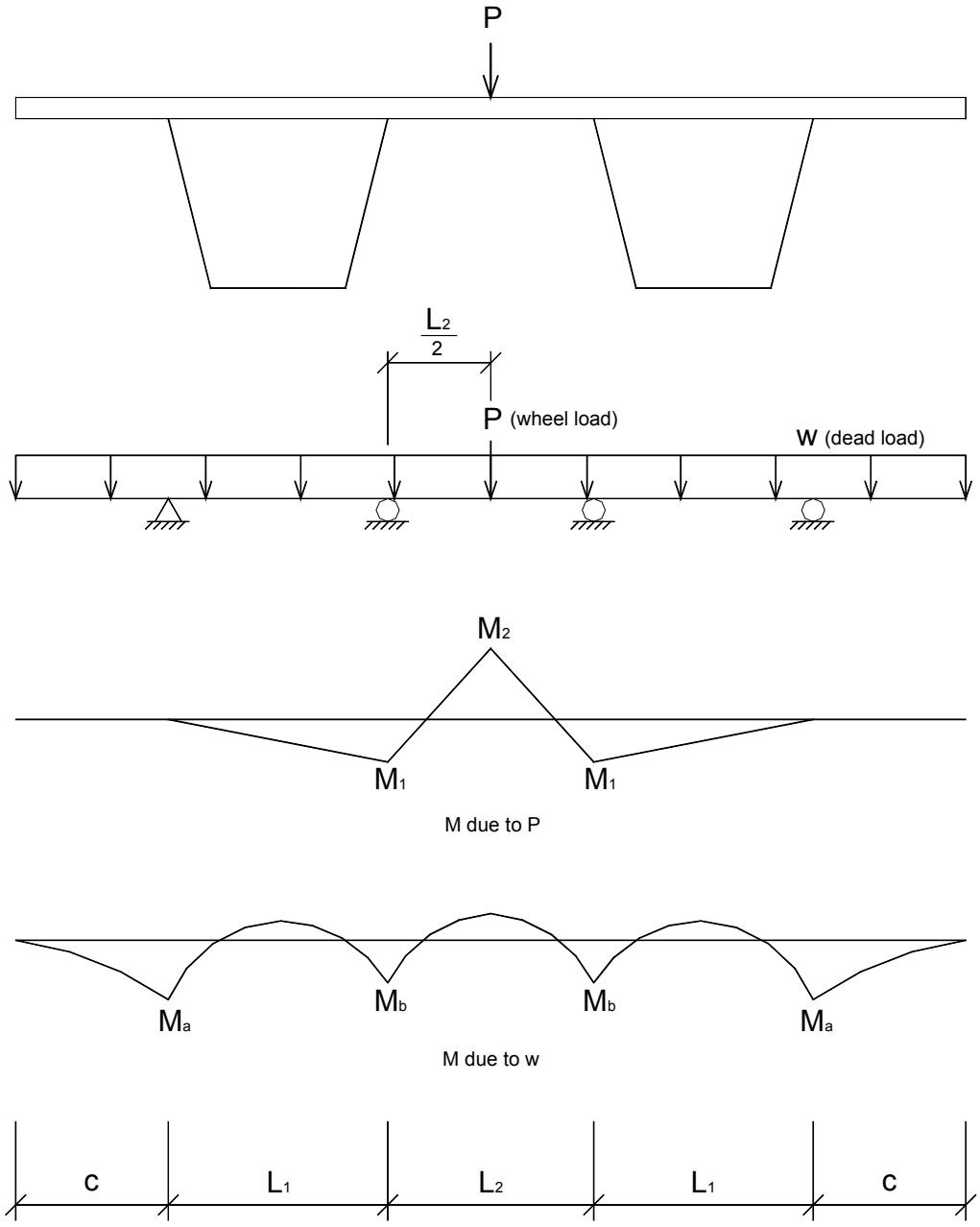

Figure 3.6 Other Slab Loads

CHAPTER 4
Design Procedure for Intermediate External Diaphragms

4.1 CURRENT DESIGN METHODS & CODES

Presently, there is no published design procedure for intermediate external diaphragms for curved steel multi-trapezoidal girder bridges. Several codes recommend or require the use of external diaphragms but do not have any specific provisions for design.

For example, Section 7.27 on Trapezoidal Box Girders of the TxDOT *Bridge Design Manual* (which is available online at http://manuals.dot.state.tx.us/dynaweb/) references *Preferred Practices For Steel Bridge Design Fabrication and Erection* (November 2000) by the Texas Steel Quality Council (TSQC). Section 9.5 of this manual, which is available online at http://www.steelbridge.org, simply states the following about external diaphragms:

> *External diaphragms are normally used to control relative displacement and rotation of girders during slab placement. They may be removed once the slab has matured sufficiently, which is done primarily for aesthetic reasons. If they are to remain in place, they should compliment the overall structure aesthetics and should contain fatigue-resistant details.*

External diaphragms should be placed at every other internal diaphragm, unless analysis indicates that they should be placed at each internal diaphragm.

This requirement is not based on any theoretical development or research. It merely represents engineering judgment.

Finite element analysis tools which are capable of modeling the details of the complex geometry and loading of curved girders do exist; however, these tools are very complex, as well as expensive and time consuming. For these reasons, they are usually only available in a research environment and not in design offices.

The placement of the intermediate external diaphragms for the highway interchange that was studied for this project were specified by TxDOT in accordance with the arbitrary requirement in the TSQC's *Preferred Practices*. There was no torsional analysis performed on the bridge to determine their required locations. Originally, intermediate external diaphragms were prescribed at every panel point. They were designed using angle members because of their cost-effectiveness. Their placement was later reduced to every other panel point after research by Chen and Topkaya showed that every other intermediate diaphragm could be removed without significantly affecting bridge stresses (Cheplak, 2001).

4.2 DESIGN CONCEPT

Within this design procedure, the intermediate external diaphragms are designed for two separate phases with distinct loading cases. The two phases are the construction phase and the in-service phase.

In the construction phase, the bridge girders are subject to rotations caused by the heavy dead loads. The main concern during this phase is constructability. Intermediate external diaphragms may be needed in order to control excessive rotations in the girders so that the actual roadway alignments and superelevation will match the roadway design as closely as possible.

During the in-service phase, the limiting factor is the slab strength. The live loads on the bridge will cause girder rotations that will induce moments in the slab. It is important to ensure that these moments do not reach the ultimate capacity in the slab. The number of diaphragms required to restrict girder rotations due to live loads during the in-service phase is typically zero. It is also important to check the bridge for this condition to determine if the intermediate external diaphragms can be removed after the concrete deck has hardened.

4.3 DESIGN FOR CONSTRUCTION PHASE

4.3.1 Girder Properties

The torsional constant J of the girder is required to calculate the maximum angle of twist of the girder caused by the loads. Before J can be calculated, the Equivalent Plate Method (EPM) must be used to determine the thickness of the "top plate" in the quasi-closed section. The EPM is introduced in Section 2.2. Once the thickness t* is known, J can be readily determined using the method described in Section 2.4.

4.3.2 Rotation Due to Dead Loads

4.3.2.1 Loading Condition

During the construction phase, the only significant loads that the girders will experience are due to self-weight of the girders themselves and also of the wet concrete. At this stage, the slab is not yet hardened and is not yet acting compositely with the girders. Because of the curvature of the girders, the dead loads will induce torsional loads that will cause rotations. Other construction loads, such as work trucks and concrete pouring equipment, are relatively minor and have little impact on the structure. During the construction phase, the girders are assumed to rotate by the same amount in the same direction, as the torsional loads on each girder are virtually equal.

For design of the intermediate external diaphragms, the loading case that causes the largest amount of rotation will be considered. This loading case occurs when the all of the concrete for the deck has been poured. The concrete is assumed to be "wet" (not hardened) and not exhibiting any composite action with the girders. This is a conservative assumption and will not actually occur; on the real bridge, composite action begins to occur within hours of the concrete placement (Topkaya, 2002). As a result, the girder cross-section will have greater stiffness and will undergo smaller rotations.

Furthermore, the entire concrete roadway slab is not poured at one time. In fact, the bridge plans for the highway interchange at IH-35 and US 290 specified that "continuous concrete placement shall not be permitted". The concrete placement of the deck for long-span bridges is done in sections and is spread out over a few days, as specified by the bridge designer. In addition to controlling stresses in the girders, separating the concrete pour into sections helps to limit shrinkage effects in the deck.

In summary, including the concrete dead load with the girder self-weight along the entire bridge will result in greater calculated rotations than these girders will actually experience. In reality, the entire deck will never be totally "wet' at one time; however, it is conservative to make this assumption because composite action in freshly-poured concrete deck slabs is not yet fully understood. Research is currently being performed on this topic by Topkaya (2002) in another phase of this project.

4.3.2.2 Worst Case Rotation

The dead load of the girders and concrete can be modeled as a uniformly distributed load along the length of the bridge. As explained in Section 2.3, the uniformly distributed load acting on the curved girders results in a parabolic distribution on the straightened member. As part of the design process, it is necessary to calculate d_0, the maximum chord distance, for each span. Once d_0 is known for each span, the theoretical torques on the bridge can be calculated. d_0 is calculated using equation 2-2. The angle of twist ϕ that is calculated using equation 2-12 is the theoretical "worst case" rotation that is used as a starting point for determining the number of intermediate external diaphragms that are required for the construction phase.

4.3.3 Required Number of Intermediate Diaphragms

Before determining the number of diaphragms required for the construction phase, it is first necessary to determine if any diaphragms are actually required in each span. The maximum angle of twist per span must be checked against the maximum allowable rotation in the girder.

The maximum allowable rotation for the construction phase is defined as rotation which causes ½ in. of differential displacement measured at the outside edge of the top flanges, or ¼ in. vertical displacement at the tip of each flange (see Figure 4.1). Differential displacement of the top flanges is defined in Section 2.6. If the maximum angle of twist is greater than the allowable rotation, then it is necessary to install intermediate diaphragms in the span to resist girder rotations.

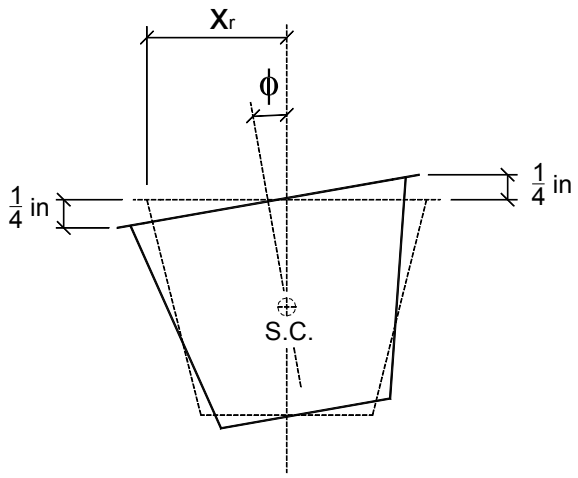

Figure 4.1 Maximum Allowable Rotation in Girders Before Deck is Poured

The reasoning for limiting the vertical displacement of the tips of the flanges at ¼ in. has to do with construction concerns. With large girder rotations, the overhang bracket, which is used to line up the metal deck, can become skewed. Also, large girder rotations would result in a "roller coaster" effect on the slab (source: John Holt of the TxDOT Bridge Design Division).

With a known girder size and maximum allowable differential displacement (½ in.), the maximum allowable angle of twist in the girder can be

easily solved using equation 2-13. For example, for a girder that is 96 inches wide at the top: $x_r = 48$ inches, and $\phi = 0.0052$ radians, or 0.3°.

If the calculated rotation due to dead loads is smaller than the maximum allowable girder rotation, then no intermediate diaphragms are required for the purposes of torsion. If the calculated rotation is larger, however, intermediate diaphragms must be added so that the calculated rotation in the girder is less than the maximum allowable rotation. The maximum spacing (s_{max}) for intermediate diaphragms due to the maximum allowable twist is determined by solving for L in equation 2-12. The number of required intermediate external diaphragms could possibly be reduced by using a step-by-step approach (i.e. adding one diaphragm at a time and then recalculating the girder rotations for each section of the span).

For convenience and also to avoid localized stresses in the webs of the girder, the intermediate external diaphragms are installed at the internal diaphragm locations (panel points). The spacing of the internal diaphragms is determined by a separate procedure.

4.3.4 Standard Diaphragm

In the event that intermediate external diaphragms are required, the engineer can select an appropriate bracing configuration (i.e. K-bracing, X-bracing). Selection of the bracing type is based on practical considerations. This design procedure does not specify a certain bracing type or diaphragm depth. The primary concern for the intermediate external diaphragms is controlling girder rotations. It does not matter how they are configured; rather, it matters how adequately they can restrain the girder rotations.

The bracing design that was chosen for the highway interchange at IH-35 and US 290 is a K-frame with the chevron opening upward, as shown in Figure

4.2. K-bracing was chosen because of its relative ease of fabrication and installation. The chevron opened upward in order to brace the longer bottom chord of the diaphragm. The diaphragm was not full-depth; it was approximately nine inches shorter than the girder on both the top and bottom. This reduction in depth made the diaphragms easier to install and remove.

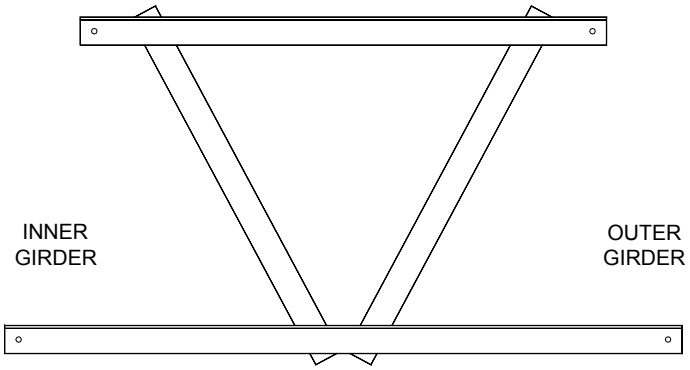

Figure 4.2 K-frame Configuation

(Cheplak, 2001)

Once the bracing configuration is determined, the intermediate external diaphragm with the largest torsional moment is analyzed to determine the forces in each member of the cross-frame. As shown in Figure 4.3, the same torsional moment is applied by each girder on the diaphragm. Each of the members are sized based on the force in the member and the unbraced length. The largest member size specified should be used in each of the members of the diaphragm for economy and ease of fabrication.

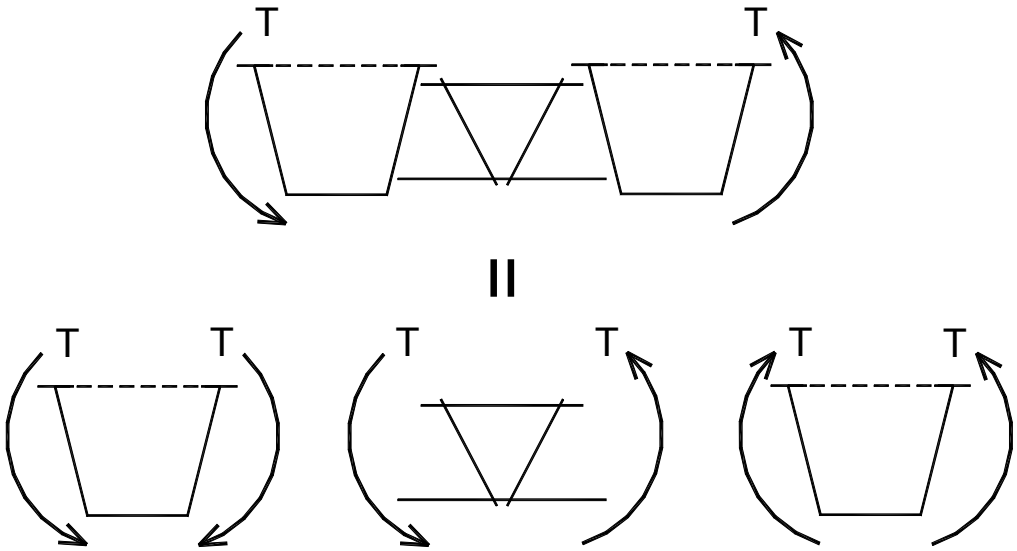

Figure 4.3 Torque Acting on Intermediate Diaphragm

It is not practical to design each diaphragm separately and specify different member sizes; rather, the one diaphragm which takes on the largest torsional moment should be designed and then made typical throughout the span. In multi-span bridges, it is economical to specify the same diaphragm throughout the entire bridge at each location where one is required.

4.4 CHECK BRIDGE IN SERVICE

4.4.1 Rotation due to Live Loads

4.4.1.1 Loading Condition

After the concrete deck has hardened, only live loads are to be considered in checking the girder for excessive rotations. At this point, rotations due to the dead loads have taken place. In-service live loads (i.e. vehicular traffic) cause girder rotations due to the bridge curvature and also due to the location of the live load on the slab. Any load that is not directly on the centerline of one of the girders will cause the girder(s) beneath it to rotate because of the eccentricity.

Similar to the construction phase, the assumed worst case during the live load phase is conservative and results in larger rotations than in the real bridge. This worst case for in-service conditions assumes that both girders rotate anti-symmetrically – in the same direction by the same angle of twist – at every point along the span. An illustration of the antisymmetric rotation in the girders is shown in Figure 4.4.

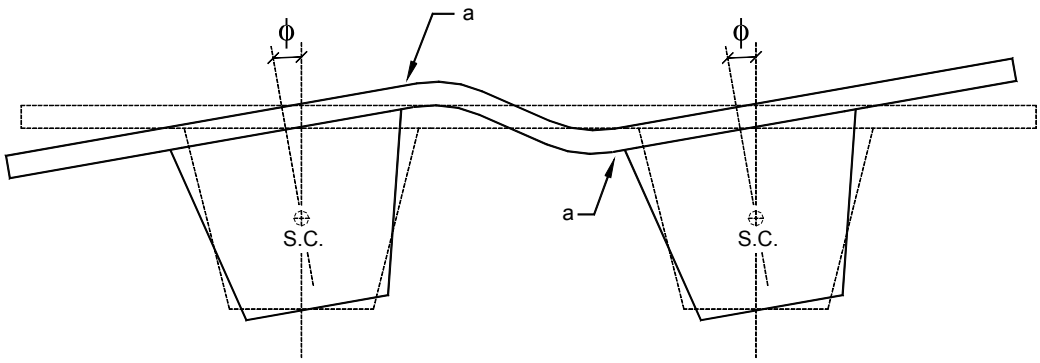

Figure 4.4 Antisymmetric Rotation due to In-Service Loads

In order for the girders to rotate antisymmetrically, the torsional loads must be identical. Although the torsional loads due to bridge curvature are equal in each girder, this is not necessarily true for eccentrically applied loads on the roadway slab and is not likely for the extreme loading cases.

From the three support displacement moment cases presented in Section 3.3 and the corresponding information provided in the Appendix, it can be seen that the largest moments in the slab occur when the girders rotate in the same direction. The calculations are much simpler if the girders rotate by the same amount, so the worst case considers two girders rotating antisymmetrically with larger-than-actual rotations. In fact, when the girders rotate in the opposite direction, the effect on the moment in the slab is reduced.

The extreme loading cases assume that the bridge is fully loaded along the entire span. This is represented in the AASHTO *Standard Specifications for Highway Bridges* as a continuous line of trucks, or a truck train. The truck train for heavy loading is modeled by a uniformly distributed load of 640 pounds per linear foot of lane and a concentrated load of 18,000 pounds at the location where it causes the maximum moment on the bridge. The distributed load is applied longitudinally at the center of a 10-foot-wide design lane, and the concentrated load is applied at the center of the span in each lane. For the design of intermediate external diaphragms, the design lanes need to be placed in such a way that they cause the largest possible rotation in the girders.

In an actual bridge, the slab is continuous over the girders, as shown in Figure 4.4. The slab will help restrain girder twist; the girders do not act independently. Once the slab cracks at location “a” (see Figure 4.4), however, this restraining effect is diminished significantly. For this reason, this restraining effect is ignored for the purposes of calculating girder rotations. The slab, therefore, is considered only to distribute the loads on it to the girders beneath.

The loads distributed to each girder are based on the tributary area of the girder. Loads that straddle the center line between two girders are distributed to both girders, thus reducing the effect on one girder alone.

Figure 4.5 shows the loading condition that would cause the worst actual rotation in a typical two-girder bridge. e denotes the eccentricity of the design lane load. The largest actual rotation occurs when one design lane is positioned as close to the edge of the slab as possible, and another design lane is flush with the centerline of the cross-section. The eccentricities of the loads over each girder are different; as a result, one girder has a larger torsional load and undergoes a larger rotation than the other. For the design procedure, though, both girders are assigned the higher girder rotation for simpler calculations and a more conservative design.

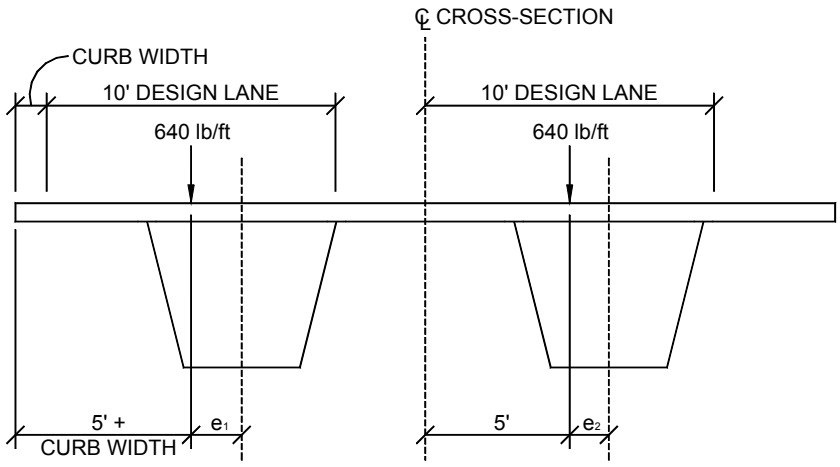

Figure 4.5 Loading Case Corresponding to Largest Actual Rotation

4.4.1.2 Girder Rotation

The design lane load that is above each of the girders has a constant eccentricity (e) respective to each girder. That translates to a uniformly distributed load of 640*e pounds per linear foot on each girder. Each girder then has three torsional loads to consider: one constantly applied torque (640*e), the parabolic torque distribution from the lane load acting on the curved bridge, and the concentrated torque from the 18,000 pound load acting at mid-span. The girder rotations due to these loads are determined from the equations in Section 2.5. It is only necessary to calculate the angle of twist for the girder with the largest eccentricity and then apply that angle of twist to both girders. For example, in a two-girder bridge where $e_1 > e_2$, it is only necessary to calculate the girder rotations for the torsional loads using e_1. Both girders are then assumed to rotate this amount for the worst design case.

The theoretical maximum angle of twist calculated for the worst case in-service loads is used to determine the theoretical amount of vertical displacement in the top flanges of the girders using the same procedure as given in Section 4.3. The girder torsional constant is significantly larger in the in-service state because the slab fully closes the section; it is no longer quasi-closed. It is necessary to calculate the maximum angle of twist in each span to determine if intermediate external diaphragms are required for the in-service phase. The method is further developed in the remainder of this section and is further explained in the design example in Chapter 5.

The top flange displacement (Δ) due to the calculated twist is determined from equation 2-15. This value is needed to calculate the moment in the slab (explained in next subsection). For example, for a girder that is 96 inches wide at the top and rotates 0.1° (0.00175 rad) about its shear center: Δ = (48 inches) * (0.00175) = 0.084 inches

4.4.2 Slab Moments

As explained in Chapter 3, there are three moment cases to consider in the slab. There are moments due to girder rotations / slab support displacements, the design wheel load, and the slab self-weight. Each of these moments can be calculated using the figures in Chapter 3 and corresponding information in the Appendix. All moment calculations assume a one-foot slab design width of the slab.

Figures 4.6 and 4.7 show typical moment envelopes in a slab with small and large girder rotations, respectively. It is apparent that with small girder rotations, the dominating moment case is that of the design wheel load; however, when the girders undergo significant rotations, the moment due to the slab support

displacements dominates. The largest moments occur at the interior slab supports.

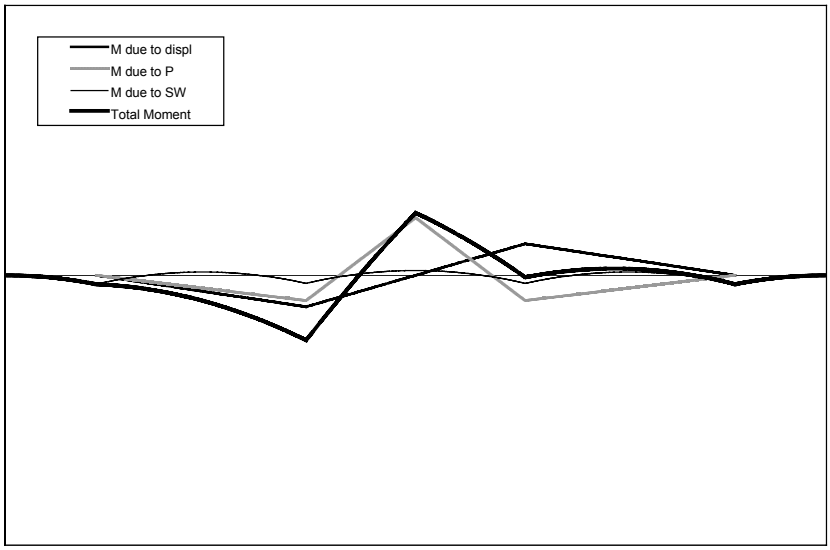

Figure 4.6 Typical Moment Envelope in Slab with Small Girder Rotations

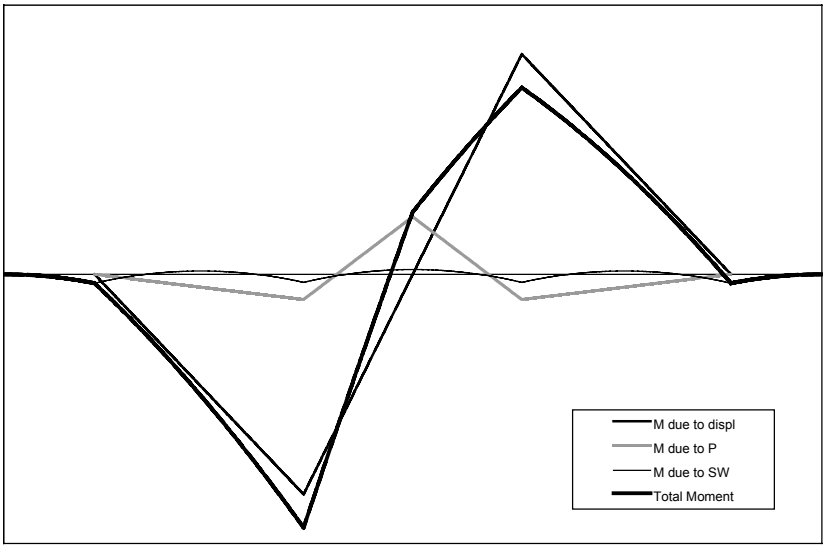

Figure 4.7 Typical Moment Envelope in Slab with Large Girder Rotations

4.4.3 Capacity of Slab

In the construction phase, the amount of rotation permitted in the girder is limited by the amount of vertical displacement of the top flanges. The criteria are different in the in-service phase; here, the ultimate moment in the slab is the limiting factor. The maximum moment from the slab moment envelope calculated for the slab must not reach the slab ultimate moment.

The ultimate moment in the slab is calculated for a one-foot-wide design strip. A drawing of the basic design strip is shown in Figure 4.8. d and c_t represent the respective depths of the bottom and top mats of steel reinforcement.

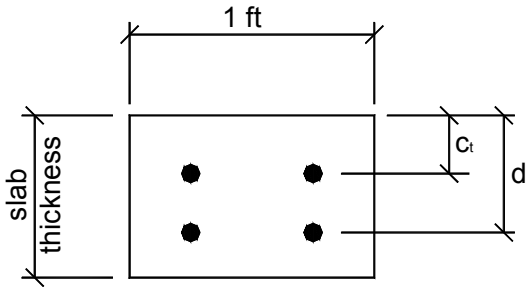

Figure 4.8 Roadway Slab Design Strip

In the typical roadway slab, the top clearance (c_t) is greater than the bottom clearance; therefore, the calculated moment capacity assuming compression in the top of the design strip is larger than the calculated moment capacity assuming compression in the bottom. However, in the real slab, this is not necessarily the case. Although its contribution is ignored in analysis, the metal deck that forms the bottom of the slab acts essentially as reinforcing steel that boosts the moment capacity of the slab. For the design procedure, it is acceptable to assume that the bending of the slab in either direction will result in

the same ultimate moment capacity, even though there is less concrete cover in the bottom.

The ultimate moment capacity assuming compression in the top of the design strip is determined using the moment-curvature relationship of the slab. Typical values for an eight-inch slab are between 20-25 kip-feet (240 – 300 kip-inches). The moment capacity of the slab is compared with the maximum moment in the slab determined from the slab moment envelope.

4.4.4 Intermediate Diaphragms for In-Service Bridge

Once the concrete slab has hardened sufficiently, the girders and slab act compositely, forming an extremely stiff section with a very large moment of inertia. For this reason, intermediate external diaphragms are often removed from curved steel trapezoidal girder bridges after the construction phase is complete. This is a reasonable assumption, as there are no known failures of these types of bridges in torsion after the intermediate external diaphragms were removed. However, it is important to evaluate the bridge with its worst case torsional loads before removing all of these diaphragms.

If the calculated rotation due to the truck train and other slab loads is smaller than the maximum allowable girder rotation, which is limited by the slab, then no intermediate diaphragms are required in the final state for the purposes of torsion. If the calculated rotation is larger, however, permanent intermediate diaphragms may be required. The diaphragm-to-girder connections for the permanent diaphragms must be designed as fatigue connections. The number of diaphragms that must remain on the bridge is calculated in a similar manner as the one by which the number of temporary diaphragms to install was determined.

4.5 LIMITATIONS OF DESIGN PROCEDURE

This design procedure assumes that warping is not a factor because of the large torsional stiffness of the quasi-closed and closed section status of the trapezoidal girder. If warping is a factor, this method is not adequate for the design of intermediate external diaphragms. Warping becomes important when the warping torsion constant (I_w) of a given member is significantly greater than the girder torsional constant (J). This occurs only in open sections, and therefore, should not be a consideration with curved steel trapezoidal girder bridge systems (Kolbrunner & Basler, 1969).

CHAPTER 5
Design Example

5.1 DESIGN PROBLEM

Consider a three-span bridge with twin steel trapezoidal girders and a concrete roadway slab. This design example is provided to explain the procedure that was introduced in Chapter 4. A plan view of the bridge is shown in Figure 5.1. The girder dimensions are given in Figure 5.2, and the final bridge cross-section is shown in Figure 5.3. The radius of curvature (R) of the centerline bridge cross-section is 535 feet, and the top lateral braces are assumed to be WT8x33.5 members.

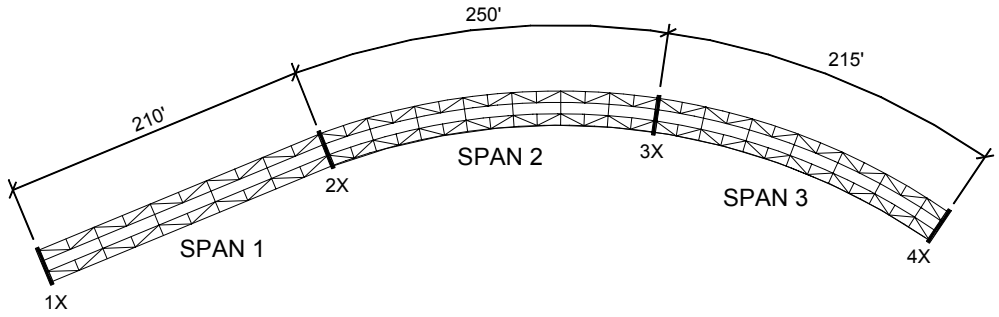

Figure 5.1 Example Bridge

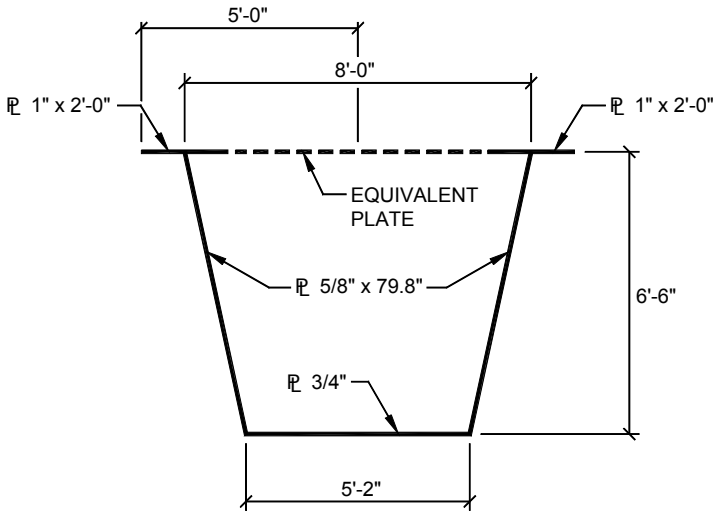

Figure 5.2 Example Girder Cross-Section

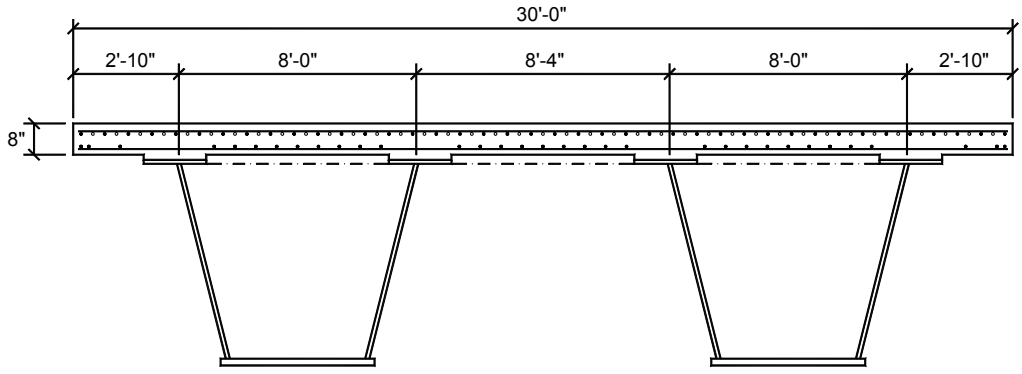

Figure 5.3 Example Bridge Cross-Section

5.2 DESIGN FOR CONSTRUCTION PHASE

5.2.1 Girder Properties

The effective top plate thickness for each span of the girder was calculated using the Equivalent Plate Method. Each span has a different internal diaphragm spacing (panel length), meaning that the equivalent plate thickness (t*) is different for each span. Figures 5.4 through 5.6 shows the calculations for t* for each span. As the panel lengths decrease, t* increases. Also shown in Figures 5.4 through 5.6 are the calculations for J for each span using equation 2-5. As t* increases, J increases.

The panel lengths are equal in both girders in the straight portion of the bridge, but they vary slightly from inside girder to outside girder in the curved spans due to the small difference in the radii of curvature at the inside and outside of the bridge cross-section. This difference in radii is insignificant, as it is a small percentage of the relatively large distance to the center of curvature of the bridge. For ease of calculation, it is acceptable to assume that both girders have the same radius of curvature and that the bridge span is measured on the centerline of the roadway slab. Then, the panel lengths can be determined by dividing the span length by the number of panels. This assumption should only be used if the difference between radii of curvature is less than 5% of R of the centerline.

For example, in the example bridge, R is given as 535 feet at the centerline of the bridge cross-section. Using the dimensions shown in Figure 5.3, it can be determined that R of the centerline of the inner girder is 526′-10″, and R of the centerline of the outer girder is 543′-2″. The difference of these two radii (16′-4″) is 3% of 535 feet, which is not a significant difference.

SPAN 1

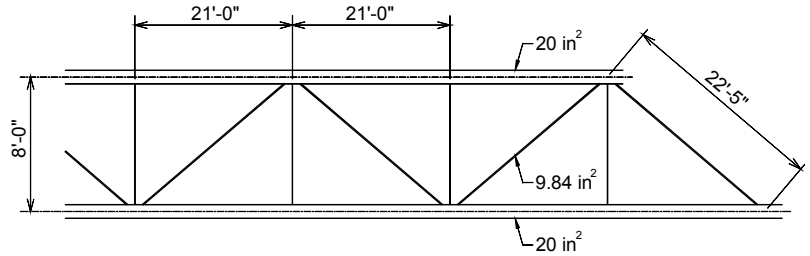

$$t^* = \left(\frac{29{,}000ksi}{11{,}200ksi}\right)\frac{(21ft)(8ft)}{\frac{(22.5ft)^3}{(0.07ft^2)} + \frac{(21ft)^3}{3}\left(\frac{1}{(0.14ft^2)} + \frac{1}{(0.14ft^2)}\right)} = 0.00210\,ft$$

$$J = \frac{4(6162in^2)^2}{\left(\frac{96in}{0.025in}\right) + 2\left(\frac{79.8in}{0.675in}\right) + \left(\frac{62in}{0.75in}\right)} = 36{,}518in^4$$

Span 1 is straight; therefore, $d_0 = 0$

Figure 5.4 Span 1 Properties

SPAN 2

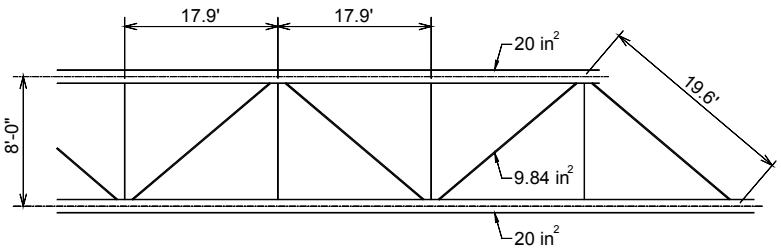

$$t^* = \left(\frac{29{,}000ksi}{11{,}200ksi}\right)\frac{(17.9\,ft)(8\,ft)}{\dfrac{(19.6\,ft)^3}{(0.07\,ft^2)} + \dfrac{(17.9\,ft)^3}{3}\left(\dfrac{1}{(0.14\,ft^2)} + \dfrac{1}{(0.14\,ft^2)}\right)} = 0.00275\,ft$$

$$J = \frac{4(6162in^2)^2}{\left(\dfrac{96in}{0.033in}\right) + 2\left(\dfrac{79.8in}{0.675in}\right) + \left(\dfrac{62in}{0.75in}\right)} = 47{,}048in^4$$

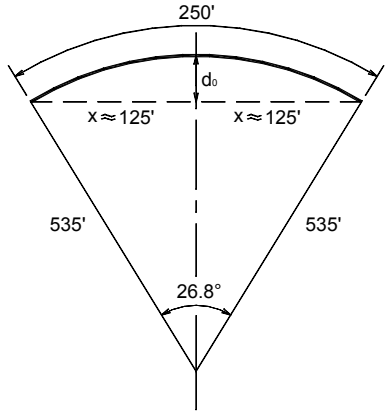

$$d_0 = (535\,ft)\left[1 - \sin\left(90° - \frac{26.8°}{2}\right)\right] = 14.56\,ft$$

Figure 5.5 Span 2 Properties

SPAN 3

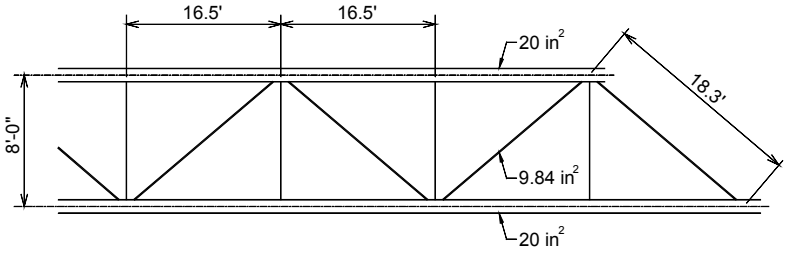

$$t^* = \left(\frac{29{,}000ksi}{11{,}200ksi}\right)\frac{(16.5\,ft)(8\,ft)}{\frac{(18.3\,ft)^3}{(0.07\,ft^2)} + \frac{(16.5\,ft)^3}{3}\left(\frac{1}{(0.14\,ft^2)} + \frac{1}{(0.14\,ft^2)}\right)} = 0.00314\,ft$$

$$J = \frac{4(6162in^2)^2}{\left(\frac{96in}{0.032in}\right) + 2\left(\frac{79.8in}{0.675in}\right) + \left(\frac{62in}{0.75in}\right)} = 45{,}760in^4$$

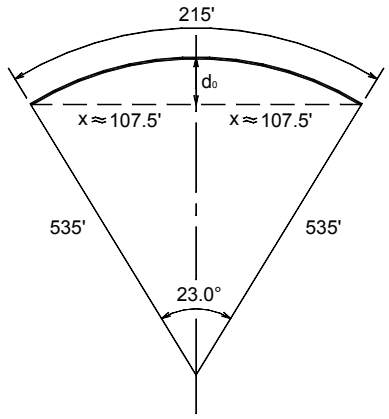

$$d_0 = (535\,ft)\left[1 - \sin\left(90° - \frac{23.0°}{2}\right)\right] = 10.74\,ft$$

Figure 5.6 Span 3 Properties

5.2.2 Loading Condition

The assumed worst case dead load during the construction phase consists of two aspects: girder self weight and weight of concrete. The steel is assumed to weigh 490 lbs/ft^3, and the concrete is assumed to weigh 150 lbs/ft^3.

The cross-sectional area of the example girder is:

$$A_{steel} = 2(1in \times 20in) + 2(0.675in \times 79.8in) + (0.75in \times 62in) = 194.23in^2$$

The self weight of the girder is:

$$w_{steel} = 1.35\,ft^2 \times 490lbs/ft^3 = 661.5lbs/ft$$

Increase the weight by 10 per cent to account for the top lateral bracing and internal cross-frames inside the girder:

$$w_{steel} = 1.1 \times (661.5lbs/ft) = 728lbs/ft$$

The weight of the concrete slab is:

$$w_{conc} = 30\,ft \times 0.67\,ft \times 150lbs/ft^3 = 3000lbs/ft$$

Total dead load per span:

$w = w_{steel} + w_{conc} = 3.73$ *kips/ft* (1.87 *kip/ft per girder*)

5.2.3 Required Number of Intermediate Diaphragms

SPAN 1

Span 1 is straight; therefore, no intermediate diaphragms are required for the purposes of torsion during the construction phase.

SPAN 2

From Eq. 2-15: $\phi_{\max} = 1/4in \div 60in = 0.0042rad = 0.24°$

From Eq. 2-12: $0.0042 = \dfrac{7(1.87kip/ft)(14.56ft)L^2}{72(1{,}612{,}800ksf)(2.27ft^4)} \rightarrow L = 76.2\,ft$

$\dfrac{250\,ft}{76.2\,ft} = 3.3 \rightarrow$ *4 intermediate diaphragms required*

Place diaphragms at fifth points of span; s = 50 ft

SPAN 3

$0.0042 = \dfrac{7(1.87kip/ft)(10.74ft)L^2}{72(1{,}612{,}800ksf)(2.21ft^4)} \rightarrow L = 87.6\,ft$

$\dfrac{215\,ft}{87.6\,ft} = 2.5 \rightarrow$ *3 intermediate diaphragms required*

Place diaphragms at quarter points of span; s = 53.8 ft

5.2.4 Axial Forces for Design Diaphragm

The torques at the locations of the intermediate diaphragms were calculated using equation 2-3. As shown in Figures 5.7 and 5.8, the diaphragm at the center of span 2, which had the largest torque, was chosen as the design diaphragm. A schematic of the design diaphragm is shown in Figure 5.9. The diaphragms are assumed to be offset nine inches from the top and bottom of the girder. The force breakdown for each member of the design diaphragm is shown in Figure 5.10. In a real bridge, these forces would be used to select member sizes.

Notes for Figure 5.10:

1. The horizontal force couple on the girders was determined by dividing the torque in the girder by the height of diaphragm (the distance between the centroidal axes of the top and bottom chords).
2. The cross-frames was treated as a truss. The space on the bottom chord in between the diagonals was not enough for Vierendeel action to occur, and the diagonals were very close to the ends of the top chord at the diaphragm-girder connections.
3. The shear force was determined from statics: V = 2M/L, where L is taken as the length of the top chord. Assuming truss analysis, the diaphragm width is equivalent to the length of the top chord.
4. A positive force indicates tension, and a negative force indicates compression.

SPAN 2

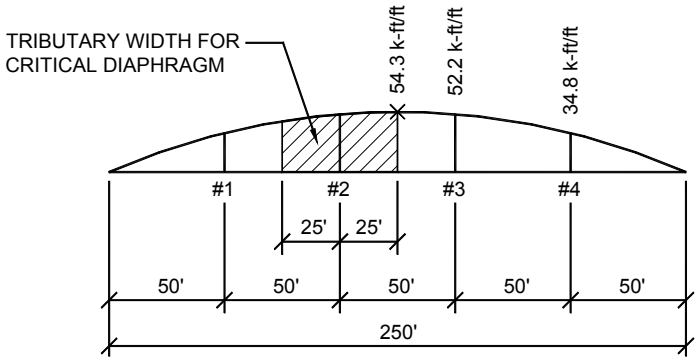

Assume torque is constant over tributary width:

T = (52.2 *k-ft/ft*)(50 *ft*) = 2610 *k-ft* (1305 *k-ft per girder*)

Figure 5.7 Critical Diaphragm in Span 2

SPAN 3

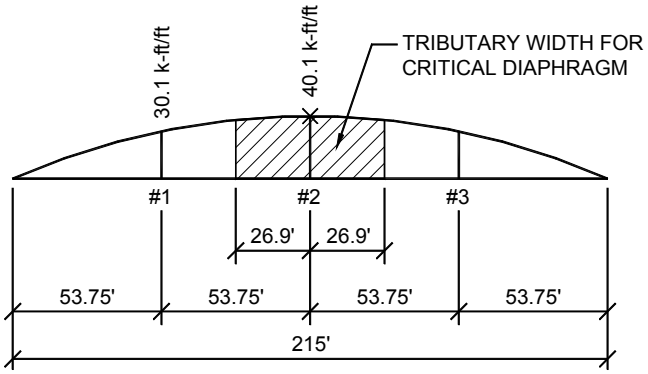

Assume torque is constant over tributary width:

T = (40.1 *k-ft/ft*)(53.75 *ft*) = 2155.4 *k-ft* (1077.7 *k-ft per girder*)

Figure 5.8 Critical Diaphragm in Span 3

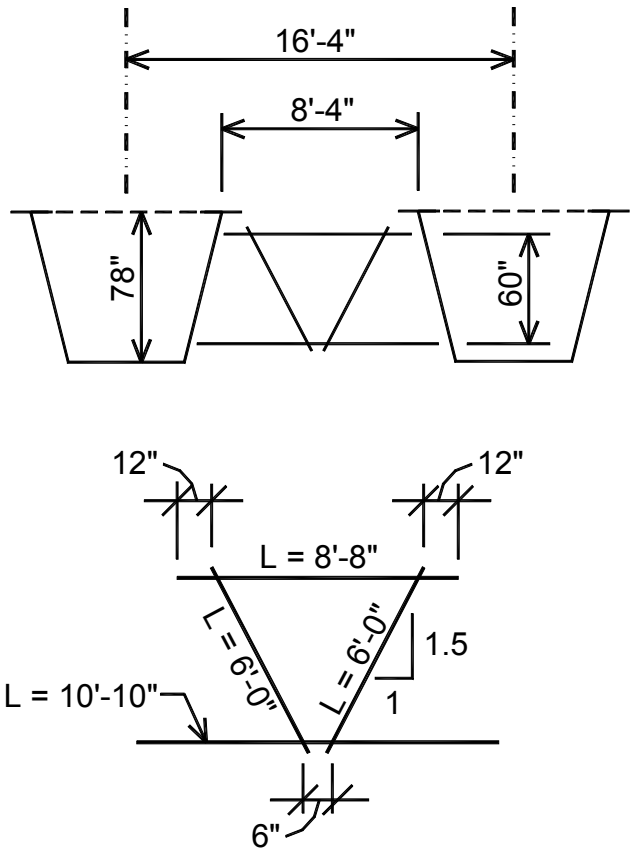

Figure 5.9 Dimensions of Typical Diaphragm

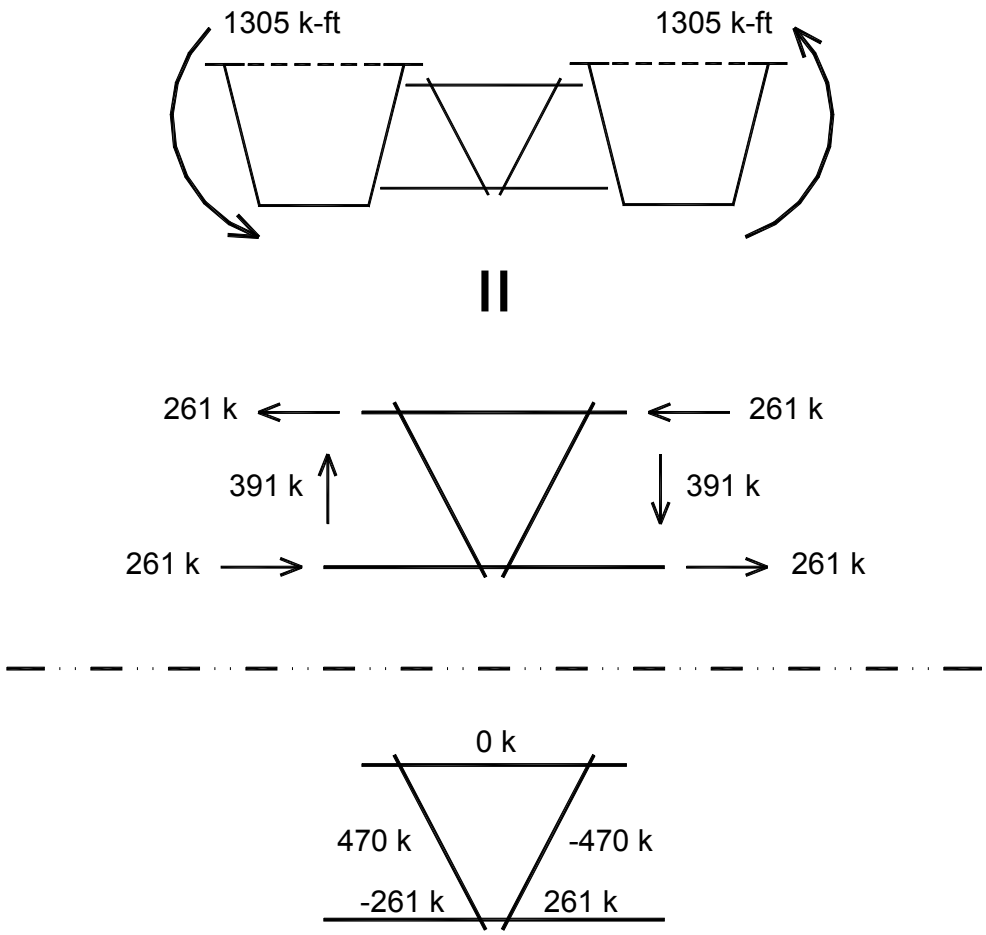

Figure 5.10 Design Forces

These are significant forces which require relatively large member sizes. The same is true for the 3-diaphragm arrangement in span 3. The addition of intermediate external diaphragms to each span can reduce the design axial forces in the diaphragm members. The design axial forces must be recalculated with the addition of each diaphragm.

5.3 CHECK BRIDGE IN SERVICE

5.3.1 Girder Properties

Recalculate J for each span including the 8" slab. The concrete has a compressive strength of 4000 psi. The modulus of elasticity of the concrete was determined using ACI Sec. 8.5.1.

$$I_{slab} = \frac{(12in)(8in)^3}{12} = 512in^3$$

$$E_{conc} = 57{,}000\sqrt{f'_c} = 3605 \times 10^3 \, psi$$

$$\eta = \frac{E_{steel}}{E_{conc}} = \frac{29{,}000ksi}{3605ksi} = 8$$

SPAN 1

$$t^* = 0.025in + \frac{8in}{\eta} = 1.025in$$

$$J = \frac{4(6162in^2)^2}{\left(\frac{96in}{1.025in}\right) + 2\left(\frac{79.8in}{0.675in}\right) + \left(\frac{62in}{0.75in}\right)} = 367{,}956in^4$$

SPAN 2

$$t^* = 0.033in + \frac{8in}{\eta} = 1.033in$$

$$J = \frac{4(6162in^2)^2}{\left(\frac{96in}{1.033in}\right) + 2\left(\frac{79.8in}{0.675in}\right) + \left(\frac{62in}{0.75in}\right)} = 368{,}603.5in^4$$

SPAN 3

$$t^* = 0.032in + \frac{8in}{\eta} = 1.032in$$

$$J = \frac{4(6162in^2)^2}{\left(\frac{96in}{1.032in}\right) + 2\left(\frac{79.8in}{0.675in}\right) + \left(\frac{62in}{0.75in}\right)} = 368{,}523in^4$$

5.3.2 Loading Condition

The bridge was checked for rotation due to the truck train loading, which is explained in Section 4.4. The truck train lane loading, shown in Figure 5.11, supplies a uniformly distributed torque of 0.53 kip-ft along the length of each girder. The total rotation due the truck train was calculated for each span using the equations in Section 2.5.

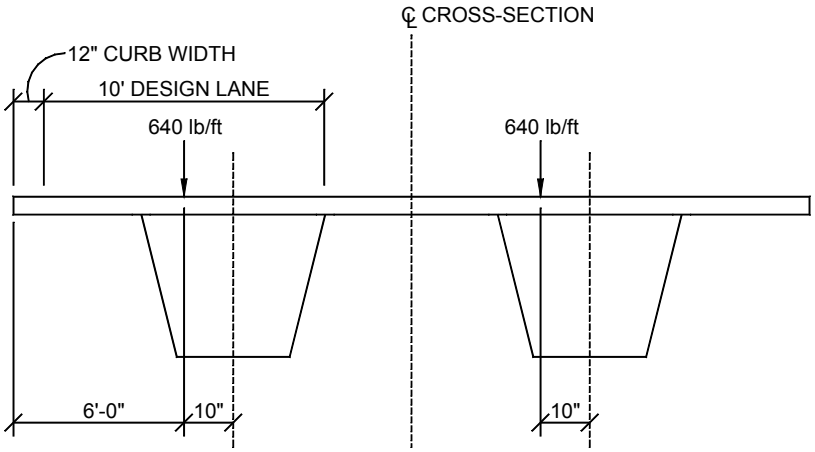

Figure 5.11 Truck Train Lane Loading

SPAN 1

Torque from 18 kip load on each girder:

T = 18 *kip* x 0.83 *ft* = 15 *k-ft*

Both girders have the same torsional load.

$$\phi(105\,ft) = \frac{(15k-ft)(105\,ft)(105\,ft)}{(1{,}612{,}800ksf)(17.74\,ft^4)(210\,ft)} = 2.75\times10^{-5}\,rad \qquad (1)$$

$$\phi(105\,ft) = \frac{(0.53k-ft)(210\,ft)^2}{8(1{,}612{,}800ksf)(17.74\,ft^4)} = 0.00010rad \qquad (2)$$

(1) rotation in outer girder due to eccentricity of 18 kip load

(2) rotation in outer girder due to constant eccentricity of lane load

total rotation = (1) + (2) = 0.00013 rad = 0.007°

$\Delta = x_r\phi \;\rightarrow\; \Delta = (48in)(0.00013rad) = 0.01in$

SPAN 2

Torque from 18 kip load on each girder:

T = 18 *kip* x 0.83 *ft* = 15 *k-ft*

Torque from 18 kip load due to bridge curvature:

T = 18 *kip* x 5.56 *ft* = 100.08 *k-ft* (inner girder)

T = 18 *kip* x 21.89 *ft* = 394.02 *k-ft* (outer girder)

Outer girder has the larger torsional load.

$$\phi(125\,ft) = \frac{(15k-ft)(125\,ft)(125\,ft)}{(1{,}612{,}800ksf)(17.78\,ft^4)(250\,ft)} = 3.27\times10^{-5}\,rad \qquad (1)$$

$$\phi(125\,ft) = \frac{(394.02k-ft)(125\,ft)(125\,ft)}{(1{,}612{,}800ksf)(17.78\,ft^4)(250\,ft)} = 0.00086rad \qquad (2)$$

$$\phi(125\,ft) = \frac{(0.53k-ft)(250\,ft)^2}{8(1{,}612{,}800ksf)(17.78\,ft^4)} = 0.00014rad \qquad (3)$$

$$\phi(125\,ft) = \frac{7(0.64kip)(21.89\,ft)(250\,ft)^2}{72(1{,}612{,}800ksf)(17.78\,ft^4)} = 0.00297rad \qquad (4)$$

(1) rotation in outer girder due to eccentricity of 18 kip load

(2) rotation in outer girder from 18 kip load due to bridge curvature

(3) rotation in outer girder due to constant eccentricity of lane load

(4) rotation in outer girder from lane load due to bridge curvature

total rotation = (1) + (2) + (3) + (4) = 0.00400 *rad*

$\Delta = x_r\phi \;\rightarrow\; \Delta = (48in)(0.00400rad) = 0.19in$

SPAN 3

Torque from 18 kip load on each girder:

T = 18 *kip* x 0.83 *ft* = 15 *k-ft*

Torque from 18 kip load due to bridge curvature:

T = 18 *kip* x 1.74 *ft* = 31.32 *k-ft* (inner girder)

T = 18 *kip* x 18.07 *ft* = 325.26 *k-ft* (outer girder)

Outer girder has the larger torsional load.

$$\phi(107.5\,ft) = \frac{(15k-ft)(107.5\,ft)(107.5\,ft)}{(1{,}612{,}800ksf)(17.77\,ft^4)(215\,ft)} = 2.81\times10^{-5}\,rad \qquad (1)$$

$$\phi(107.5\,ft) = \frac{(325.26k-ft)(107.5\,ft)(107.5\,ft)}{(1{,}612{,}800ksf)(17.77\,ft^4)(215\,ft)} = 0.00061rad \qquad (2)$$

$$\phi(107.5\,ft) = \frac{(0.53k-ft)(215\,ft)^2}{8(1{,}612{,}800ksf)(17.77\,ft^4)} = 0.00011rad \qquad (3)$$

$$\phi(107.5\,ft) = \frac{7(0.64kip)(18.07\,ft)(215\,ft)^2}{72(1{,}612{,}800ksf)(17.77\,ft^4)} = 0.00181rad \qquad (4)$$

(1) rotation in outer girder due to eccentricity of 18 kip load

(2) rotation in outer girder from 18 kip load due to bridge curvature

(4) rotation in outer girder due to constant eccentricity of lane load

(4) rotation in outer girder from lane load due to bridge curvature

total rotation = (1) + (2) + (3) + (4) = 0.00256 *rad*

$\Delta = x_r\phi \;\rightarrow\; \Delta = (48in)(0.00256rad) = 0.12in$

5.3.3 Slab Moments

The moments in a 1-ft strip of the slab were determined using the method presented in Chapter 3. The slab moments for the three spans are presented in Figures 5.12, 5.13, and 5.14. The maximum and minimum moments are indicated in the figures. Location "a" is defined in Section 4.4.

SPAN 1

Moment due to Slab Support Displacements:

$$M_{\Delta} = 6(3605ksi)(512in^4)(0.01)\left[\frac{1}{(96in)^2} - \left(\frac{1}{(96in)^2} - \frac{2}{(100in)^2}\right)\left(\frac{1}{1+\frac{2(96in)}{100in}}\right)\right]$$

M_{Δ} = 15.5 *k-in* = 1.3 *k-ft*

Moment due to Design Wheel Load:

Design Wheel Load (P_{20}) = 16 kips

Effective Span Length (S) = clear distance between girders + ½ flange width

= 6′-8″ + 10″ = 7′-4″

$$E = \left(\frac{8S}{S+2}\right) = 7.82 \qquad P = \frac{P_{20}}{E} = 2.05kip$$

$$M_1 = \frac{(2.05kip)(100in)}{8}\left(\frac{3}{3+\frac{2(96in)}{100in}}\right) = 15.6\ k\text{-}in = 1.3\ k\text{-}ft$$

$$M_2 = \frac{(2.05kip)(100in)}{4} - M_1 = 36.0\ k\text{-}in = 3.0\ k\text{-}ft$$

Moment due to Self-Weight of Slab:

The weight of the concrete slab is:

$$w_{conc} = 1ft \times 0.67\,ft \times 150lbs/\,ft^3 = 100.5lbs/\,ft$$

$$DF = \frac{3}{3 + \frac{2L_1}{L_2}} = 0.61$$

$$M_a = \frac{(.1kip/\,ft)(2.83\,ft)^2}{2} = 0.4\ kip\text{-}ft$$

$$M_b = \frac{(.1kip/\,ft)(8\,ft)^2}{8}(1 - DF) + \frac{(.1kip/\,ft)(2.83\,ft)^2}{4}(DF - 1)$$

$$+ \frac{(.1kip/\,ft)(8.33\,ft)^2}{12}(DF)$$

$$M_b = 0.6\ kip\text{-}ft$$

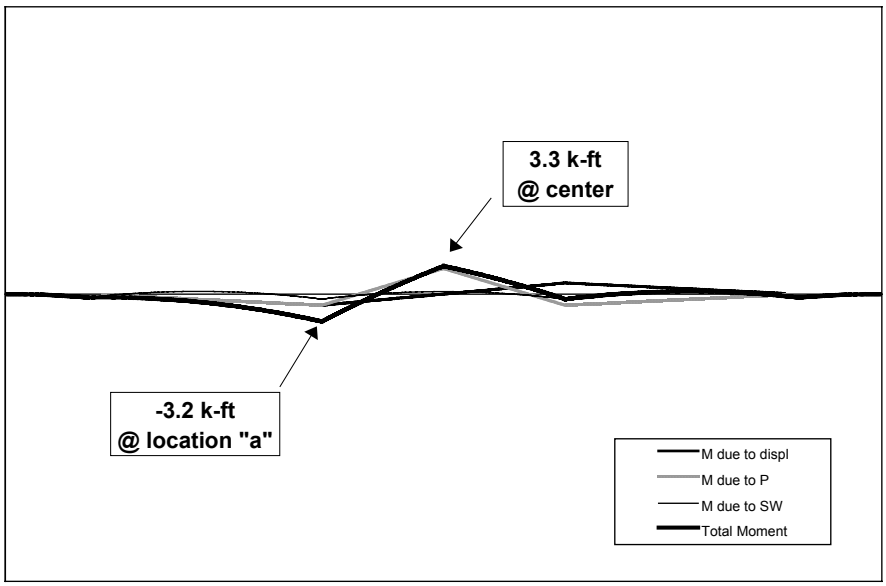

Figure 5.12 Span 1 Slab Moments

SPAN 2

Moment due to Slab Support Displacements:

$$M_{\Delta} = 6(3605ksi)(512in^4)(0.19)\left[\frac{1}{(96in)^2} - \left(\frac{1}{(96in)^2} - \frac{2}{(100in)^2}\right)\left(\frac{1}{1+\frac{2(96in)}{100in}}\right)\right]$$

$M_{\Delta} = 294.5$ *k-in* $= 24.5$ *k-ft*

The moments due to the design wheel load and the self-weight of the slab are the same as those calculated for span 1.

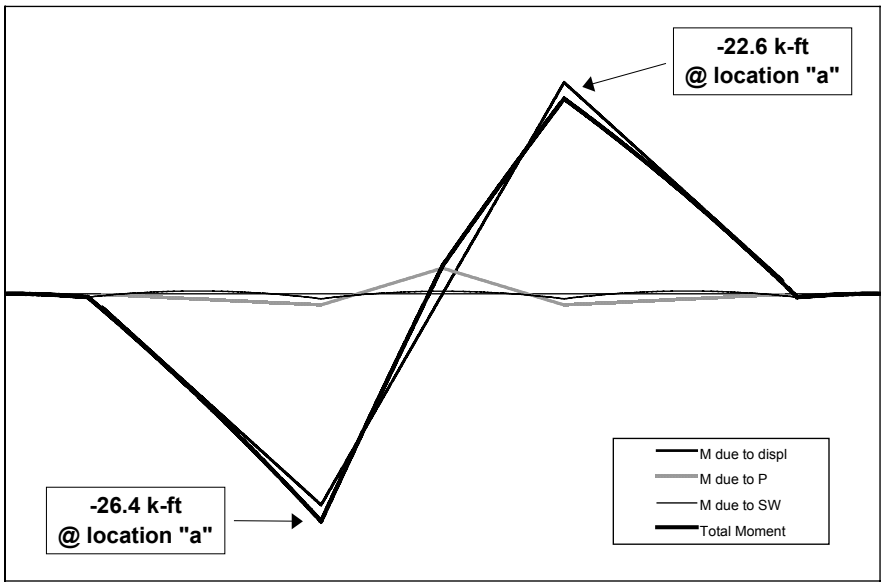

Figure 5.13 Span 2 Slab Moments

SPAN 3

Moment due to Slab Support Displacements:

$$M_{\Delta} = 6(3605ksi)(512in^4)(0.12)\left[\frac{1}{(96in)^2} - \left(\frac{1}{(96in)^2} - \frac{2}{(100in)^2}\right)\left(\frac{1}{1+\frac{2(96in)}{100in}}\right)\right]$$

M_{Δ} = 186.0 *k-in* = 15.5 *k-ft*

The moments due to the design wheel load and the self-weight of the slab are the same as those calculated for span 1.

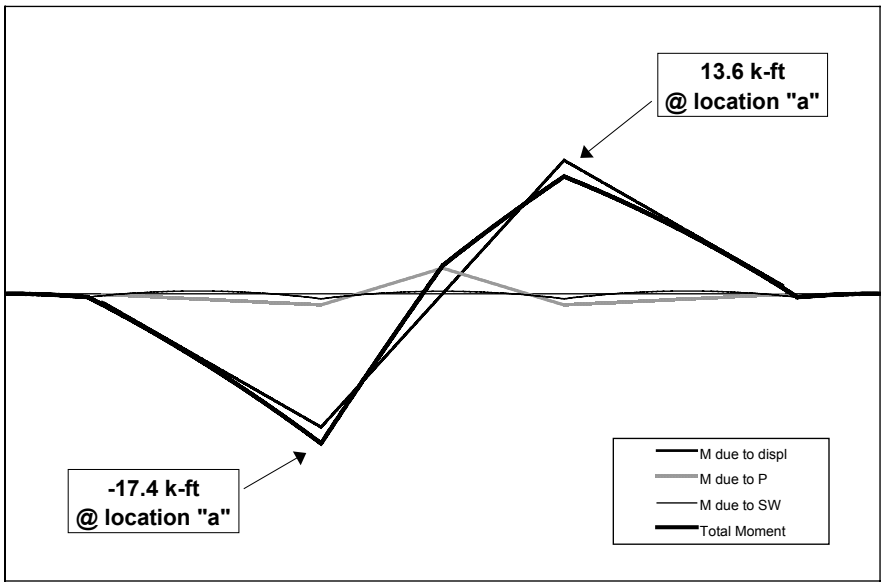

Figure 5.14 Span 3 Slab Moments

5.3.4 Capacity of Slab

The ultimate moment capacity of a 1-ft strip of the slab was obtained using the slab moment-curvature relationship. A cross-section of that 1-ft strip is shown in Figure 5.15. The ultimate moment capacity was determined to be 21.4 k-ft. This value was calculated using a regular stress block and disregarding strain hardening in the steel reinforcing bars.

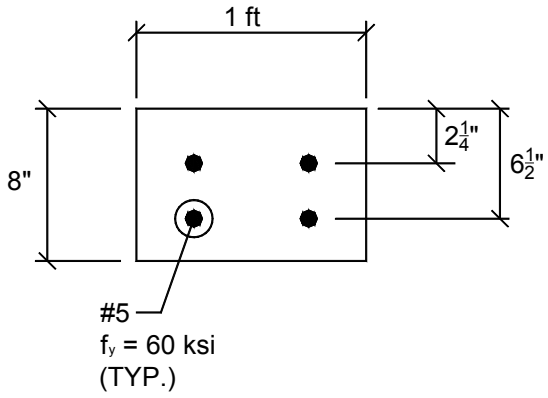

Figure 5.15 Cross-Section of Slab Design Strip

5.3.5 Intermediate Diaphragms for In-Service Bridge

SPAN 1

Maximum +M = 3.3 *k-ft*
Maximum –M = -3.2 *k-ft*

3.3 *k-ft* < 21.4 *k-ft* → *no intermediate diaphragms required*

SPAN 2

Maximum +M = 22.6 *k-ft*
Maximum –M = -26.4 *k-ft*

26.4 *k-ft* > 21.4 *k-ft* → *intermediate diaphragms required*

Insert one diaphragm at midspan and recheck moments in slab:
d_0 = *3.65 ft*

Torque from 18 kip load due to bridge curvature:
T = 18 *kip* x -6.65 *ft* = -119.7 *k-ft* (inner girder) #
T = 18 *kip* x 10.98 *ft* = 197.6 *k-ft* (outer girder)
# *the negative sign indicates that the twist is in the opposite direction*

Outer girder has the larger torsional load.

$$\phi(62.5ft) = \frac{(15k-ft)(62.5ft)(62.5ft)}{(1{,}612{,}800ksf)(17.78ft^4)(125ft)} = 1.63\times10^{-5}rad \qquad (1)$$

$$\phi(62.5ft) = \frac{(197.6k-ft)(62.5ft)(62.5ft)}{(1{,}612{,}800ksf)(17.78ft^4)(125ft)} = 0.00022rad \qquad (2)$$

$$\phi(62.5ft) = \frac{(0.53k-ft)(125ft)^2}{8(1{,}612{,}800ksf)(17.78ft^4)} = 3.61\times10^{-5}rad \qquad (3)$$

$$\phi(62.5ft) = \frac{7(0.64kip)(10.98ft)(125ft)^2}{72(1{,}612{,}800ksf)(17.78ft^4)} = 0.00037rad \qquad (4)$$

total rotation = (1) + (2) + (3) + (4) = 0.00064 *rad*

$\Delta = x_r\phi \;\rightarrow\; \Delta = (48in)(0.00064rad) = 0.03in$

Moment due to Slab Support Displacements:

$$M_\Delta = 6(3605ksi)(512in^4)(0.03)\left[\frac{1}{(96in)^2} - \left(\frac{1}{(96in)^2} - \frac{2}{(100in)^2}\right)\left(\frac{1}{1+\frac{2(96in)}{100in}}\right)\right]$$

M_Δ = 46.5 *k-in* = 3.9 *k-ft*

The moments due to the design wheel load and the self-weight of the slab are the same as those calculated previously.

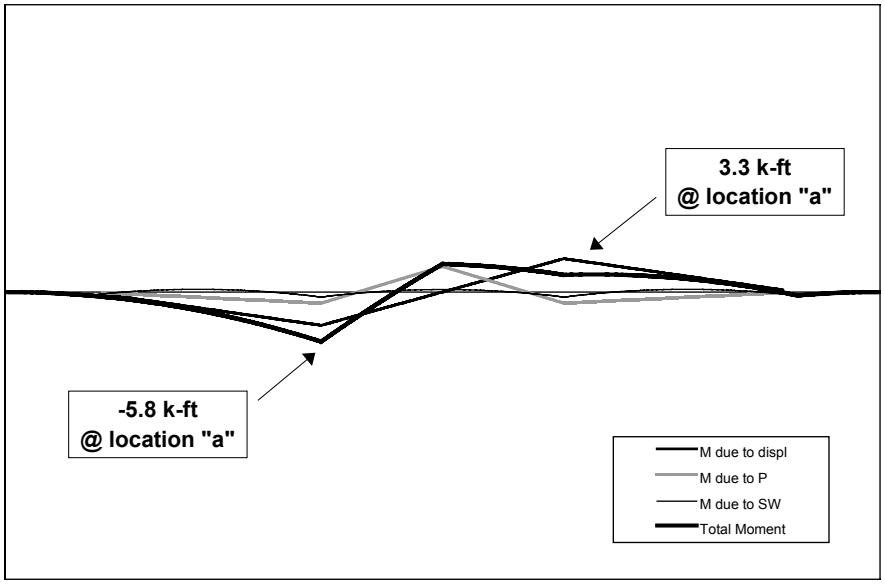

Figure 5.16 Span 2 Slab Moments (2nd Pass)

Maximum +M = 3.3 *k-ft*

Maximum –M = -5.8 *k-ft*

5.8 *k-ft* < 21.4 *k-ft* → *no additional intermediate diaphragms required*

SPAN 3

Maximum +M = 13.6 *k-ft*

Maximum –M = -17.4 *k-ft*

17.4 *k-ft* < 21.4 *k-ft* → *no intermediate diaphragms required*

5.4 DESIGN SUMMARY

The intermediate external diaphragm requirements for the bridge are summarized below in Table 5.1; a total of seven intermediate diaphragms were required for the entire bridge. Each of the seven diaphragms has the dimensions as shown in Figure 5.9 and member sizes as determined using the design axial forces in Figure 5.10. The member axial forces in the permanent diaphragm in span 2 due to the truck train are less than the design axial forces; it is not necessary to redesign for the in-service phase. The diaphragm that is installed at mid-span for the construction phase can remain in place, and the diaphragm-to-girder connections must be designed as fatigue connections.

Table 5.1 Intermediate External Diaphragms for Example Bridge

Span	Construction Phase	In-Service Phase
1	*0*	*0*
2	*4 at fifth points (min.)*	*1 at midspan*
3	*3 at quarter points (min.)*	*0*

The requirement for an intermediate external diaphragm at the mid-span of span 2 as determined by the design procedure is based on conservative assumptions and simplifications of actual bridge behavior. For instance, in the completed bridge, the two girders do not act independently of each other; the slab ties the two girders together and plays a major role in restraining girder rotations. Therefore, the calculated girder rotations in section 5.3 are overestimated, and permanent intermediate external diaphragms would likely not be required in reality. This is discussed further in Chapter 6.

CHAPTER 6
Evaluation and Comparison of Design Method with Bridge K

6.1 INTRODUCTION

Data were recorded for the concrete deck pours on bridge K, as well as a live load test on bridge K after the concrete deck had hardened past its 28-day strength. Presented in this chapter are results from the pours and load test for two instrumented intermediate external diaphragms. In addition, those measured values are compared with the values that would be expected using the design procedure that is introduced in Chapter 4. The concrete deck pours were completed over a one-week period in March 2001, and the live load test was conducted on June 7, 2001.

6.2 DATA ACQUISITION SYSTEM

6.2.1 Description

Two intermediate external diaphragms were instrumented on Bridge K, both located in the center span. In addition, a total of eight top flange lateral braces and six individual girder cross sections were also instrumented, and temperatures were monitored at two separate locations inside the outer girder. Figure 6.1 shows the locations of the various instrumented members and cross-sections throughout the bridge. Refer to the figures in section 1.2 for the orientation of the bridge.

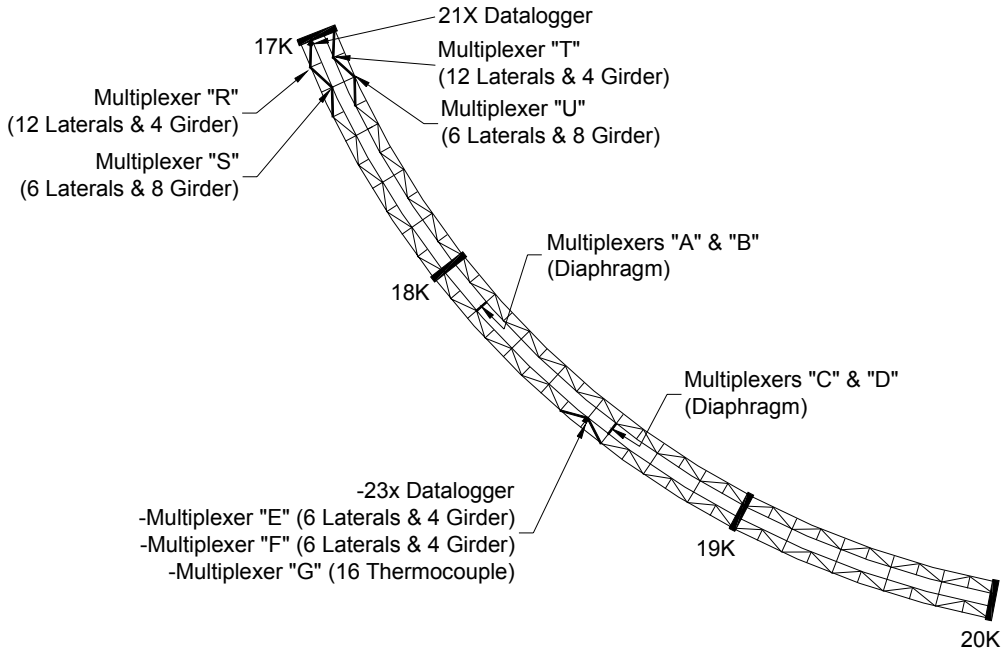

Figure 6.1 Instrumented Locations on Bridge K

(Cheplak, 2001)

As displayed in Figure 6.1, the data acquisition system on Bridge K consisted of two dataloggers, which were connected to a total of 11 multiplexers. There were a total of 136 strain gauges and 16 thermocouples to instrument the bridge. The methods for instrumenting the bridge and calculating forces and stresses, as well as specifications and recommendations for the data acquisition system, are presented in detail in Chapter 2 of Cheplak (2001). Additional information about the data acquisition system used in bridge K and the validity of the field results can be found in Cheplak et al (2002).

During each of the concrete pours, the data acquisition system collected strain gauge and thermocouple readings every 10 minutes. During the live load

test, the readings were collected every 10 seconds for an average of 12 data points per position. The data was either downloaded using a laptop directly connected to the datalogger or via modem.

6.2.2 Overview of Diaphragm Instrumentation on Bridge K

Two intermediate external diaphragms were instrumented on bridge K and monitored for the concrete deck pours and live load test. As shown in Figure 6.1, the two diaphragms were both located in the center span of bridge K. The instrumented diaphragm close to pier 18K was labeled #11, and the diaphragm near the mid-span was labeled #18. These diaphragms, as well as the other intermediate diaphragms that were installed on the bridge, were K-frames made out of angle members with the chevrons opening upward.

Each of the diaphragms contains five angle members and was assigned a number for identification purposes. An illustration of the member numbering system is shown in Figure 6.2.

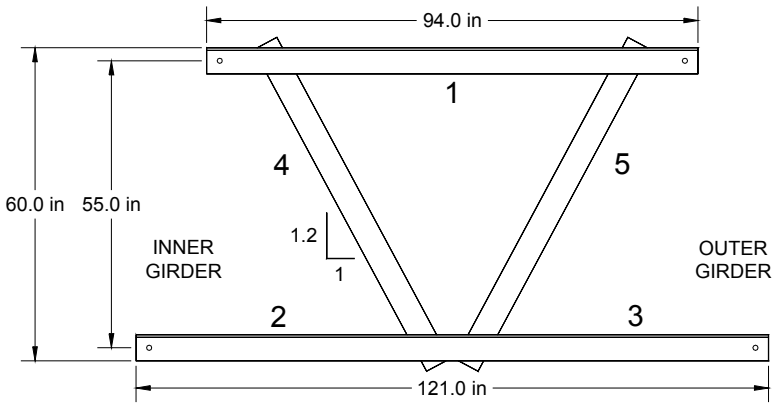

Figure 6.2 Member Numbering System

(Cheplak, 2001)

A picture of diaphragm #11 installed on the bridge can be seen in Figure 6.3. The two gray boxes shown are steel enclosures through which the strain gauges on the diaphragm were wired. Diaphragm #18 was instrumented in an identical fashion.

Figure 6.3 External Diaphragm #11 -- Looking South

(Cheplak, 2001)

6.3 BRIDGE K CONCRETE POURS

6.3.1 Description

The pouring sequence of Bridge K is illustrated in Figure 6.4. There were approximately two-and-a-half days in between the first two pours; however, pours 2 through 5 were conducted on three consecutive nights (refer to pour schedule in Table 6-1). Pours 4 and 5 were conducted on the same night.

The weather was generally not a factor during the pours; Pour 1 occurred in the morning with some cloud cover and temperatures in the mid 60s (°F). The other four pours were completed in the overnight hours with some cloud cover and temperatures in the 40s.

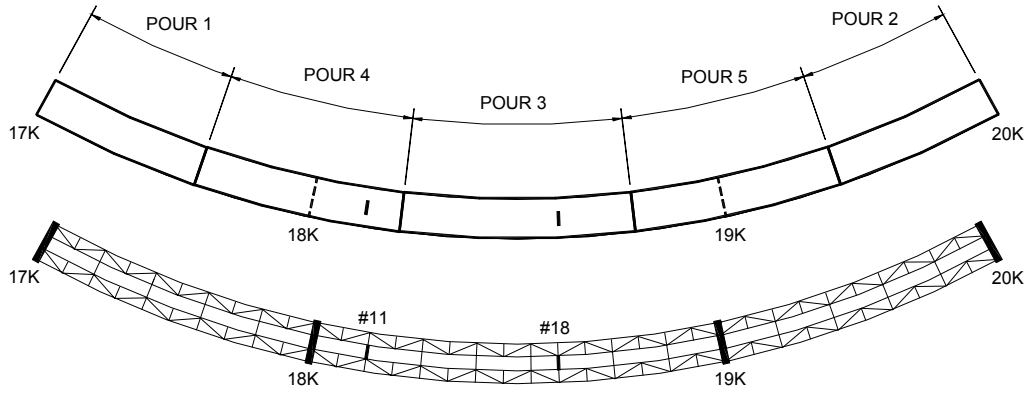

Figure 6.4 Bridge K Pouring Sequence

Table 6.1 Bridge K Pouring Schedule

POUR	START		END		DURATION
1	3/13/01	8:39 A.M.	3/13/01	11:10 A.M.	2 hr 31 min
2	3/16/01	12:27 A.M.	3/16/01	2:05 A.M.	1 hr 38 min
3	3/17/01	12:00 A.M.	3/17/01	3:20 A.M.	3 hr 20 min
4	3/17/01	10:30 P.M.	3/18/01	12:30 A.M.	2 hr 0 min
5	3/18/01	1:06 A.M.	3/18/01	2:54 A.M.	1 hr 48 min

ALL POURS ADVANCED TOWARDS 20K

6.3.2 Field Results for Diaphragms for Concrete Pours

The calculated values of axial forces in the instrumented locations and cross-sections were used to determine the measured change in axial force caused by each pour individually. This measured force is simply an absolute change in axial force; the values at the time immediately before the start time of each pour were subtracted from the values at the time immediately after the end time of each pour. For example, pour 1 began at 12:27 A.M. and ended at 2:05 A.M. The axial force starting values were taken at 12:20 A.M., and the ending values were taken at 2:10 A.M. In all cases, the data showed very little change before the start time and after the stop time.

The changes in axial force (kips) during the concrete pours for each diaphragm member are presented in Tables 6.2 (diaphragm #11) and 6.3 (diaphragm #18). A positive force change indicates tension, and a negative force change indicates compression. Refer to Figure 6.4 to relate the location of the pours with the corresponding changes in axial force in the diaphragm members. For example, diaphragm #18, which was near mid-span, was not affected greatly

by pours 1 and 2, which were at the ends of the bridge. Pour 3, however, was poured over diaphragm #18 and caused the most significant changes in axial force.

There is no field data for members 2 and 4 of diaphragm #18 because of a problem with a power cable. That problem was corrected before pour 3, and the system functioned normally for the remainder of the concrete pours and the live load test.

The total change in the diaphragm member forces is defined as the sum of the changes in each of the pours. This is presented because it most closely matches the theoretical worst case rotation that is described in section 4.3. The total change is not the change in force from the start of the first pour to the end of the last pour. During the time in between pours, the bridge components were loaded due to the normal daily temperature cycles; therefore, the measured axial force is not the same at the end of one pour and at the start of the next.

Table 6.2 Changes in Axial Force in Diaphragm #11 During Concrete Pours

External #11	Member 1	Member 2	Member 3	Member 4	Member 5
Change due to Pour 1	3.3	0.7	0.2	0.1	0.4
Change due to Pour 2	-0.2	0.0	-0.3	-0.8	0.4
Change due to Pour 3	0.8	-2.3	-0.8	1.9	-2.1
Change due to Pour 4	8.1	1.3	1.4	0.1	-0.1
Change due to Pour 5	-1.0	0.4	0.2	-0.3	0.2
Total Change	11.0	0.1	0.7	1.0	-1.2

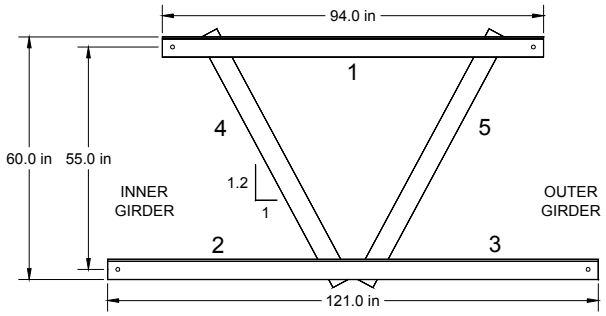

Figure 6.5 Member Numbering System

Table 6.3 Changes in Axial Force in Diaphragm #18 During Concrete Pours

External #18	Member 1	Member 2	Member 3	Member 4	Member 5
Change due to Pour 1	2.3	-----	0.4	-----	1.3
Change due to Pour 2	-1.6	-----	0.3	-----	-1.2
Change due to Pour 3	15.9	-0.5	-4.4	-6.8	8.3
Change due to Pour 4	-0.2	-0.2	-0.2	0.0	0.1
Change due to Pour 5	0.0	0.6	0.4	-0.2	-0.1
Total Change	16.4	-----	-3.5	-----	8.4

The results from tables 6.2 and 6.3 are also presented in bar charts, which can be found in the Appendix. A sample bar chart is presented in Figure 6.6. The forces for the member presented are small, even during the concrete pour that is directly over that diaphragm.

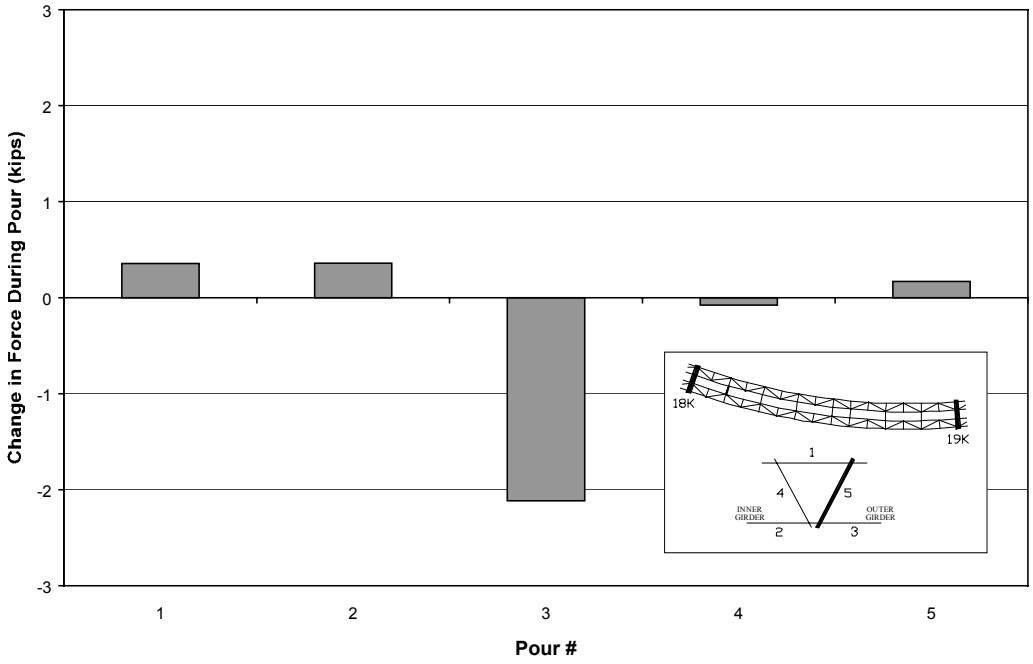

Figure 6.6 Diaphragm #11-5 During K Concrete Pours

6.3.3 Expected Forces in Diaphragms

In this section, the expected forces in the diaphragms that were calculated using the design procedure are compared with the actual forces that were measured on the bridge during the concrete pours. Recall that the assumed worst case torsional loading occurs when the bridge is fully covered with wet concrete. The expected forces in diaphragms #11 and #18 were calculated according to this

loading condition and the arrangement of intermediate external diaphragms on bridge K.

Span 18 of bridge K, which is illustrated in plan view in Figure 6.7, included both diaphragms #11 and #18. It has a nominal length of 242 feet and a radius of curvature of 572.96 feet. d_0 was calculated to be 12.73 feet.

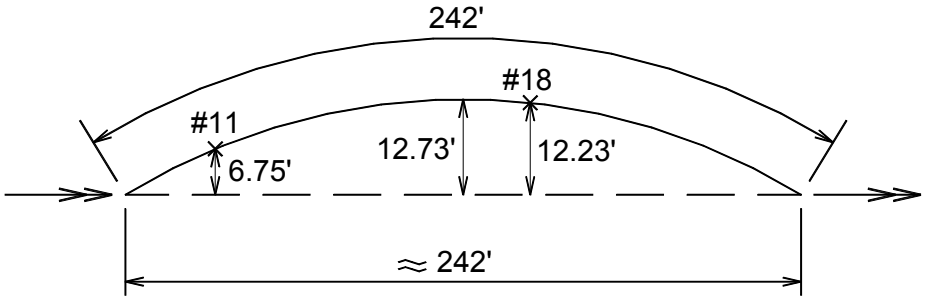

Figure 6.7 Plan View of Bridge K Span 18

The total dead load on the girders amounted to 3 kips per linear foot for the dead load of the concrete slab. The self-weight of the girders is not counted in this instance because at the time that the corresponding measurements were taken, the rotations due to the self-weight of the girder had already taken place. Half of the uniformly distributed load from the wet concrete was assigned to each girder. The uniformly distributed load and associated torque on each girder is illustrated in Figure 6.8.

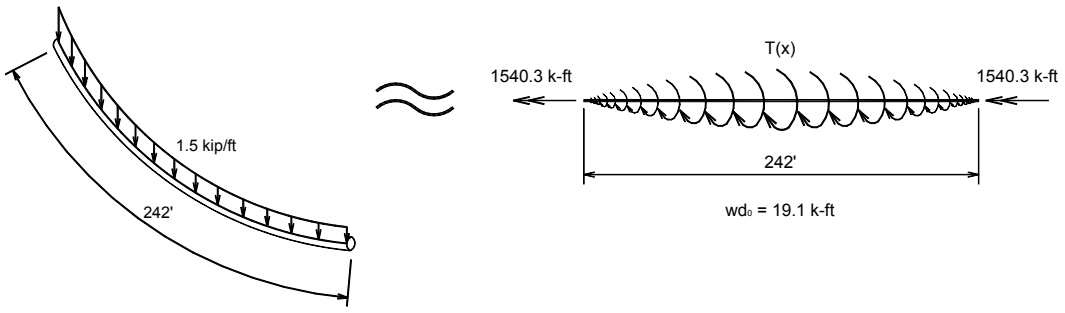

Figure 6.8 Total Dead Load on Bridge K Span 18

The torque distribution in span 18 was broken down using equation 2-3 to find the torque carried by diaphragms #11 and #18. The torque values for each girder at each diaphragm location are shown in Figure 6.9. The tributary widths for diaphragms #11 and #18 are shaded in the figure. The calculations for the expected torques transferred from each girder to diaphragms #11 and #18 are presented in Figures 6.10 and 6.11, respectively.

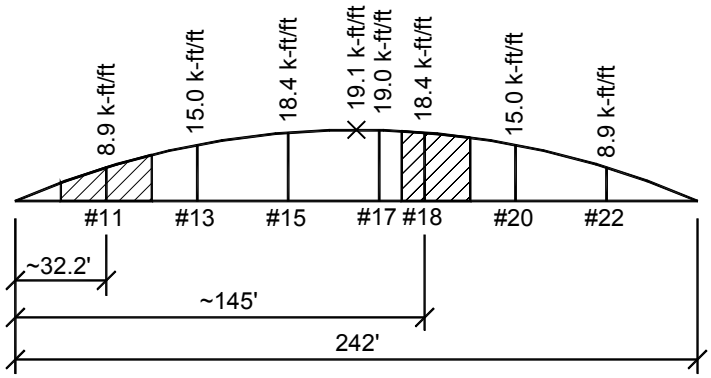

Figure 6.9 Torque at Intermediate External Diaphragms in Span 18

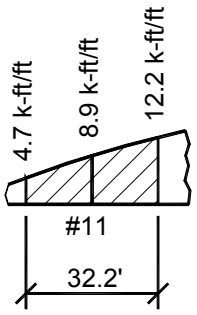

$$T = (32.2\ ft)(4.7\ k\text{-}ft/ft) + (2/3)(32.2\ ft)(12.2 - 4.7\ k\text{-}ft/ft) = 312.3\ k\text{-}ft$$

Figure 6.10 Torque From Each Girder on Diaphragm #11

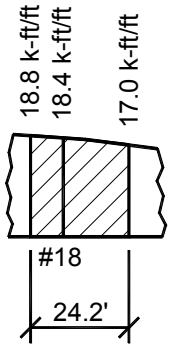

$$T = (24.2\ ft)(17.0\ k\text{-}ft/ft) + (2/3)(24.2\ ft)(18.8 - 17.0\ k\text{-}ft/ft) = 440.4\ k\text{-}ft$$

Figure 6.11 Torque From Each Girder on Diaphragm #18

The torques at diaphragms #11 and #18 from each girder were used to calculate the expected forces in the diaphragms for the assumed worst case torsional loading. Summaries of the expected forces are shown in Figures 6.12 and 6.13. Note: Figures 6.12 and 6.13 follow the same provisions as Figure 5.10.

Table 6.4 is a comparison of the expected worst case forces and the measured total changes in axial force for all of the pours. Also presented in Table 6.4 are predicted changes in axial force from finite element analyses of bridge K that were performed by Topkaya (2002). The finite element analytical model is described in detail in section 1.5 of Cheplak (2001).

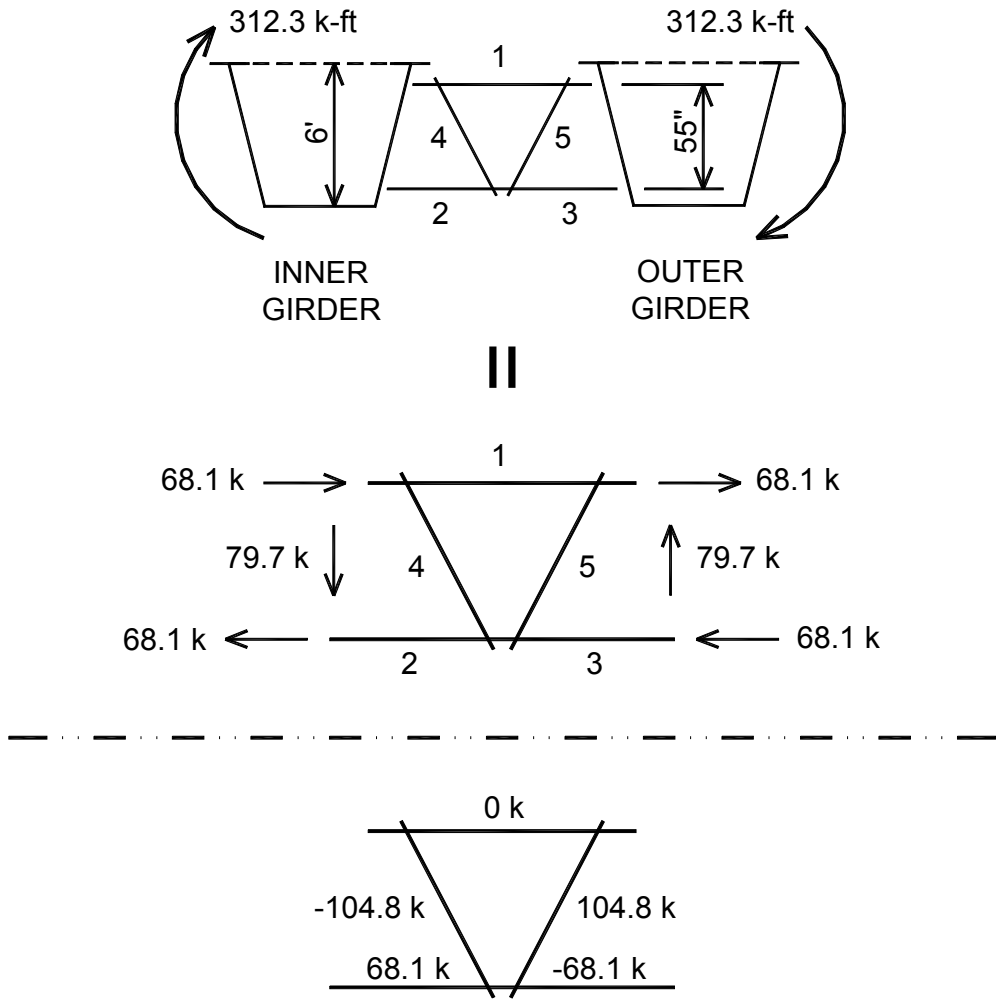

Figure 6.12 Expected Forces in Diaphragm #11 from Worst Case

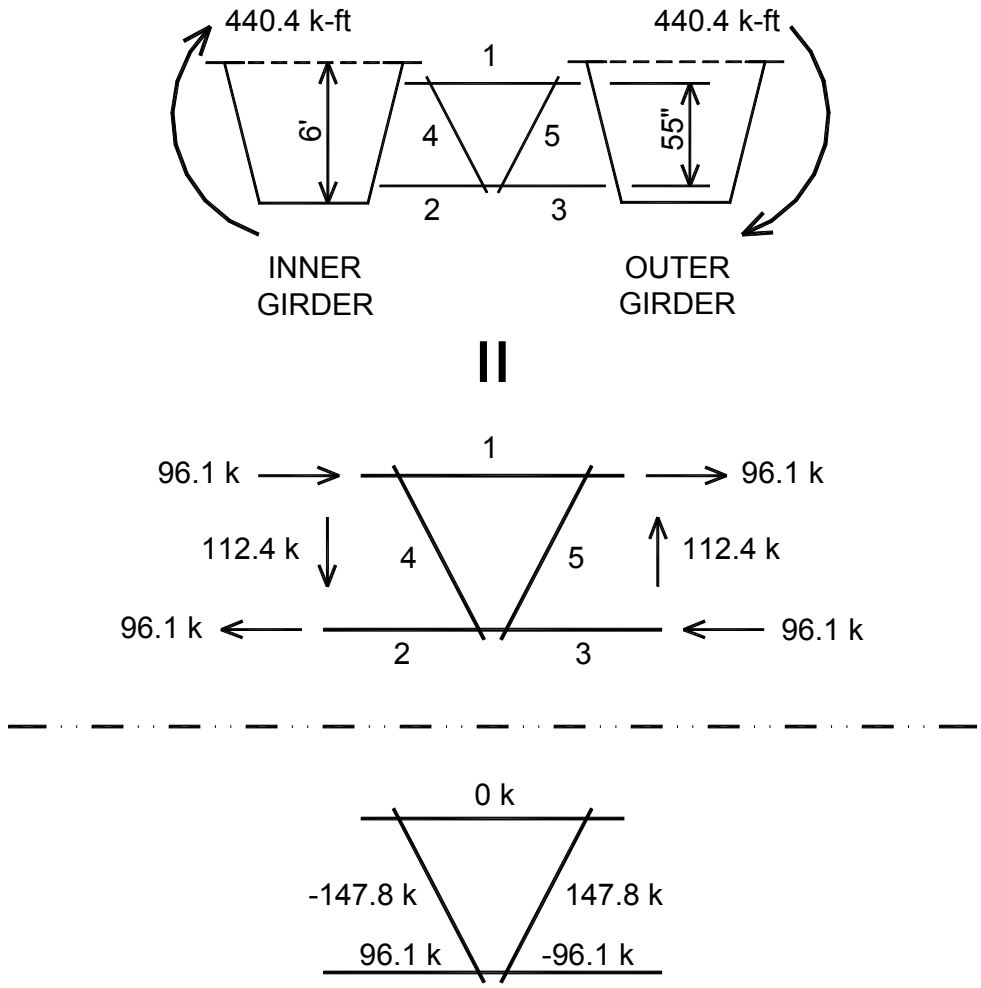

Figure 6.13 Expected Forces in Diaphragm #18 from Worst Case

Table 6.4 Changes in Axial Force (kips) due to K Concrete Pours

	Diaphragm #11			Diaphragm #18		
Member	**Meas.**	**Exp.**	**Pred.**	**Meas.**	**Exp.**	**Pred.**
1	11.0	0.0	4.7	16.4	0.0	8.7
2	0.1	68.1	-12.5	-----	96.1	12.4
3	0.7	-68.1	10.4	-3.5	-96.1	-16.5
4	1.0	-104.8	16.8	-----	-147.8	-21.2
5	-1.2	104.8	-16.8	8.4	147.8	21.2

Meas. = Measured force changes with data acquisition system on Bridge K

Exp. = Expected force changes from design procedure in Chapter 4

Pred. = Predicted force changes from finite element analysis (Topkaya, 2002)

For both diaphragms #11 and #18, there is little correlation between the measured and expected force changes. This is most likely because the design method assumed that only the diaphragms resisted the torsional loads. All of the measured changes in force in diaphragm #11 are very low, even in the top chord (stress = 2.3 ksi), which is much larger than any of the other members. Similarly, in diaphragm #18, the top chord experienced the largest amount of force change out of any of the five members (stress = 3.5 ksi).

With the exception of the top chords, the predicted force changes for each member from the finite element analysis are significantly larger than the measured force changes. They are larger most likely because the finite element analytical model ignored composite action in the bridge cross-section, and the diaphragm stiffness may have been overestimated by not correctly modeling the girder-to-diaphragm connection (Cheplak, 2001).

The expected force changes for both diaphragms are also significantly greater in magnitude then the measured force changes and are approximately five times greater than the predicted force changes (excluding the top chords). This is most likely of the assumption that the diaphragms resisted all of the torsional loads and that the girders had no effect.

It is uncertain why the forces in the top chords of both diaphragms #11 and #18 were so large relative to those of the diagonals and bottom chords. According to the truss analysis, the top chord should not have had any axial force as a result of the torsion in the girders. It is likely that these axial forces are a result of some other force condition, as the forces in the top chords did not have an effect on the forces in the other members of the diaphragms. A possible cause for this top chord axial force is unknown interactions between the girder-to-diaphragm connection. Figure 6.14 illustrates how forces transferred through the diaphragms would increase forces in the top chords only.

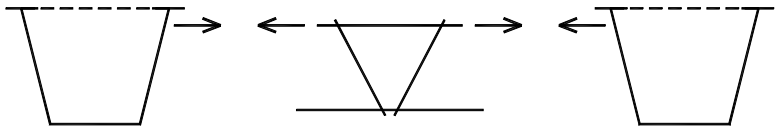

Figure 6.14 Forces Transferred to Top Chord

The largest forces in the top chords occurred during the pours directly above each of the respective diaphragms. As shown in Figure 6.4, diaphragm #11 was located near the end of pour 4, and diaphragm #18 was located approximately at the 2/3 point of pour 3. Figures 6.15 and 6.16 plot the force-time histories of the top chords of diaphragms #11 and #18, respectively, during the pour that resulted in the maximum axial force change for the member. It can be seen in Figure 6.15 that the change in axial force in the top chord of diaphragm #11

experienced significant increases as pour 4 progressed and passed over diaphragm #11 and was virtually unaffected by the air temperature at the bridge site. Similarly, it can be seen in Figure 6.16 that the change in axial force in the top chord of diaphragm #18 depended on the progress of pour 4 and that air temperature was also not a factor. During other pours, as indicated by Tables 6.2 and 6.3, the force-time histories for the top chords show little changes in axial force.

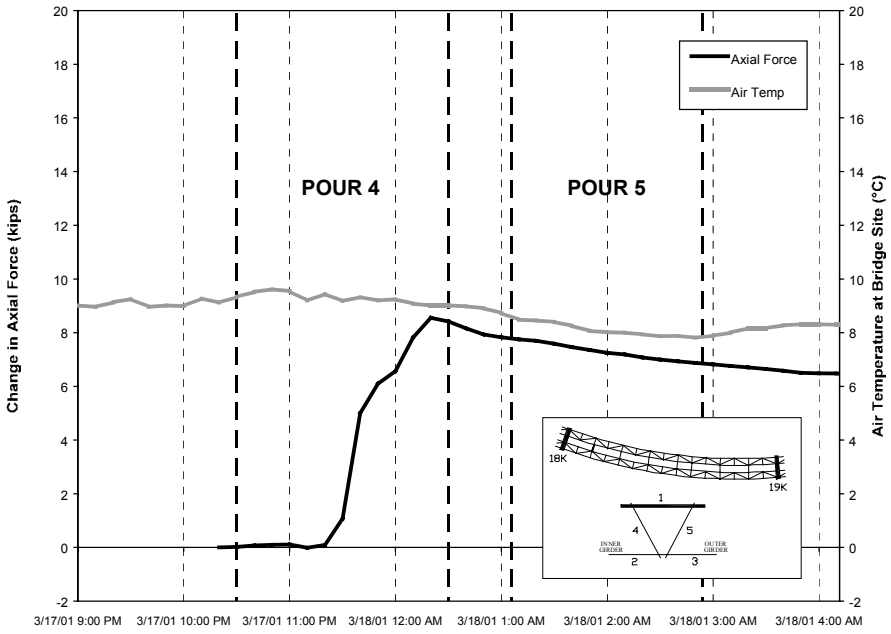

Figure 6.15 Top Chord in Diaphragm #11 During K Pours 4 & 5

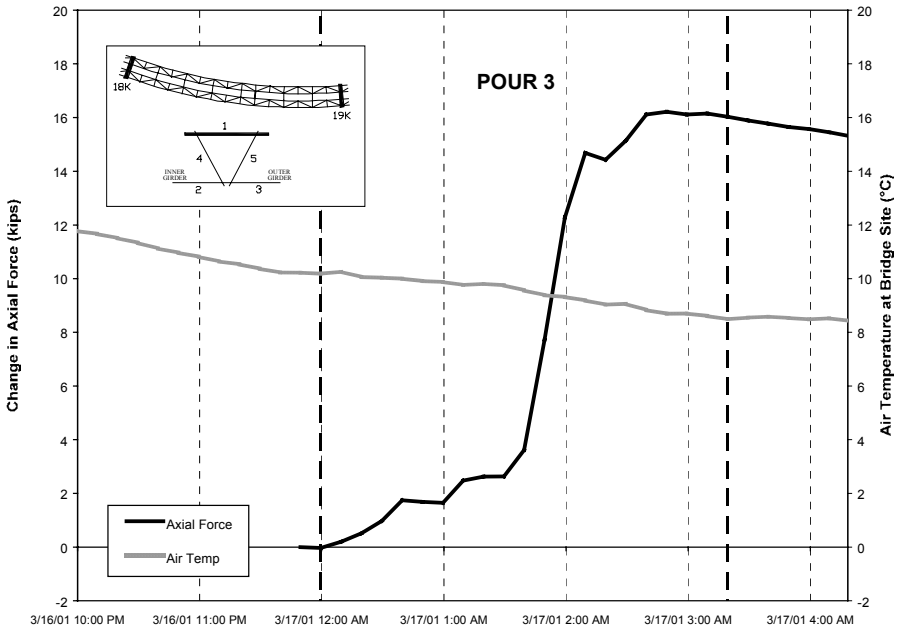

Figure 6.16 Top Chord in Diaphragm #18 During K Pour 3

Even though the measured top chord axial forces were high relative to the forces in the other members of the diaphragms, they did not cause any problems in the performance of the diaphragms. The axial forces in the top chord were very low (maximum stress = 3.3 ksi), and the member size chosen for the diaphragm was much more than adequate to carry this force.

6.3.4 Expected Girder Rotation

The largest girder rotation during the construction phase was expected at mid-span, where the torsional loads are the highest. The maximum expected rotation occurred between diaphragms #15 and #17. The torque diagram for this portion of the girder is shown in Figure 6.17.

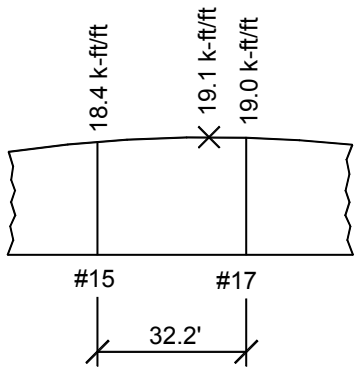

Figure 6.17 Torque at Mid-Span

For ease of calculations, the torque was assumed to be constant for the entire section. If the exact angle of twist were calculated by superimposing different cases, the resulting value would not be significantly lower and would occur close to the center of the section. It is acceptable in this case to use the conservative assumption of a constant torque in this portion of the span with the maximum angle of twist in the center.

The maximum angle of twist was calculated using equation 2-10:

$$\phi\left(\frac{L}{2}\right) = \frac{tL^2}{8GJ} \quad \rightarrow \quad \phi(16.1ft) = \frac{(19.1k - ft)(32.2ft)^2}{8(1{,}612{,}800ksf)(1.92ft^4)} = 0.00080rad$$

The maximum angle of twist was converted to vertical displacement at the tip of the top flange using equation 2-15:

$$\Delta = x_r\phi \quad \rightarrow \quad \Delta = (56in)(0.00080rad) = 0.045in$$

This calculated displacement is well below the maximum allowable amount (0.25 inches), as described in section 4.3.

The low expected girder rotation indicates that the diaphragm spacing is adequate, as the vertical displacement of the top flanges is less than the allowable amount. In fact, the calculated vertical displacement (a conservative value) was only 1/5 of the acceptable limit. It can be concluded that fewer intermediate external diaphragms were necessary to control the girder rotations in bridge K.

6.4 BRIDGE K LIVE LOAD TEST

6.4.1 Description

A live load test was conducted on bridge K on June 7, 2001, from 11:50 A.M. to 3:00 P.M. in order to monitor the response of the instrumented cross-sections when two overloaded TxDOT dumptrucks stopped at 30 different locations across the bridge. The 30 locations are illustrated in Figure 6.18.

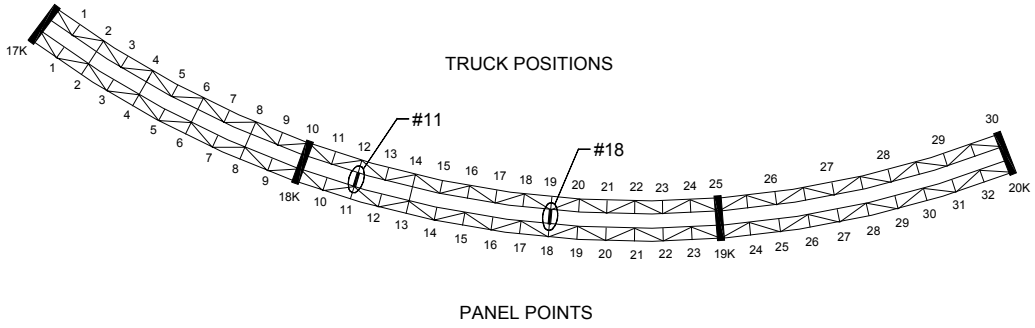

Figure 6.18 Live Load Test Truck Positions for Bridge K

From 11:50 A.M. to 1:15 P.M., the trucks moved over the outside girder of the bridge, and from 1:35 P.M. to 3:00 P.M., the trucks moved over the inside

girder. The trucks remained in each position for approximately two minutes in order to collect a large data sample for each location. A similar test was conducted on bridge Z on November 9, 2000, as reported by Cheplak (2001).

The two trucks were positioned back-to-back in order to generate the largest possible torsional response on the bridge, as shown in Figure 6.19. The combined axle weights of the trucks gave a total load of 88.5 kips. The trucks remained 40 inches away from the edge of the bridge deck for safety reasons.

Figure 6.19 Truck Positioning During K Live Load Test

In between the concrete pours and the live load test, some of the intermediate external diaphragms were removed from bridge K. Because most of the bridge was directly over the interstate, the diaphragms could only be taken

down when the highway was closed down to allow lift access. The contractor had very limited opportunities to close the highway, so the decision was made to remove all of the diaphragms over the highway, with the exception of instrumented diaphragm #18. The diaphragms that were not over the highway, including all of the diaphragms in span 17 and diaphragm #11, were left in place until after the live load test was completed. This was accounted for in the analysis and comparison of predicted and measured values. Figure 6.20 shows a plan view of bridge K with the external diaphragms that remained in place for the live load test.

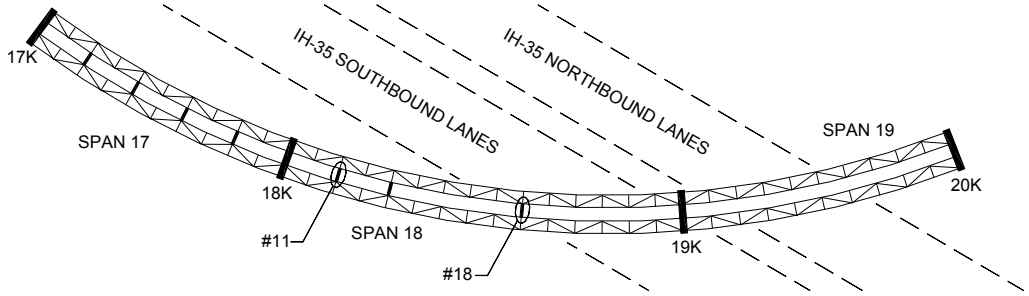

Figure 6.20 External Diaphragms In Place for K Live Load Test

6.4.2 Field Results for Diaphragms for Live Load Test

The values of axial force determined from the strain gauge data in the instrumented locations were used to create influence curves of axial force versus truck position. The axial forces at each position were calculated by averaging all of the values collected at that position. For example, the trucks were at outer girder position 6 during the live load test from approximately 12:10 P.M. until approximately 12:12 P.M. The axial forces presented for this position is the

average of all 12 readings (one reading each 10 seconds). In all cases, there was little scatter in the readings at each position.

Each truck run (outer and inner) was considered as a separate test. Because of temperature effects, the strain values were zeroed before each run when the dumptrucks were off the bridge. The temperature effects prevented the strain values from returning to zero at the end of each test.

All of the instrumented members experienced insignificant to minor temperature effects during the outer test. During the inner run, only the horizontal members of the diaphragms experienced any temperature effect; the diagonals were basically unaffected by the change in temperature. The top horizontal member in each diaphragm showed a minor effect, while there was a very large effect on the bottom horizontal members. The largest temperature effect recorded was in the bottom horizontal members of diaphragm #18. There were approximately 6 kips of axial force in these members due to temperature at the end of the inner truck run.

This temperature effect was accounted for by applying a linear temperature correction to all of the data from the live load test, as explained in section 5.3 of Cheplak (2001). The temperature-corrected data at any time during the test run were determined by linear interpolation. For example, the axial force due to temperature in member #18-2 at the final position of the inner test was -6.2 kips (the duration of the inner test was approximately 1.4 hours). This converts to -4.4 kips/hr. At the middle of test, approximately 0.7 hours into the test, the temperature correction applied was approximately +3.1 kips. A full plot of the axial force in member #18-2 during the inner girder truck run before and after temperature correction is shown in Figure 6.21 as an example.

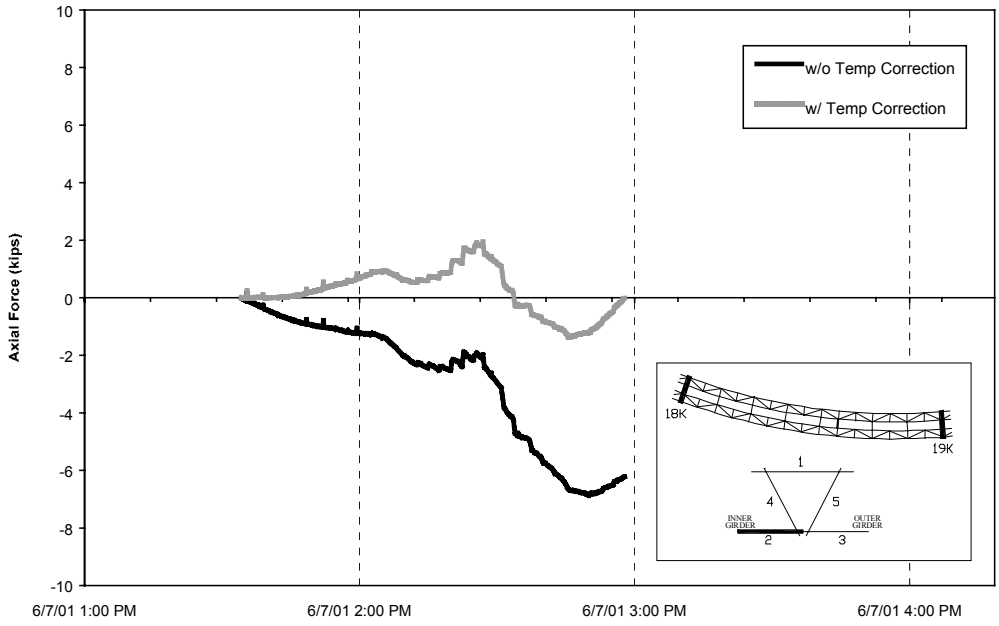

Figure 6.21 Temperature Correction for Diaphragm #18-2 During K Live Load Test Over Inner Girder

After the temperature corrections were made, influence curves were generated for each of the diaphragm members for both the outer and inner truck runs. These influence curves are available in the Appendix; a sample is shown in Figure 6.22. The values plotted in the influence curves, which are the average axial force values in the members with the trucks at each position along the bridge, are tabulated in the Appendix.

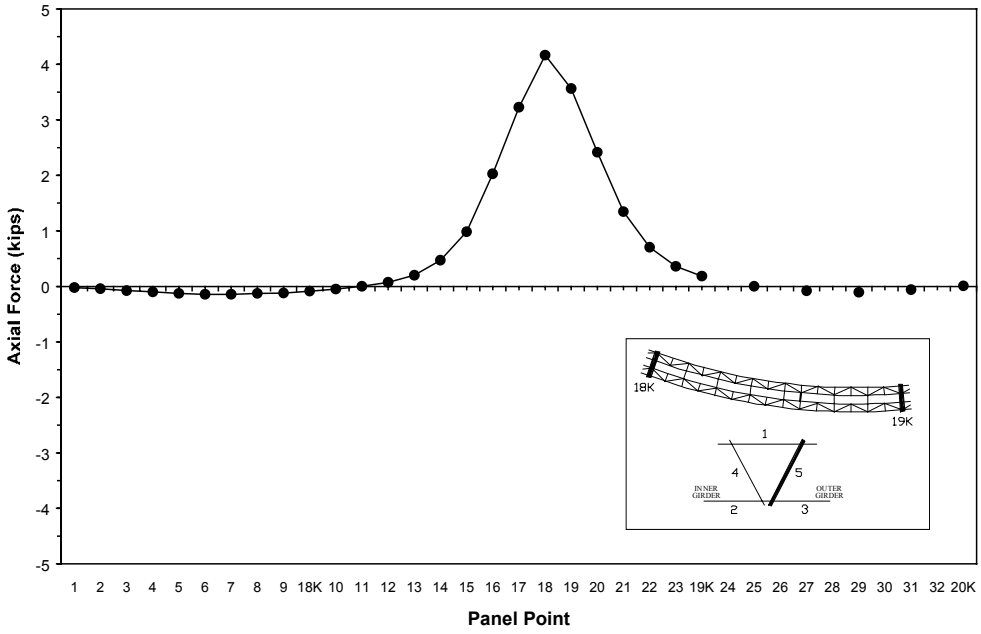

Figure 6.22 Axial Force in Diaphragm #18-5 During K Live Load Test Over Inner Girder

6.4.3 Expected Forces in Diaphragms

The expected forces in the diaphragms calculated using the design procedure were compared with the actual forces that were measured on the bridge during the live load test. In this case, the largest forces in each diaphragm occurred when the dumptrucks were located directly above that diaphragm. As shown in Figure 6.18, truck position #12 corresponded to diaphragm #11, and truck position #19 corresponded to diaphragm #18. Using this loading condition and the modified intermediate external diaphragm arrangement for the live load test (see Figure 6.20), the expected forces in diaphragms #11 and #18 were compared with the measured forces in order to determine the applicability of the design procedure to an in-service bridge.

During the run over the outer girder, the trucks are assumed only to have loaded the outer girder, and during the inner run, the trucks are assumed only to have loaded the inner girder. The torque generated by the dumptrucks on the girders had two components: a torque due to the bridge curvature and a torque due to the eccentricity of the load. In curved bridges, the eccentricity can add or reduce the total torque on the girder, depending on the direction of curvature.

The total load of the dumptrucks used for the live load test was 88.5 kips. Each truck had three axles: one underneath the cab and two in the rear. Because the dumptrucks were positioned back-to-back, the four rear axles of the two trucks were very close together (see Figure 6.19). The combined weight of these four axles (62.8 kips) was modeled as a point load in between the two trucks, resulting in a concentrated torque on the girder. At positions #12 and #19, this concentrated torque was assumed to be carried entirely by the diaphragm. In reality, the torque was distributed among the slab, girder, and diaphragm at these locations.

Figures 6.23 and 6.24 show the positioning of the load on the diaphragms from the dumptrucks during the live load test, and Figure 6.25 illustrates the concentrated torque due to curvature acting on the loaded girder. Figure 6.26 shows how the torque from the dumptrucks transfers to the diaphragms by idealizing the diaphragms as a straight-line member connecting the two trapezoidal girders. As shown in the Figure, only the loaded girder is assumed to rotate. This is a conservative idealization, as there would be some rotation in the non-loaded girder in an actual bridge because the roadway slab ties the two girders together. The reduction in moment at the left end in Figure 6.26 depends on the amount of rotation at that end and the flexibility of the girder.

Table 6.5 provides the appropriate *a*, *b*, and *d* values for diaphragms #11 and #18. Using the information presented in Figures 6.23 through 6.25 and Table

6.5, the torques from the dumptrucks during the live load test were calculated using the equations in Chapter 2.

The expected forces in the diaphragms as a result of these concentrated torques are presented in Figures 6.27 thru 6.30. During the outer truck runs, the eccentricity of the dumptrucks adds to the torque on the girder; the opposite is true during the inner truck runs. Note: Figures 6.27 thru 6.30 follow the same provisions as Figure 5.10.

The eccentricity from the positioning of the dumptrucks and the bridge curvature resulted in the following torques during the live load test:

Diaphragm #11: 62.8 *k-ft* x (5.87 *ft* + 0.833 *ft*) = 421 *k-ft* (outer run)

62.8 *k-ft* x (5.87 *ft* – 0.833 *ft*) = 316.3 *k-ft* (inner run)

Diaphragm #18: 62.8 *k-ft* x (12.23 *ft* + 0.833 *ft*) = 820.4 *k-ft* (outer run)

62.8 *k-ft* x (12.23 *ft* – 0.833 *ft*) = 715.7 *k-ft* (inner run)

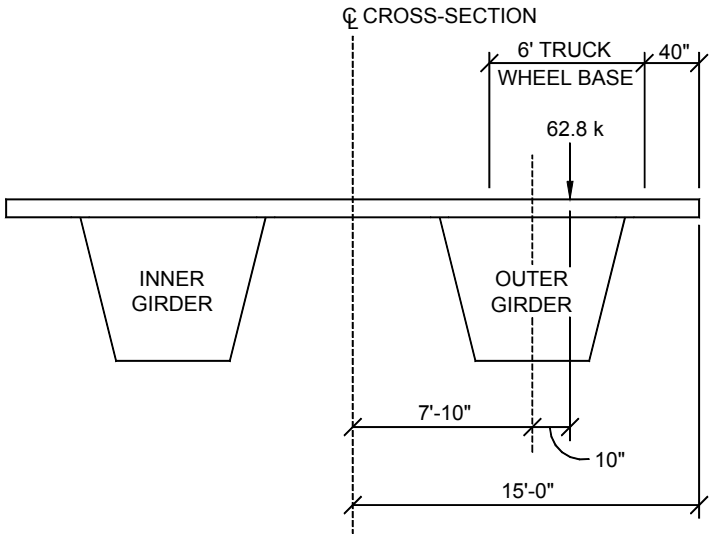

Figure 6.23 Live Load Test Setup on Bridge K (Outer Run)

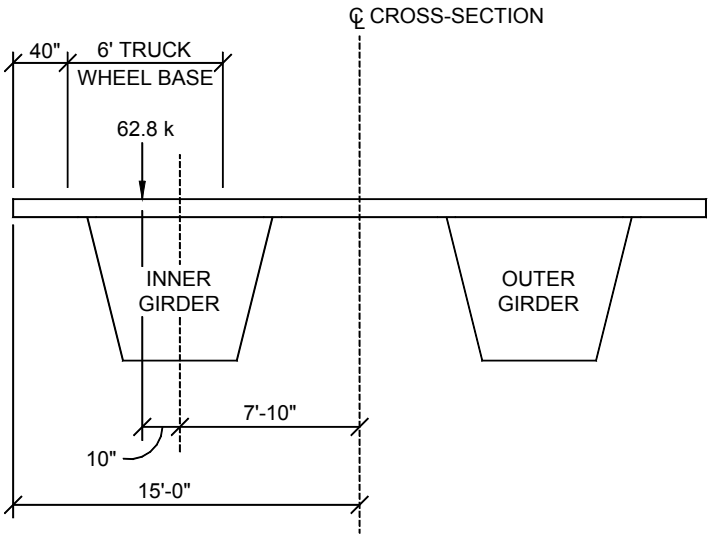

Figure 6.24 Live Load Test Setup on Bridge K (Inner Run)

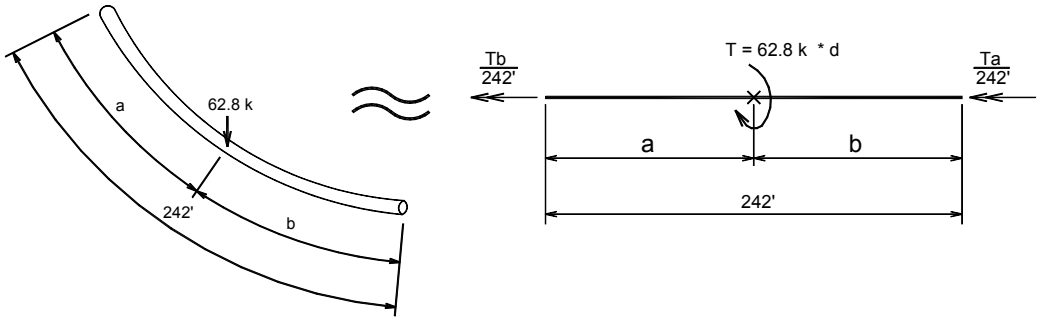

Figure 6.25 Concentrated Load from Dumptrucks

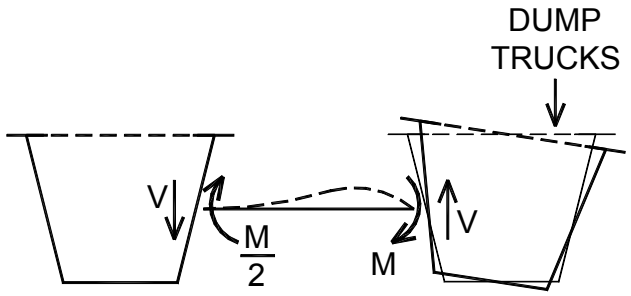

Figure 6.26 Torques Transferred to Diaphragms

Table 6.5 Locations of Instrumented Diaphragms

Diaphragm	a	b	d
#11	32.2 ft	209.8 ft	5.87 ft
#18	145 ft	97 ft	12.23 ft

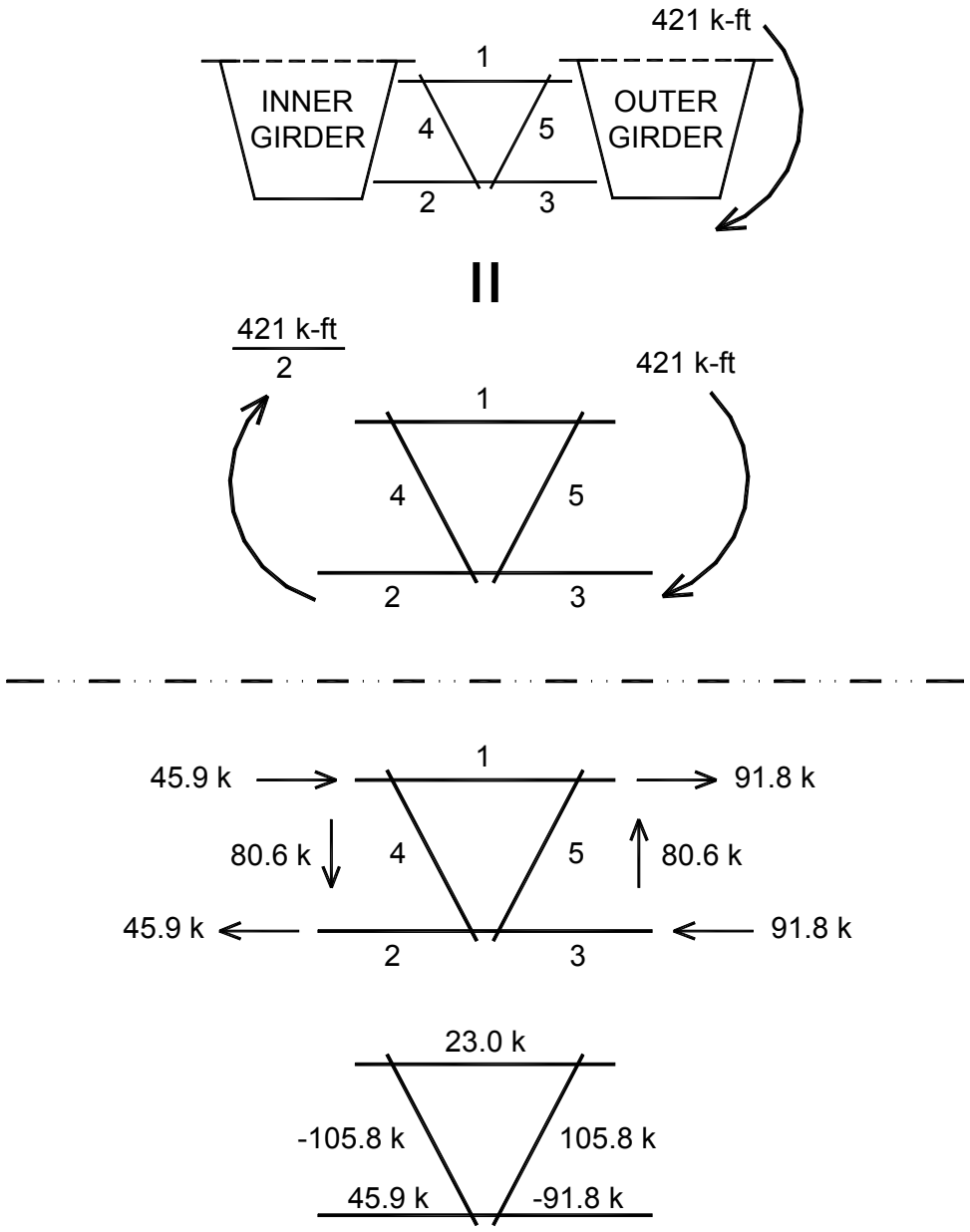

Figure 6.27 Expected Forces in Diaphragm #11 (Outer Run)

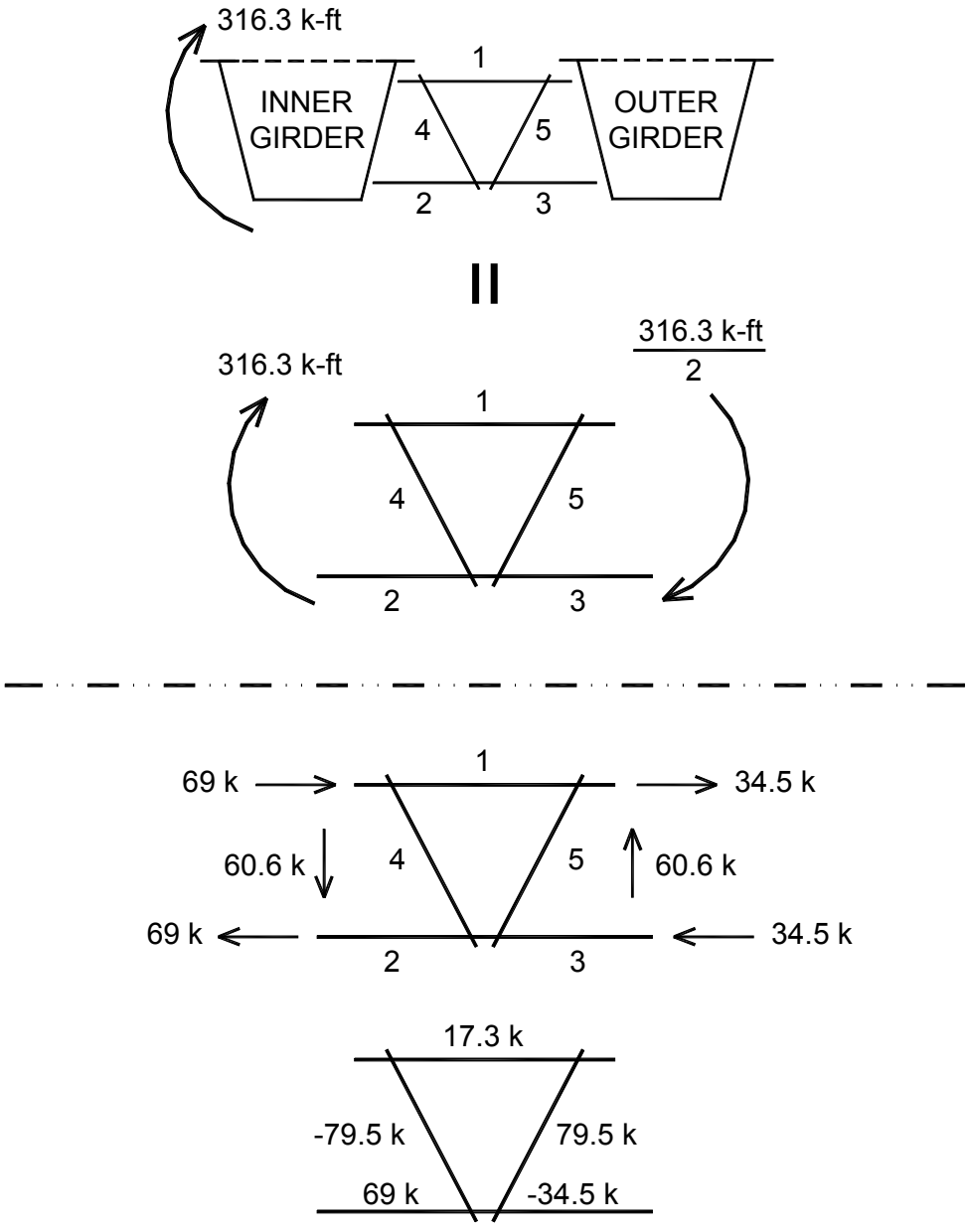

Figure 6.28 Expected Forces in Diaphragm #11 (Inner Run)

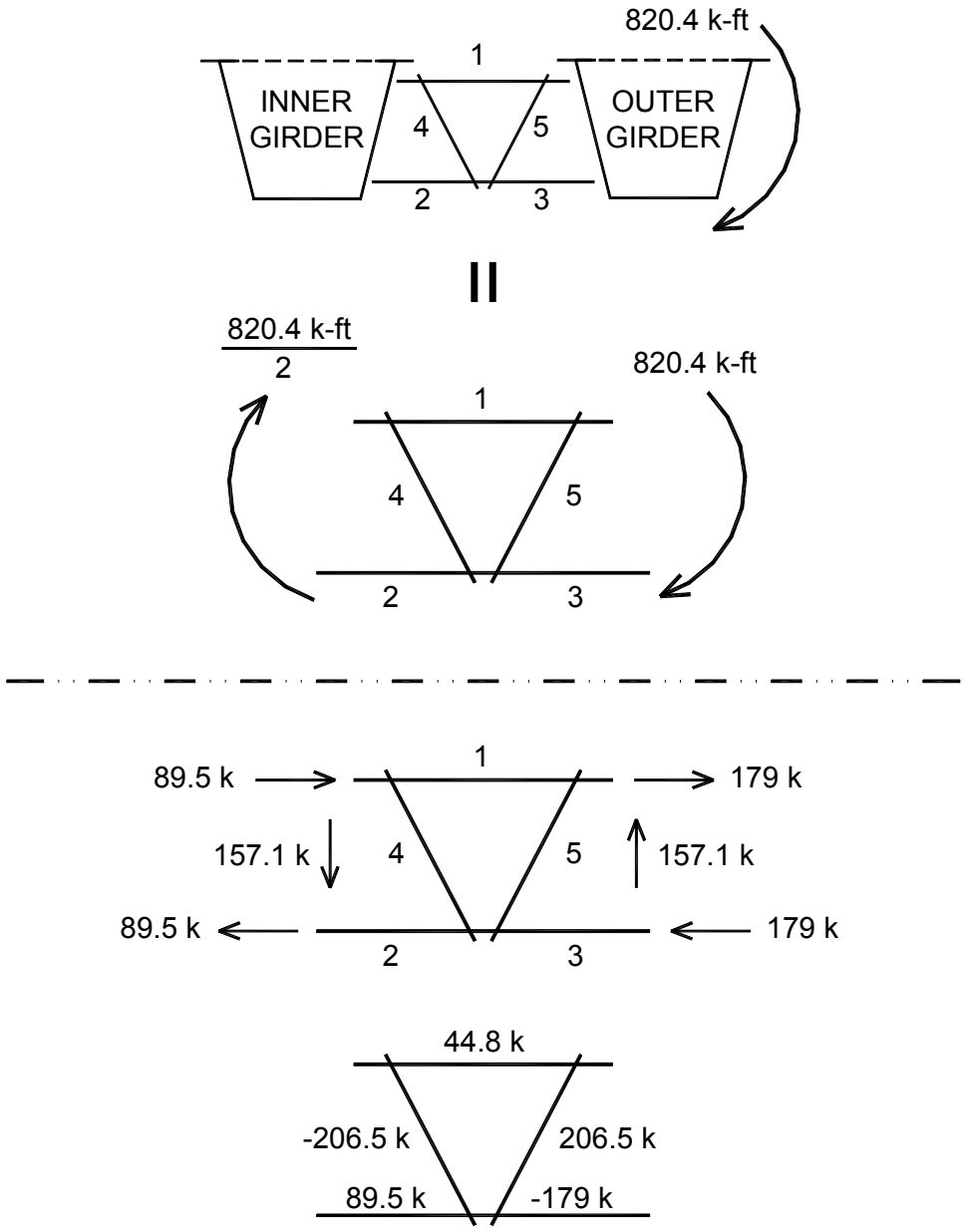

Figure 6.29 Expected Forces in Diaphragm #18 (Outer Run)

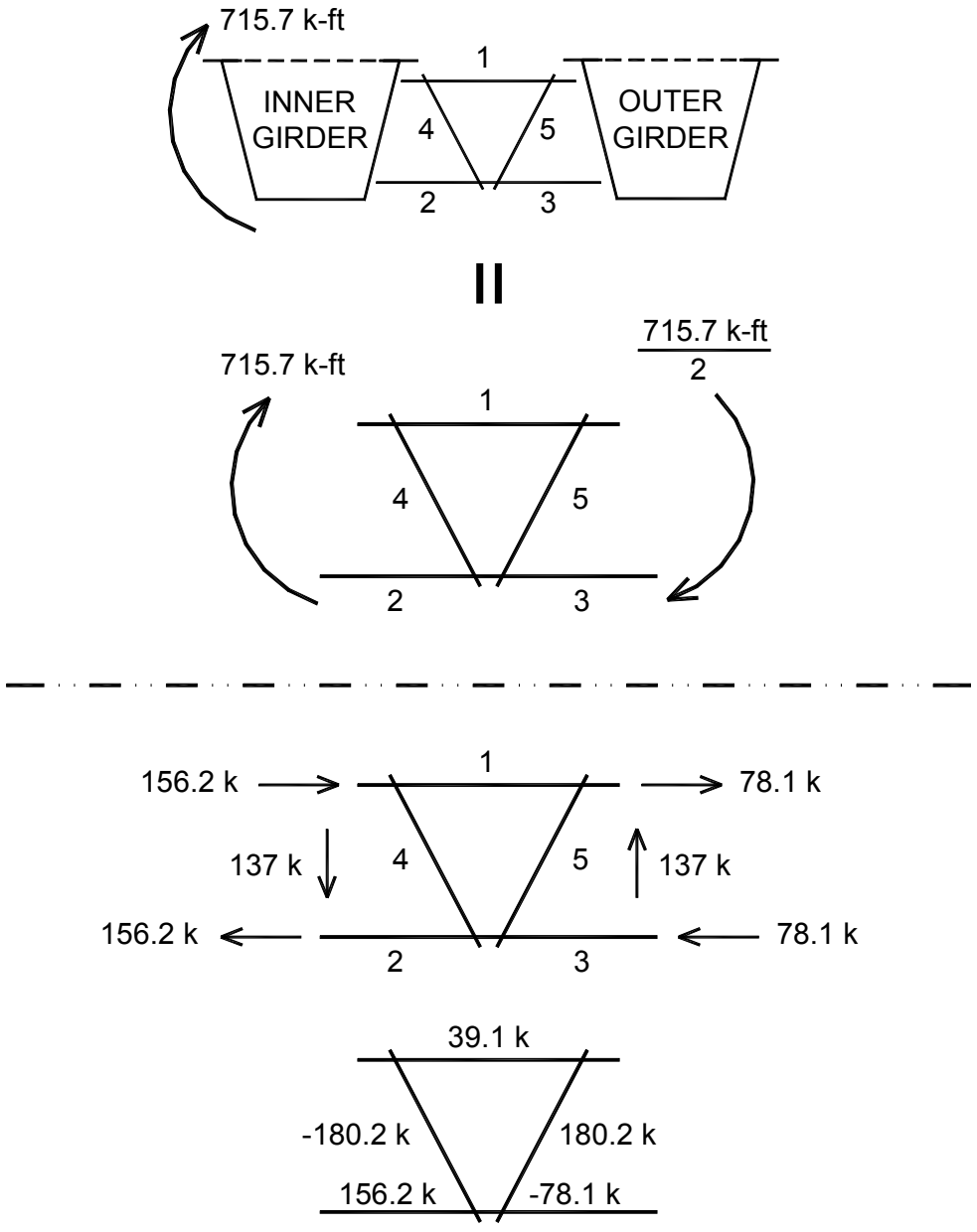

Figure 6.30 Expected Forces in Diaphragm #18 (Inner Run)

Table 6.6 Axial Force in Diaphragms During Live Load Test

(Trucks over Outer Girder)

	Trucks at Diaphragm #11			**Trucks at Diaphragm #18**		
Member	**Meas.**	**Exp.**	**Pred.**	**Meas.**	**Exp.**	**Pred.**
1	-0.6	23.0	0.1	-0.3	44.8	0.7
2	-0.7	45.9	-4.9	0.1	89.5	-6.3
3	0.7	-91.8	3.6	1.6	-179.0	4.5
4	1.9	-105.8	6.2	2.0	-206.5	7.9
5	-1.9	105.8	-6.2	-2.6	206.5	-7.9

Meas. = Measured forces with data acquisition system on Bridge K

Exp. = Expected forces from design procedure in Chapter 4

Pred. = Predicted force changes from finite element analysis (Topkaya, 2002)

Table 6.7 Axial Force in Diaphragms During Live Load Test

(Trucks over Inner Girder)

	Trucks at Diaphragm #11			Trucks at Diaphragm #18		
Member	**Meas.**	**Exp.**	**Pred.**	**Meas.**	**Exp.**	**Pred.**
1	-0.1	17.3	0.2	-0.1	39.1	0.9
2	1.5	69.0	5.4	1.8	156.2	8.9
3	0.0	-34.5	-3.9	-0.1	-78.1	-6.4
4	-2.0	-79.5	-6.8	-3.2	-180.2	-11.2
5	2.1	79.5	6.8	4.2	180.2	11.2

Overall, the expected forces in the diaphragm during the live load test calculated using the design procedure in Chapter 4 greatly overestimated the actual forces on the bridge. Additionally, the expected forces are in the opposite direction as the measured and predicted forces during the outer run of the live load test. The differences are most likely due to composite action in between the girders and the slab and also because the conservative assumption was made that the girders in bridge K acted separately when loaded with the dumptrucks. This apparently did not occur, as the slab tied the two girders together and provided significant stiffness that in turn, reduced the effect on the external diaphragms.

Furthermore, the expected forces in Tables 6.6 and 6.7 assume that the diaphragm is taking all of the torque from the dumptrucks. In actuality, some of the torque also goes into both the slab and the girder. Diaphragm #11, which was close to a support, experienced smaller forces than diaphragm #18, which was

near mid-span. This is an indicator of composite action within the bridge cross-section.

The response of the intermediate external diaphragms during the live load test appears to have been dominated by differential displacement between the two girders instead of torsional moments from the dumptrucks. During the live load test, the loaded girder deflects while the other girder does not, and the resulting differential displacement induces axial forces in the diaphragms. The directions of these forces for displacement in both the outer and inner girders are shown in Figures 6.31 and 6.32, respectively. The directions of the forces shown, which ignore the effect of the slab, are the same as the directions of both the measured and predicted forces that are presented in Tables 6.6 and 6.7. The small forces measured in the diaphragms during the live load test (maximum stress = 0.9 ksi) indicate that the differential displacement in the girders was very low. This was expected because of the large stiffness of the composite bridge cross-section comprised of the two girders and roadway slab.

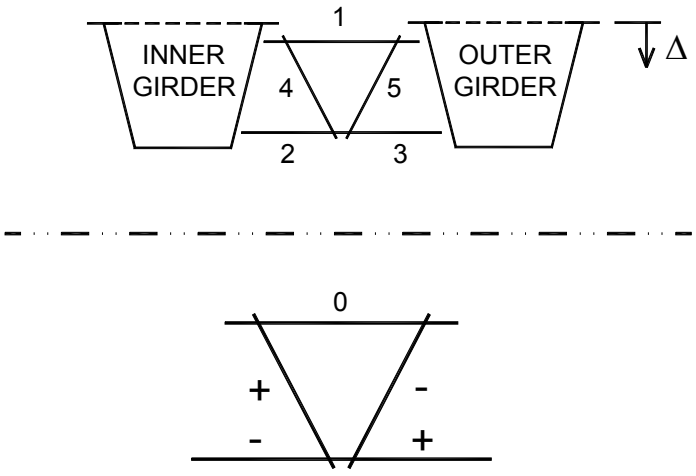

Figure 6.31 Axial Forces due to Deflection of Outer Girder

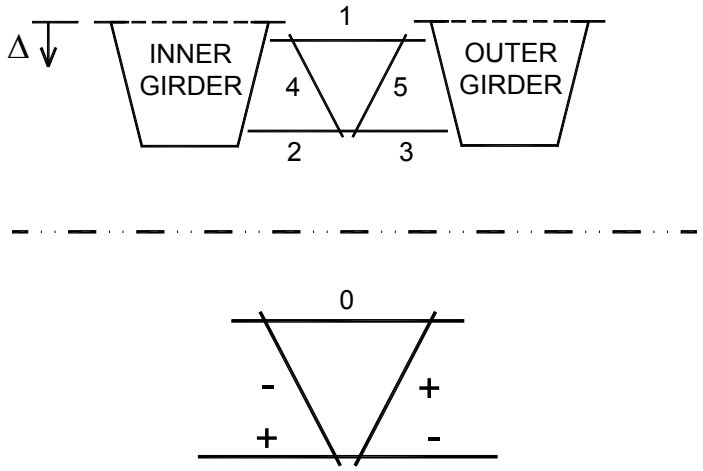

Figure 6.32 Axial Forces due to Deflection of Inner Girder

The predicted forces for each member from the finite element analysis correlated well with the actual forces. This is because the finite element analytical model included the effect of the slab and interaction between the two girders. However, difficulty in modeling the girder-to-diaphragm connection resulted in the predicted forces being three to four times greater than the actual forces.

6.4.4 Expected Girder Rotation

The largest girder rotation during the load test was expected with the dumptrucks positioned midway between two intermediate external diaphragms. Recall that some of the diaphragms in span 18 were removed before the live load test occurred (see Figure 6.15). The longest distance in between diaphragms was

from diaphragm #18 to pier 19K: 97 feet. The girder torsional stiffness was significantly increased by the addition of the slab (316,000 in^4 vs. 40,000 in^4).

The maximum angle of twist was calculated using equation 2-8:

$$\phi(a) = \frac{Tab}{GJL} \rightarrow \phi(48.5\,ft) = \frac{(53.2k - ft)(48.5\,ft)(48.5\,ft)}{(1{,}612{,}800ksf)(15.24\,ft^4)(97\,ft)} = 5.25\times10^{-5}\,rad \quad (1)$$

$$\phi(a) = \frac{Pdab}{GJL} \rightarrow \phi(48.5\,ft) = \frac{(62.8k)(8.16\,ft)(48.5\,ft)(48.5\,ft)}{(1{,}612{,}800ksf)(15.24\,ft^4)(97\,ft)} = 0.00051rad \quad (2)$$

(1) rotation in girder due to eccentricity of dumptrucks

(2) rotation in girder due to bridge curvature

total rotation = (1) + (2) = 0.00056 *rad*

The maximum angle of twist was converted to vertical displacement in the top flange using equation 2-15:

$\Delta = x_r\phi \rightarrow \Delta = (46in)(0.00056rad) = 0.03in$

The maximum moment generated from this calculated displacement using the method described in Chapter 3 is well below the ultimate moment capacity of the slab.

The girder rotation was also checked with the dumptrucks at mid-span, which was in between diaphragms #13 and #18. These diaphragms were 80.6 ft apart and were in the central region of the span (see Figure 6.15).

The maximum angle of twist was calculated using equation 2-8:

$$\phi(a) = \frac{Tab}{GJL} \rightarrow \phi(56.6\,ft) = \frac{(53.2k - ft)(56.6\,ft)(24\,ft)}{(1{,}612{,}800ksf)(15.24\,ft^4)(80.6\,ft)} = 3.65\times10^{-5}\,rad \quad (1)$$

$$\phi(a) = \frac{Pdab}{GJL} \rightarrow \phi(56.6\,ft) = \frac{(62.8k)(12.73\,ft)(56.6\,ft)(24\,ft)}{(1{,}612{,}800ksf)(15.24\,ft^4)(97\,ft)} = 0.00046rad \quad (2)$$

(1) rotation in girder due to eccentricity of dumptrucks

(2) rotation in girder due to bridge curvature

total rotation = (1) + (2) = 0.00049 *rad*

The maximum angle of twist was converted to vertical displacement in the top flange using equation 2-15:

$\Delta = x_r\phi \rightarrow \Delta = (46in)(0.00049rad) = 0.02in$

This calculated displacement is less than the amount in between diaphragm #18 and pier 19K; therefore, the maximum moment in the slab is lower, as well.

The fact that the expected girder rotations during the live load test were so small even with the heavy load from the dumptrucks and using the conservative assumption that the slab has no effect indicates that the actual rotations would be much smaller. The calculated rotations resulted in moments that did not even reach the cracking moment in the slab. Because of this, bridge K is expected to be able to handle large torques without failure of the slab in the final state with all of the intermediate diaphragms removed.

6.5 SUMMARY

The design procedure presented in Chapter 4 demonstrated limited applicability to an actual bridge in service (bridge K). The design procedure proved to be very conservative for the construction phase, as it provided diaphragm member design forces that were significantly larger than the actual member forces that were caused by the concrete deck pours. This is most likely because the design method assumed that only the diaphragms resisted the torsional loads and that the girders had no effect. In addition, the design procedure ignored composite action during the concrete pours. Information about composite action during concrete deck pours is presented by Topkaya (2002).

Forces calculated using the design procedure did not relate well with measured or predicted forces during the live load test; therefore, the applicability of the design procedure to in-service bridges is not certain. Although the design procedure ignores the effect of the slab in increasing stiffness and strength of the bridge cross-section and treats each girder as if it is acting separately and independently, the behavior of the slab due to live load appears to dominate the actual overall bridge response to live loads. Including the effect of the slab (i.e. modeling the slab with elastic supports) requires a more sophisticated analysis of the bridge, which is beyond the scope of this study.

In summary, it is difficult to accurately predict forces in the diaphragms using the design procedure. This uncertainty should be taken into account when selecting member sizes for intermediate external diaphragms in future bridges. Regardless, the diaphragms are not likely to experience very large forces during both the construction and in-service phases. It is important to minimize the number of intermediate external diaphragms used in the construction of a bridge of this type because of their high cost of installation and removal.

CHAPTER 7
Summary and Conclusions

7.1 SUMMARY

A design method was developed for intermediate external diaphragms for curved steel trapezoidal box girder bridges from a study of torsion in curved girders and its effect on twin-trapezoidal girder bridge systems. The design method was evaluated by comparing results with a highway bridge in Austin, Texas, that was opened to traffic in September 2001. Two intermediate external diaphragms on the bridge were instrumented with strain gauges and monitored during the concrete deck pours and a live load test after the deck had hardened. The live load test was conducted with two TxDOT dumptrucks that were placed at 30 different positions on the bridge deck on both the inner and outer portions of the curve.

7.2 DESIGN PROCEDURE

The design concept is to design the intermediate external diaphragms to resist girder rotations caused by dead loads during the construction phase. The bracing configuration and member sizes are selected based on practical considerations. The maximum spacing of the intermediate diaphragms is limited by the maximum allowable girder rotation, which is a function of the girder size.

The bridge is then checked for rotations due to the worst case load in the in-service phase (one AASHTO truck train per girder at the location on the slab where it will cause the largest torsional loads on the girder) with no intermediate diaphragms. If the rotations in the girders do not exceed the allowable girder

rotation, then no permanent intermediate external diaphragms are required. The allowable girder rotations are limited by the moment capacity in the slab. Typically, the bridge cross-section is significantly stiff with respect to torsion in the final state, and the bridge does not require permanent intermediate diaphragms.

Summary of Design Procedure:

I. Design for Construction Phase:

1. Girder Properties:

- $$t^* = \left(\frac{E}{G}\right)\frac{ab}{\frac{d^3}{A_d} + \frac{a^3}{3}\left(\frac{1}{A_0} + \frac{1}{A_u}\right)}$$ **(2-1)**

- $$A_0 = \frac{1}{2}(b_1 + b_3)h$$ **(2-4)**

- $$J = \frac{4A_0^2}{\sum(b_i / t_i)}$$ **(2-5)**

2. Rotation Due to Dead Loads:

- $$d_0 = R\left[1 - \sin\left(90° - \frac{\alpha}{2}\right)\right]$$ **(2-2)**

- $$\phi_{\max} = \phi\left(\frac{L}{2}\right) = \frac{7wd_0L^2}{72GJ}$$ **(2-12)**

3. Required Number of Intermediate Diaphragms:

- $\phi_{\max} = \frac{¼}{x_r} = \frac{7wd_0L^2}{72GJ}$
- Solve for L to determine the maximum spacing.

4. Standard Diaphragm:

- Determine the diaphragm with the largest torque from the girder torsional load diagram
- Determine the member design forces with an appropriate factor-of-safety
- Select bracing configuration and size members

II. Check Bridge In Service:

1. Rotation Due to Live Loads:

- Calculate rotations in girders caused by worst case live load (truck train) using appropriate angle of twist (ϕ) formulas in Section 2.5.
- $\Delta = x_r\phi$ **(2-15)**

2. Evaluate Concrete Deck

- Calculate moments per foot of deck using appropriate moment cases in Chapter 3
- Calculate ultimate moment capacity per foot of deck
- If moments in deck are less than ultimate moment capacity, no intermediate external diaphragms are needed in the final state

7.3 EVALUATION OF DESIGN PROCEDURE

Overall, the design procedure exhibited limited applicability to bridge K, which indicates that it is somewhat applicable to other curved steel trapezoidal box girder bridges. Expected force changes due to the concrete deck pours on bridge K were significantly larger than the actual member forces, demonstrating the conservative nature of the design procedure. The expected rotations in the girders due to the dead loads, which neglected the effect of composite action with the slab, were small relative to the maximum allowable rotation, therefore suggesting that bridge K could have been successfully built with fewer temporary intermediate external diaphragms.

Expected forces from the live load case did not did not correlate well with the measured forces from the same loading condition. The slab plays a significant role in the bridge response to live loads and would have to be included using a more rigorous analysis in order to achieve greater accuracy. The measured diaphragm member forces on bridge K were small (maximum stress = 0.9 ksi), thus indicating the substantial effect of the slab in reducing girder rotations due to live loads. In addition, expected rotations during the live load test were small even without the help of the slab. In this capacity, the design method was able to provide support for the decision made by TxDOT engineers to remove all of the temporary intermediate external diaphragms on bridge K. Based on the analysis, it is expected that bridge K is able to handle large torques from the worst case live load without failure of the slab.

APPENDIX A

Slab Moment Cases

Case 1: Two Equal and Opposite Support Displacements

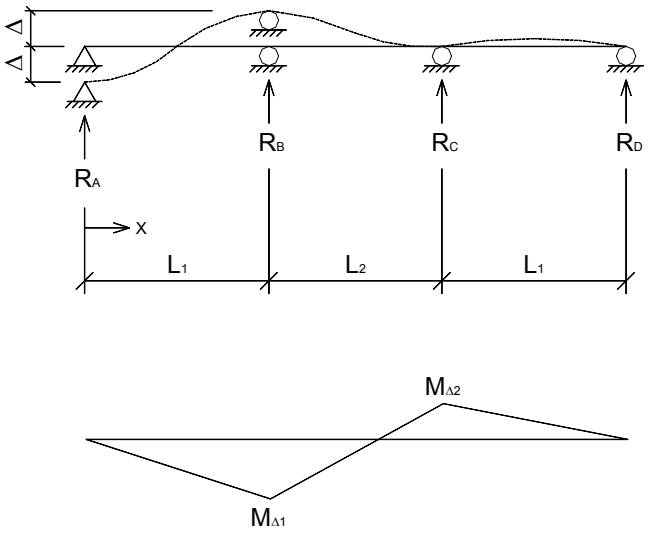

Figure A.1 Case 1

$$M_{\Delta 1} = \frac{2EI}{L_2}\left(\frac{3\Delta}{L_2} + 2d_2 + d_3\right) \qquad M_{\Delta 2} = \frac{-2EI}{L_1}\left(2d_3 + d_4\right)$$

$$R_A = \frac{-M_{\Delta 1}}{L_1} \qquad R_D = \frac{M_{\Delta 2}}{L_1}$$

$$R_B = -R_A + \frac{M_{\Delta 1} + M_{\Delta 2}}{L_2} \qquad R_C = -R_D - \frac{M_{\Delta 1} + M_{\Delta 2}}{L_2}$$

$$0 \le x < L_1: \qquad M = \frac{M_{\Delta 1}}{L_1} = -R_A x$$

$$L_1 \le x < L_1 + L_2: \qquad M = \left(\frac{M_{\Delta 1} + M_{\Delta 2}}{L_2}\right)\left(x - L_1\right) - M_{\Delta 1}$$

$$L_1 + L_2 \le x \le 2L_1 + L_2: \; M = -\frac{M_{\Delta 2}}{L_1}\left[x - \left(L_1 + L_2\right)\right] + M_{\Delta 2} = R_D\left[x - \left(L_1 + L_2\right)\right] - M_{\Delta 2}$$

$$d_1 = -\frac{d_2}{2} + \frac{3\Delta}{L_1} \qquad d_2 = \frac{6\Delta A}{B} - \left[\frac{\dfrac{12\Delta}{L_2^3}\left(\dfrac{2L_2 A}{B} + 1\right)}{\dfrac{4}{L_2^2 B} - B}\right]$$

$$d_3 = \frac{\dfrac{6\Delta}{L_2^2}\left(\dfrac{2L_2 A}{B} + 1\right)}{\dfrac{4}{L_2^2 B} - B} \qquad d_4 = -\frac{d_3}{2}$$

$$A = \frac{1}{L_1^2} - \frac{1}{L_2^2} \qquad B = \frac{3}{L_1} + \frac{4}{L_2}$$

Case 2: Pair of Equal and Opposite Support Displacements (Antisymmetric)

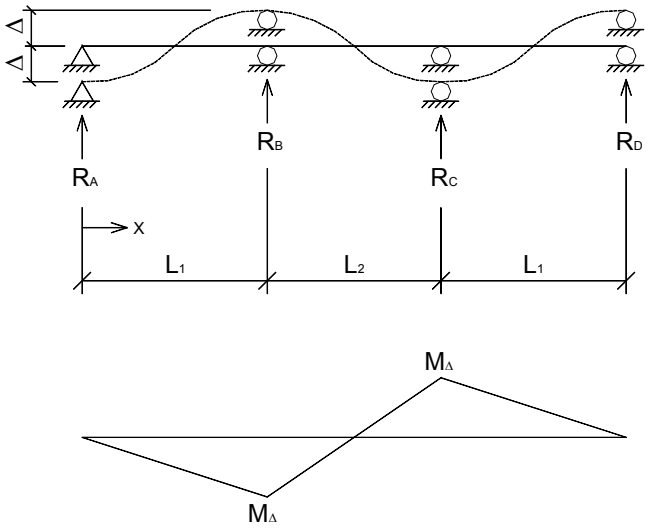

Figure A.2 Case 2

$$M_\Delta = 6EI\Delta\left[\frac{1}{L_1^2}-\left(\frac{1}{L_1^2}-\frac{2}{L_2^2}\right)\left(\frac{1}{1+\frac{2L_1}{L_2}}\right)\right] = 6EI\Delta\left[-\frac{2}{L_2^2}-\left(\frac{1}{L_1^2}-\frac{2}{L_2^2}\right)\left(\frac{2}{2+\frac{L_2}{L_1}}\right)\right]$$

$$R_A = R_D = -\frac{M_\Delta}{L_1} \qquad R_B = R_C = \frac{M_\Delta}{L_1}+\frac{2M_\Delta}{L_2} = -R_A+\frac{2M_\Delta}{L_2}$$

$$0 \le x < L_1: \qquad M = \frac{M_\Delta}{L_1}x = -R_A x$$

$$L_1 \le x \le L_1+\frac{L_2}{2}: \; M = \frac{2M_\Delta}{L_2}\left(x-L_1\right)-M_\Delta$$

ANTISYMMETRIC

Case 3: Pair of Equal and Opposite Support Displacements (Symmetric)

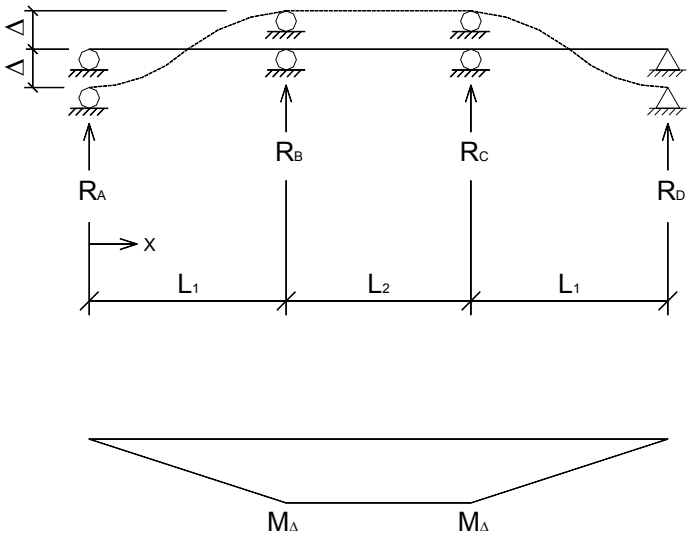

Figure A.3 Case 3

$$M_\Delta = \left(\frac{2}{2 + \frac{3L_2}{L_1}} \right) \times \left(\frac{6EI\Delta}{L_1^2} \right)$$

$$R_A = R_D = -\frac{M_\Delta}{L_1} \qquad R_B = R_C = \frac{M_\Delta}{L_1} = -R_A = -R_D$$

$$0 \le x < L_1 : \qquad M = \frac{M_\Delta}{L_1} x = -R_A x$$

$$L_1 \le x \le L_1 + \frac{L_2}{2} : \; M = M_\Delta$$

SYMMETRIC

Case 4: Concentrated Load at Mid-Span of Three-Span Continuous Member

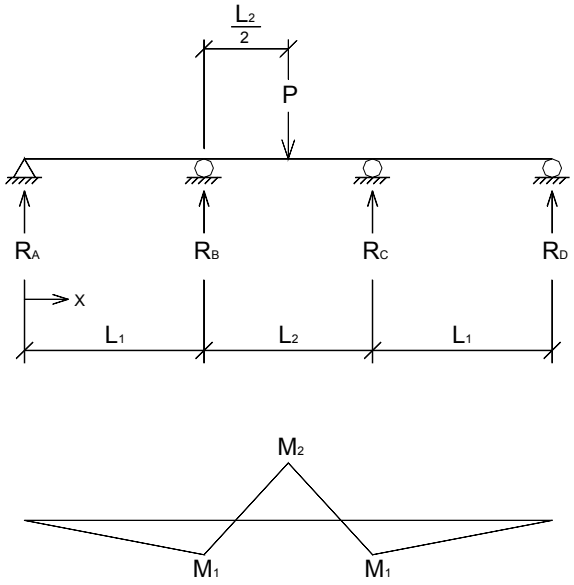

Figure A.4 Case 4

$$M_1 = \frac{PL_2}{8}\left(\frac{3}{3+\frac{2L_1}{L_2}}\right) \qquad M_2 = \frac{PL_2}{4} - M_1$$

$$R_A = R_D = -\frac{M_1}{L_1} \qquad R_B = R_C = \frac{P}{2} + \frac{M_1}{L_1}$$

$$0 \le x < L_1: \qquad M = \frac{M_1}{L_1}x = -R_A x = -R_D x$$

$$L_1 \le x \le L_1 + \frac{L_2}{2}: \; M = \frac{2}{L_2}(M_1 + M_2)(x - L_1) - M_1$$

SYMMETRIC

Case 5: Uniformly Distributed Load on Three-Span Continuous Member

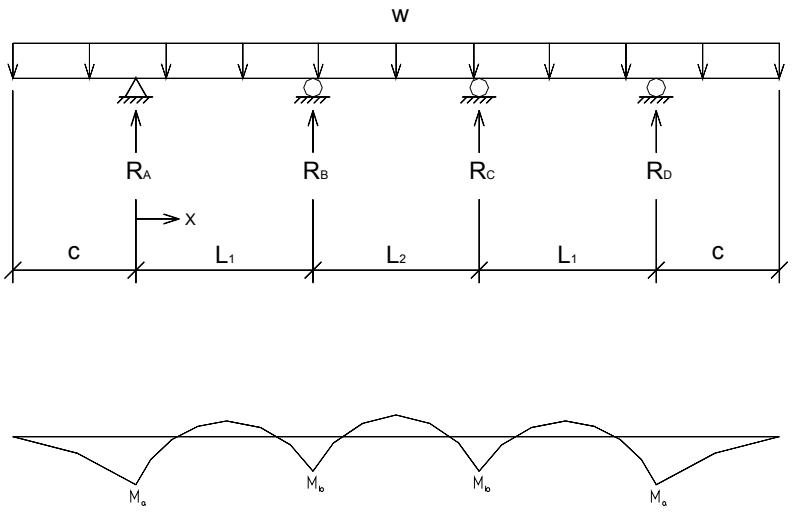

Figure A.5 Case 5

$$M_a = \frac{wc^2}{2} \qquad M_b = \frac{wL_1^2}{8}(1-DF) + \frac{wc^2}{4}(DF-1) + \frac{wL_2^2}{12}(DF) \qquad DF = \frac{3}{3+\frac{2L_1}{L_2}}$$

$$R_A = R_D = \frac{wL_1}{2} + \frac{M_a - M_b}{L_1} + wc \qquad R_B = R_C = \frac{w}{2}(2c + 2L_1 + L_2) - R_A$$

$0 \le x < c$: $\qquad M = -\frac{wx^2}{2}$

$c \le x < c + L_1$: $\qquad M = R_A(x-c) - \frac{wx^2}{2}$

$c + L_1 \le x \le c + L_1 + \frac{L_2}{2}$: $\quad M = R_A(x-c) + R_B[x-(c+L_1)] - \frac{wx^2}{2}$

SYMMETRIC

APPENDIX B

Bridge K Concrete Pour Data

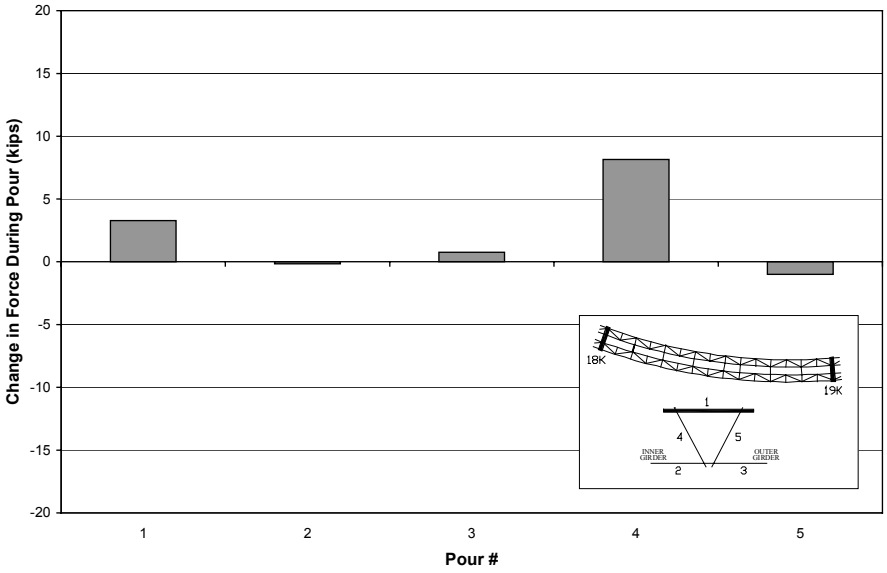

Figure B.1 Diaphragm #11-1 During K Concrete Pours

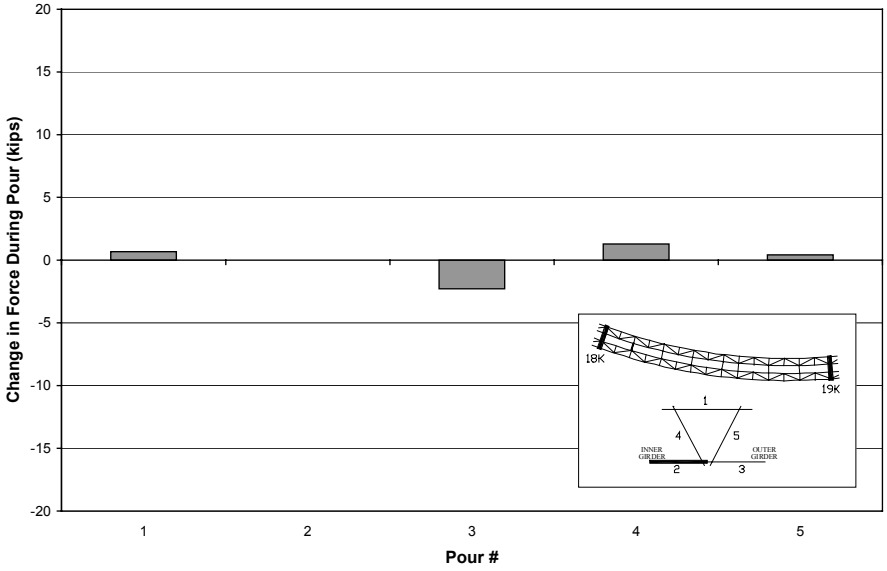

Figure B.2 Diaphragm #11-2 During K Concrete Pours

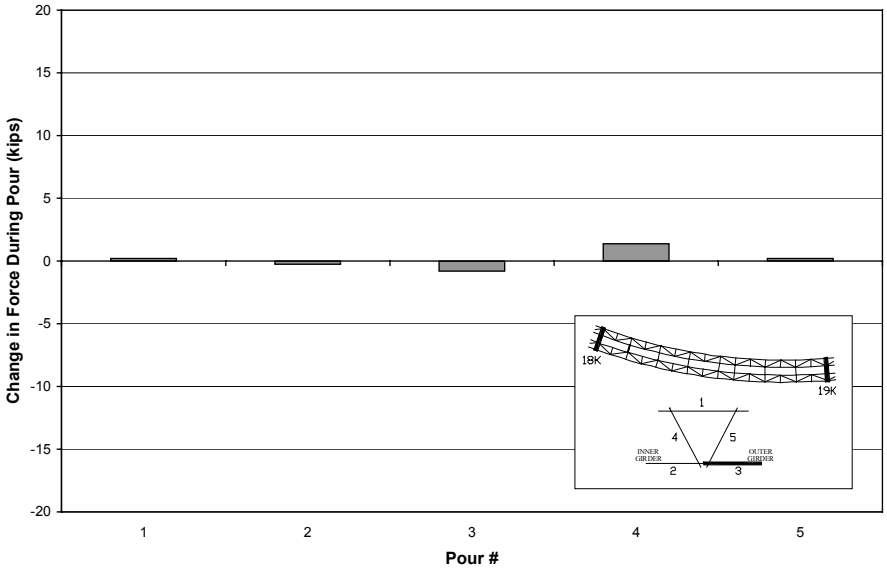

Figure B.3 Diaphragm #11-3 During K Concrete Pours

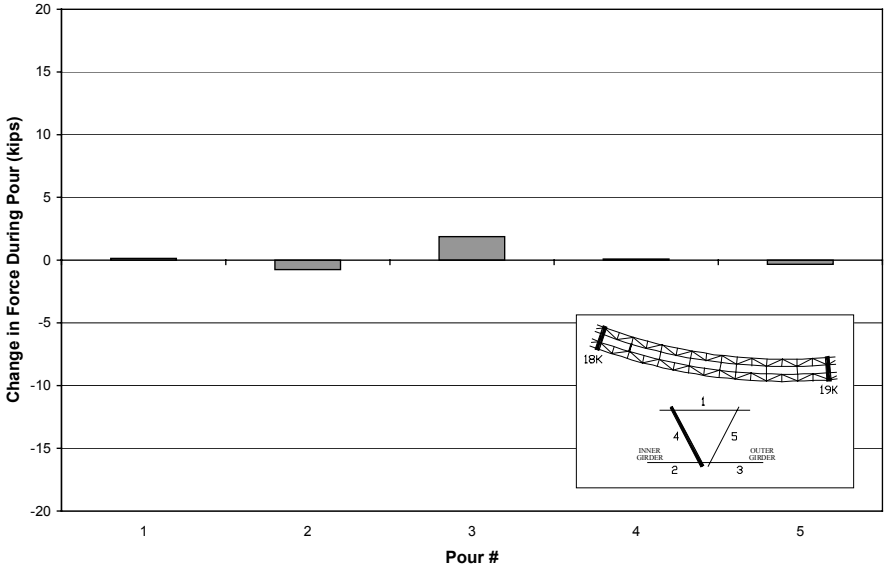

Figure B.4 Diaphragm #11-4 During K Concrete Pours

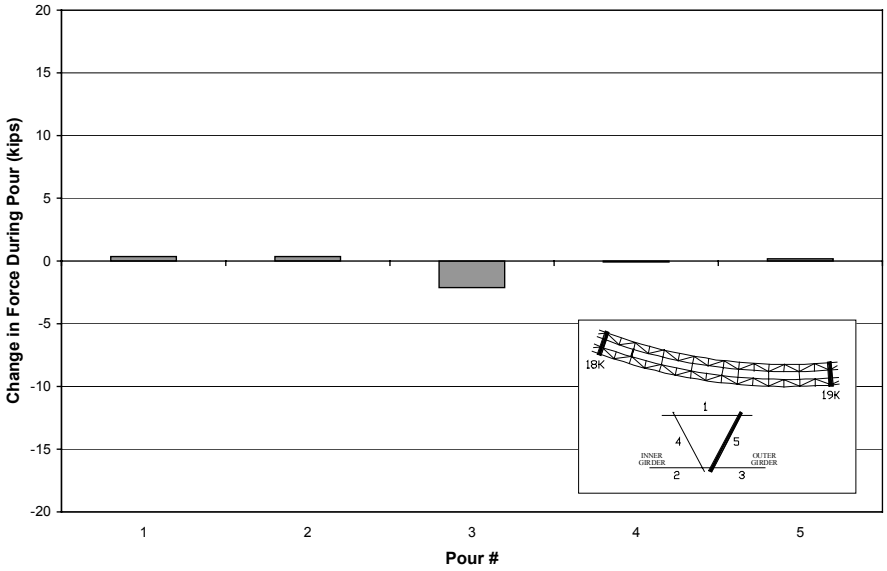

Figure B.5 Diaphragm #11-5 During K Concrete Pours

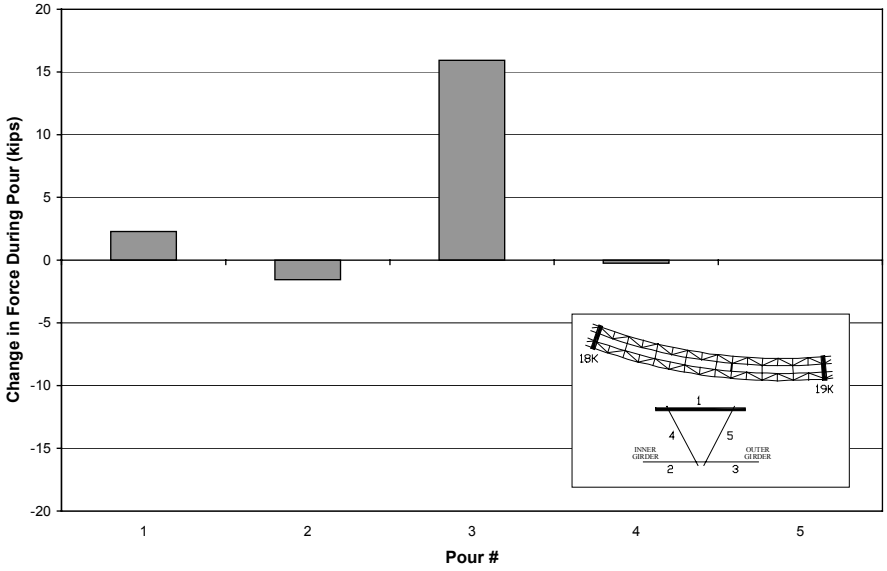

Figure B.6 Diaphragm #18-1 During K Concrete Pours

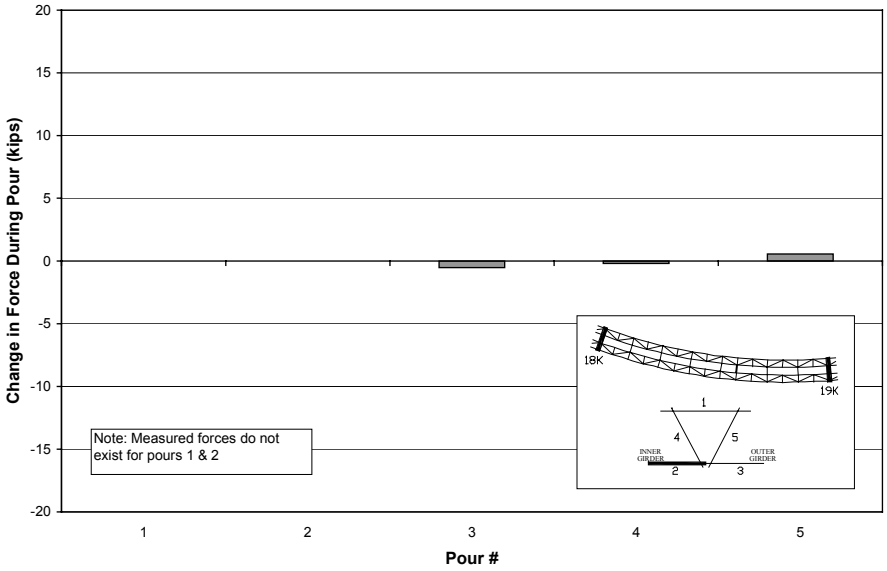

Figure B.7 Diaphragm #18-2 During K Concrete Pours

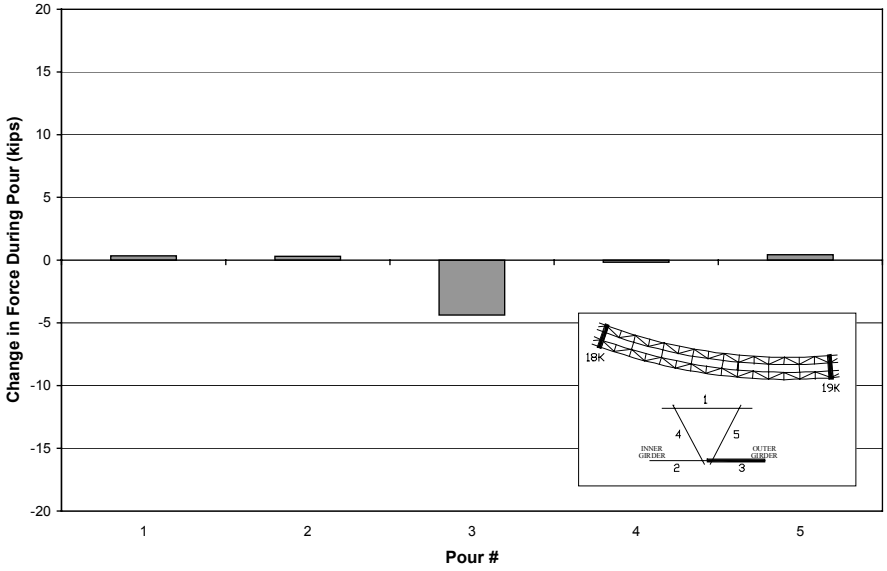

Figure B.8 Diaphragm #18-3 During K Concrete Pours

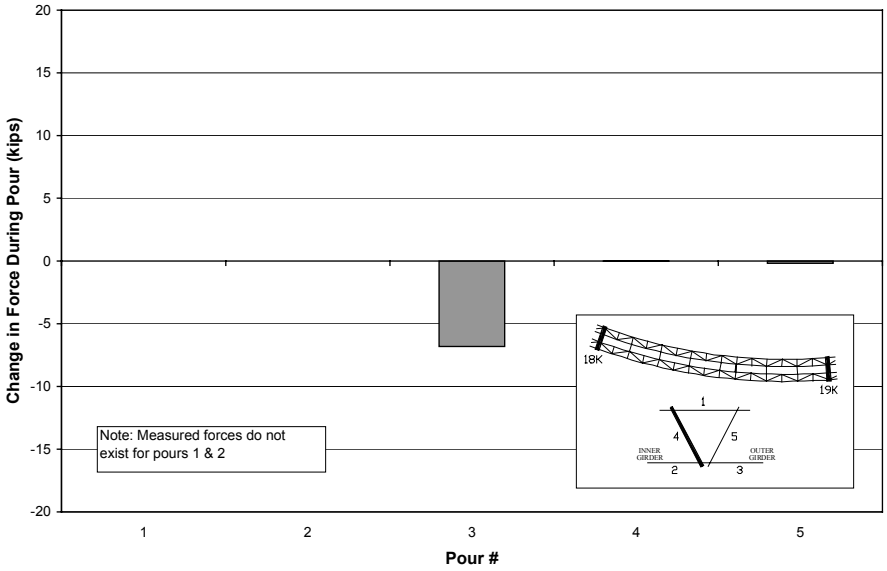

Figure B.9 Diaphragm #18-4 During K Concrete Pours

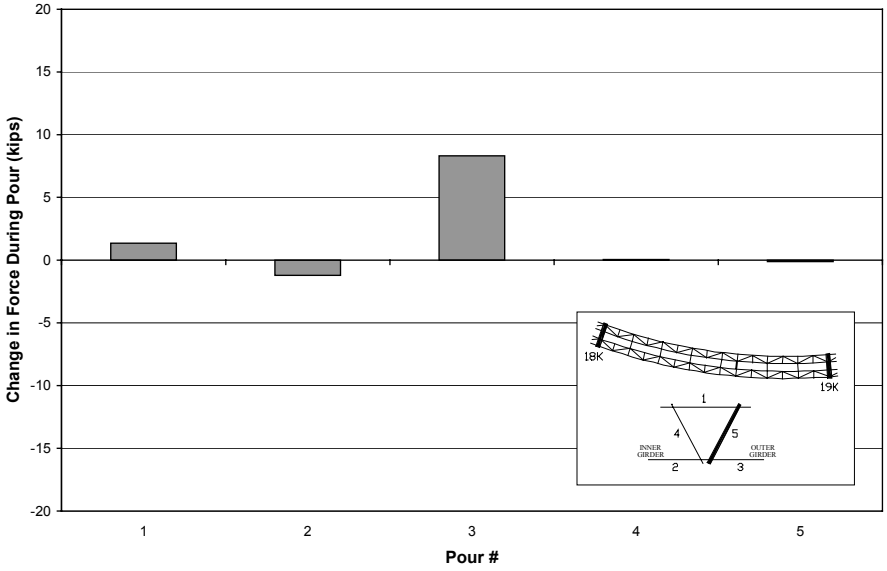

Figure B.10 Diaphragm #18-5 During K Concrete Pours

APPENDIX C
Bridge K Live Load Test Data

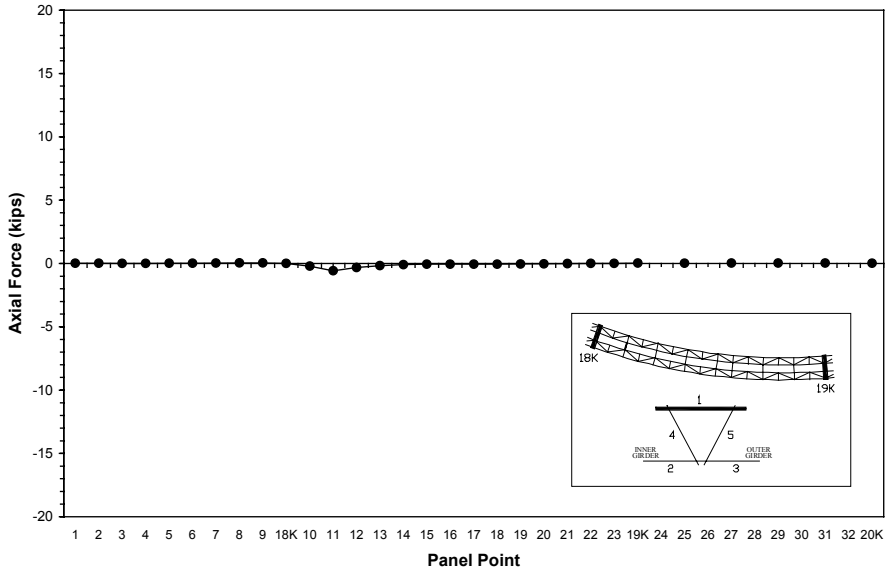

Figure C.1 Diaphragm #11-1 During K Live Load Test (Outer)

Note: the line connecting each of the data points along the influence curves stops for the panel points in span 19 because of plotting issues with Microsoft Excel 2000, the program with which these influence curves were created. As shown in Figure 6.12, truck positions were located only at every other panel point in span 19. Data points only exist for every other panel in that span: panel points 25, 27, 29, 31, and at pier 20K (trucks straddling the expansion joint). Excel can only plot graph lines in between data points on consecutive locations of the x-axis.

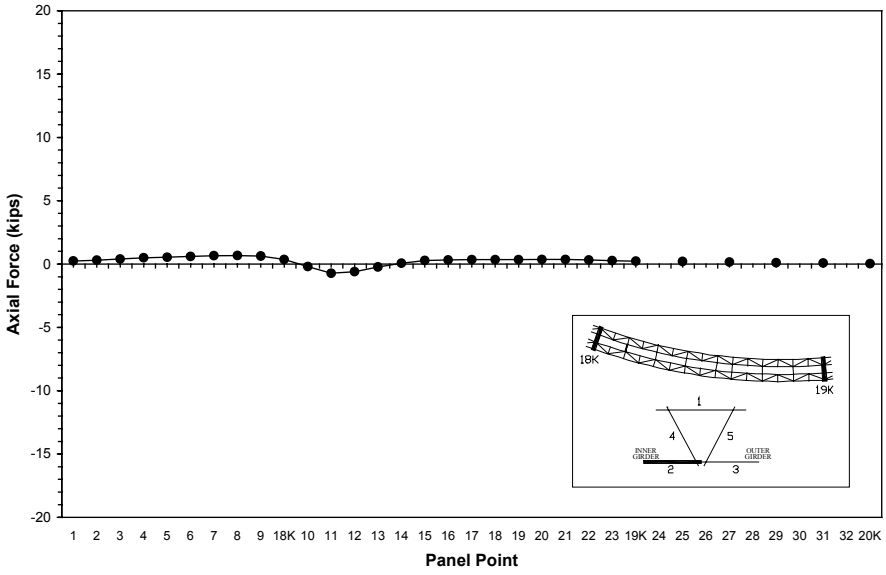

Figure C.2 Diaphragm #11-2 During K Live Load Test (Outer)

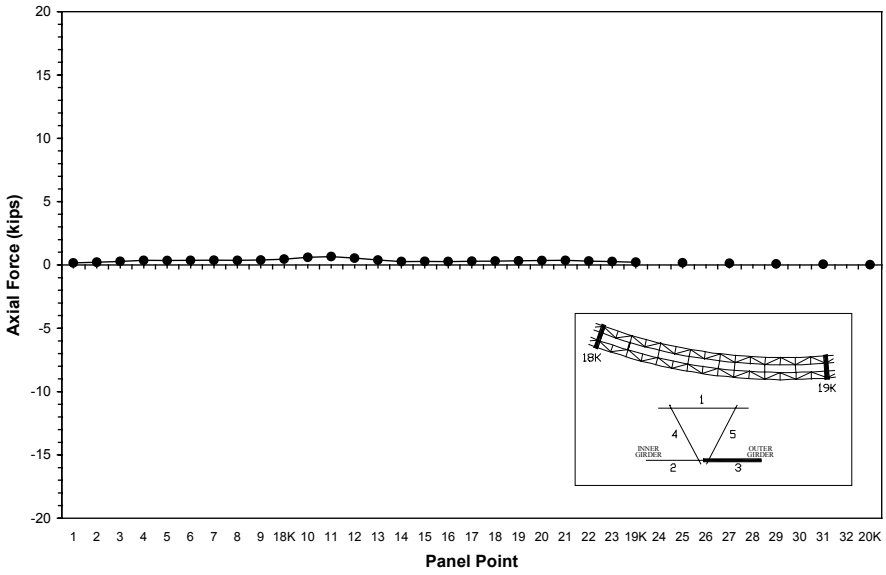

Figure C.3 Diaphragm #11-3 During K Live Load Test (Outer)

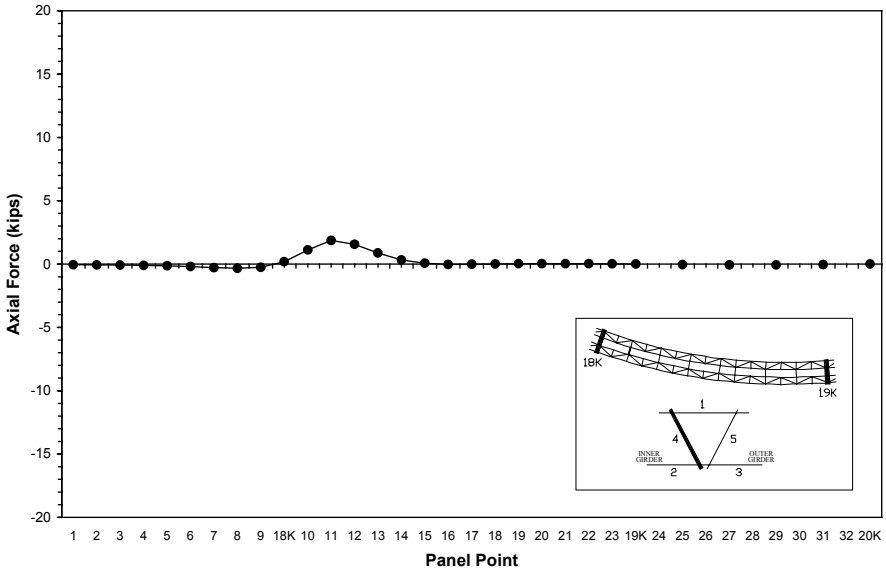

Figure C.4 Diaphragm #11-4 During K Live Load Test (Outer)

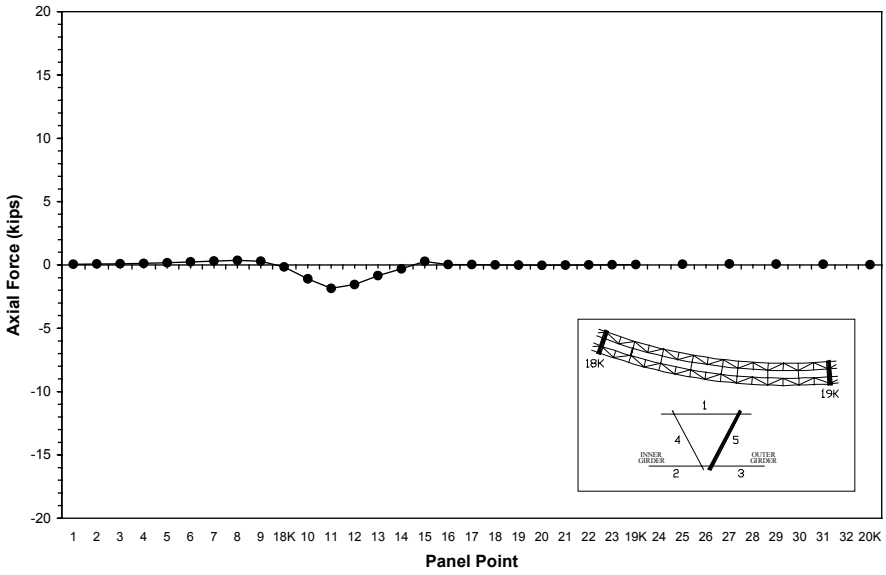

Figure C.5 Diaphragm #11-5 During K Live Load Test (Outer)

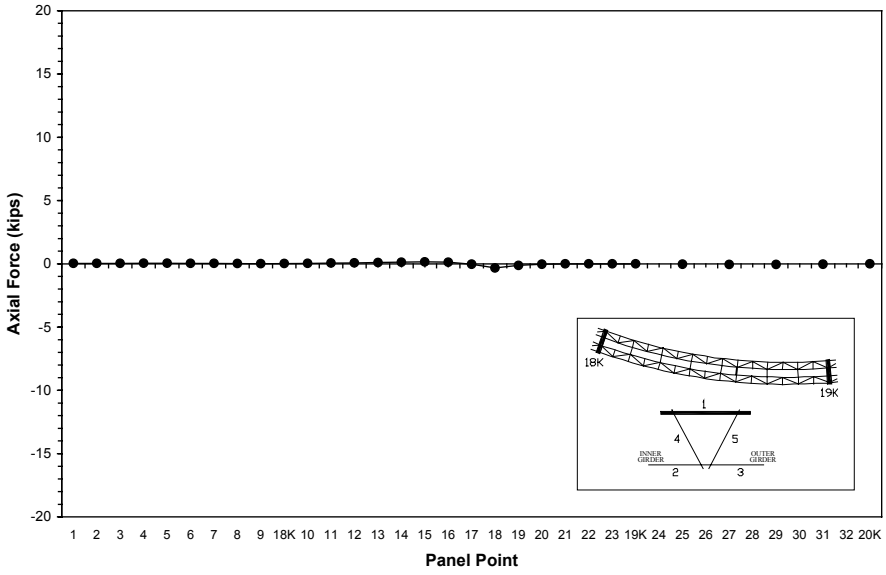

Figure C.6 Diaphragm #18-1 During K Live Load Test (Outer)

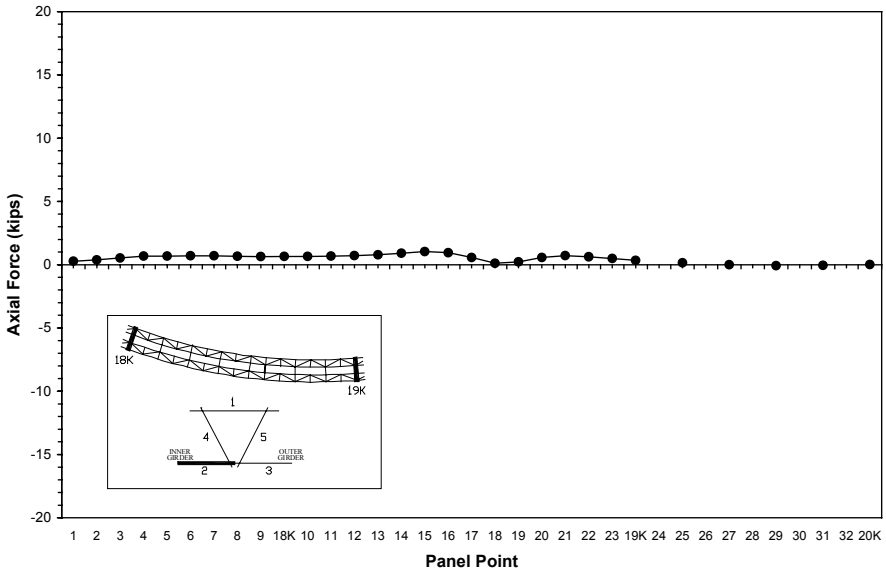

Figure C.7 Diaphragm #18-2 During K Live Load Test (Outer)

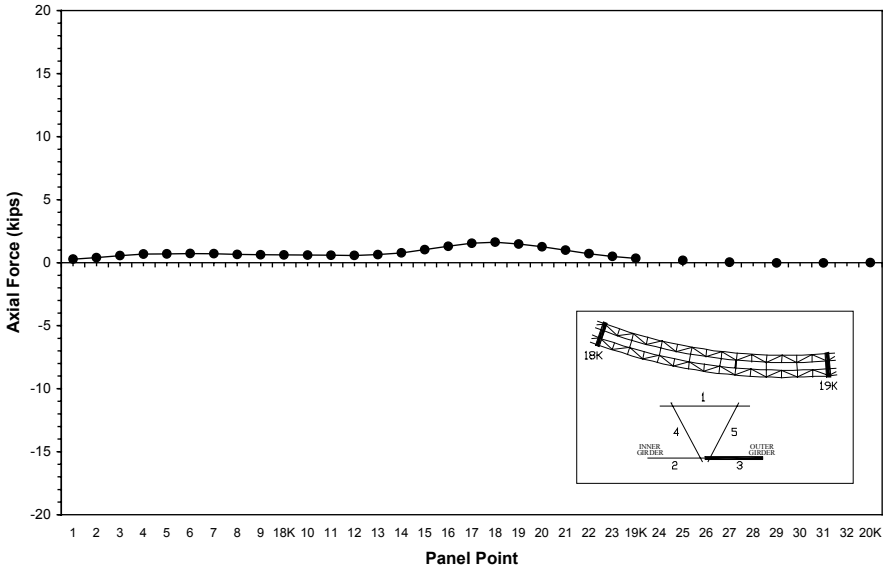

Figure C.8 Diaphragm #18-3 During K Live Load Test (Outer)

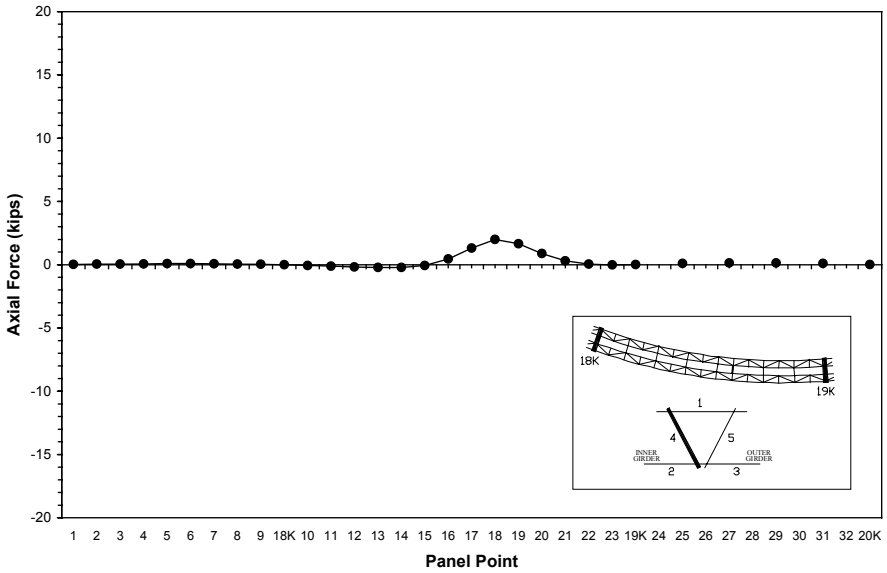

Figure C.9 Diaphragm #18-4 During K Live Load Test (Outer)

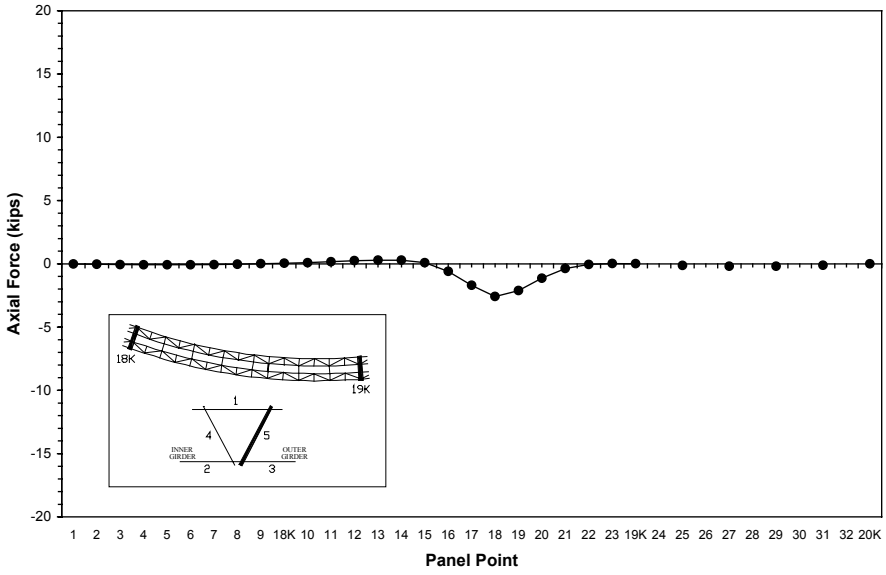

Figure C.10 Diaphragm #18-5 During K Live Load Test (Outer)

Table C.1 Axial Forces in Diaphragm #11 During K Live Load Test

(Trucks Over Outer Girder)

Panel Point	Position	#11-1	#11-2	#11-3	#11-4	#11-5
1	**1**	0.0	0.2	0.2	-0.1	0.1
2	**2**	0.0	0.3	0.2	-0.1	0.1
3	**3**	0.0	0.4	0.3	-0.1	0.1
4	**4**	0.0	0.5	0.4	-0.1	0.1
5	**5**	0.0	0.5	0.4	-0.1	0.2
6	**6**	0.0	0.6	0.4	-0.2	0.2
7	**7**	0.0	0.7	0.4	-0.3	0.3
8	**8**	0.0	0.7	0.4	-0.3	0.4
9	**9**	0.0	0.6	0.4	-0.3	0.3
18K	**10**	0.0	0.4	0.5	0.2	-0.2
10	**11**	-0.2	-0.2	0.6	1.1	-1.1
11	**12**	-0.6	-0.7	0.7	1.9	-1.9
12	**13**	-0.3	-0.6	0.5	1.6	-1.5
13	**14**	-0.2	-0.2	0.4	0.9	-0.8
14	**15**	-0.1	0.1	0.3	0.3	-0.3
15	**16**	0.0	0.3	0.3	0.1	0.3
16	**17**	-0.1	0.3	0.3	0.0	0.0
17	**18**	-0.1	0.3	0.3	0.0	0.0
18	**19**	-0.1	0.3	0.3	0.0	0.0
19	**20**	0.0	0.3	0.3	0.0	0.0
20	**21**	0.0	0.4	0.3	0.0	0.0
21	**22**	0.0	0.4	0.4	0.0	0.0
22	**23**	0.0	0.3	0.3	0.0	0.0
23	**24**	0.0	0.3	0.3	0.0	0.0
19K	**25**	0.0	0.2	0.2	0.0	0.0
24	**-----**	-----	-----	-----	-----	-----
25	**26**	0.0	0.2	0.2	0.0	0.1
26	**-----**	-----	-----	-----	-----	-----
27	**27**	0.0	0.2	0.1	-0.1	0.1
28	**-----**	-----	-----	-----	-----	-----
29	**28**	0.0	0.1	0.1	-0.1	0.1
30	**-----**	-----	-----	-----	-----	-----
31	**29**	0.0	0.1	0.1	0.0	0.1
32	**-----**	-----	-----	-----	-----	-----
20K	**30**	0.0	0.0	0.0	0.0	0.0

Table C.2 Axial Forces in Diaphragm #18 During K Live Load Test

(Trucks Over Outer Girder)

Panel Point	Position	#11-1	#11-2	#11-3	#11-4	#11-5
1	**1**	0.0	0.3	0.3	0.0	0.0
2	**2**	0.0	0.4	0.4	0.0	0.0
3	**3**	0.0	0.5	0.6	0.1	-0.1
4	**4**	0.1	0.7	0.7	0.1	-0.1
5	**5**	0.0	0.7	0.7	0.1	-0.1
6	**6**	0.0	0.7	0.7	0.1	-0.1
7	**7**	0.0	0.7	0.7	0.1	-0.1
8	**8**	0.0	0.7	0.7	0.0	0.0
9	**9**	0.0	0.6	0.6	0.0	0.0
18K	**10**	0.0	0.6	0.6	0.0	0.0
10	**11**	0.0	0.7	0.6	-0.1	0.1
11	**12**	0.1	0.7	0.6	-0.1	0.2
12	**13**	0.1	0.7	0.6	-0.2	0.2
13	**14**	0.1	0.8	0.6	-0.2	0.3
14	**15**	0.1	0.9	0.8	-0.2	0.3
15	**16**	0.2	1.0	1.0	-0.1	0.1
16	**17**	0.1	0.9	1.3	0.4	-0.6
17	**18**	0.0	0.6	1.5	1.3	-1.7
18	**19**	-0.3	0.1	1.6	2.0	-2.6
19	**20**	-0.1	0.2	1.5	1.7	-2.1
20	**21**	0.0	0.6	1.3	0.9	-1.1
21	**22**	0.0	0.7	1.0	0.3	-0.4
22	**23**	0.0	0.6	0.7	0.1	-0.1
23	**24**	0.0	0.5	0.5	0.0	0.0
19K	**25**	0.0	0.3	0.3	0.0	0.0
24	**-----**	-----	-----	-----	-----	-----
25	**26**	0.0	0.1	0.2	0.1	-0.1
26	**-----**	-----	-----	-----	-----	-----
27	**27**	0.0	0.0	0.0	0.1	-0.2
28	**-----**	-----	-----	-----	-----	-----
29	**28**	0.0	-0.1	0.0	0.1	-0.2
30	**-----**	-----	-----	-----	-----	-----
31	**29**	0.0	0.0	0.0	0.1	-0.1
32	**-----**	-----	-----	-----	-----	-----
20K	**30**	0.0	0.0	0.0	0.0	0.0

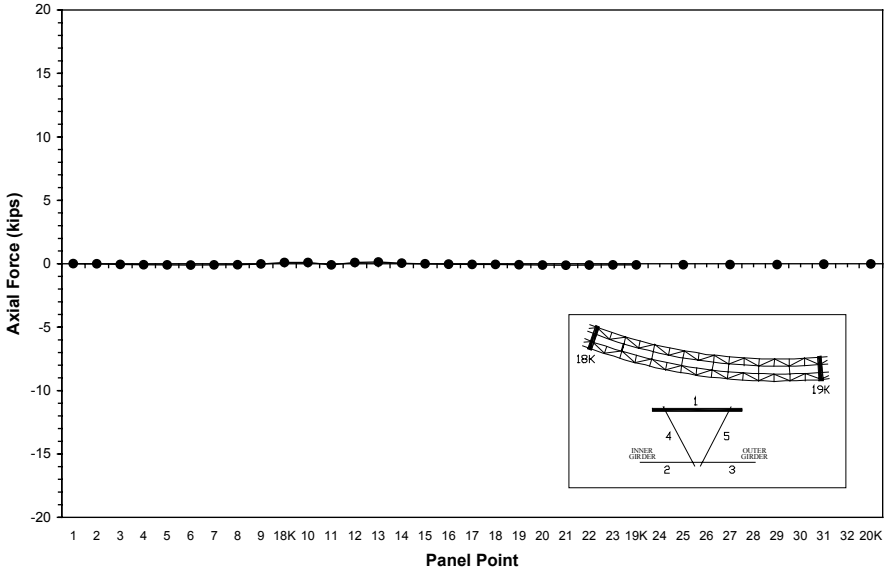

Figure C.11 Diaphragm #11-1 During K Live Load Test (Inner)

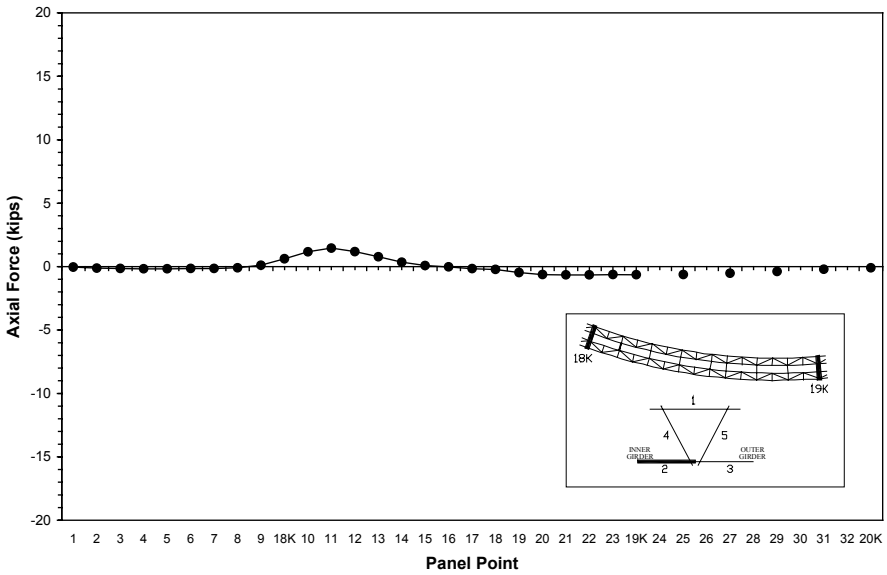

Figure C.12 Diaphragm #11-2 During K Live Load Test (Inner)

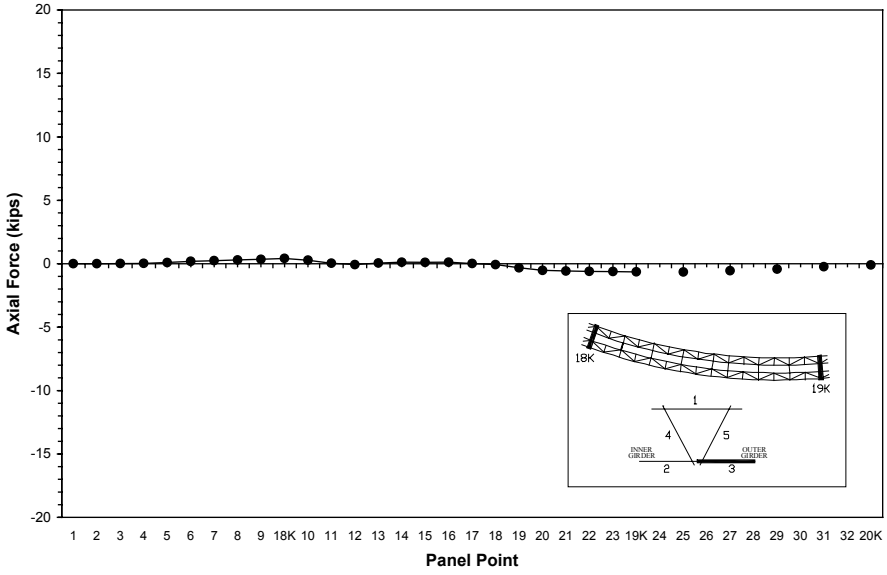

Figure C.13 Diaphragm #11-3 During K Live Load Test (Inner)

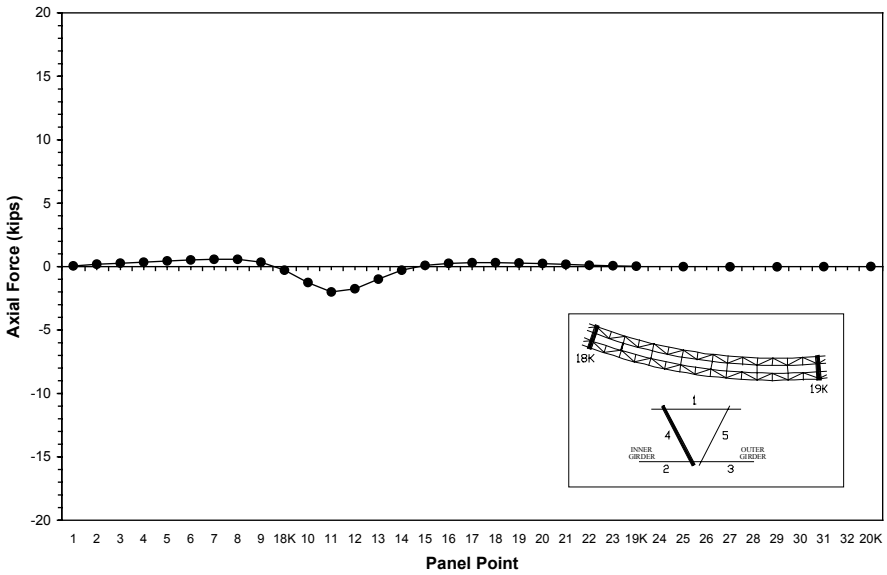

Figure C.14 Diaphragm #11-4 During K Live Load Test (Inner)

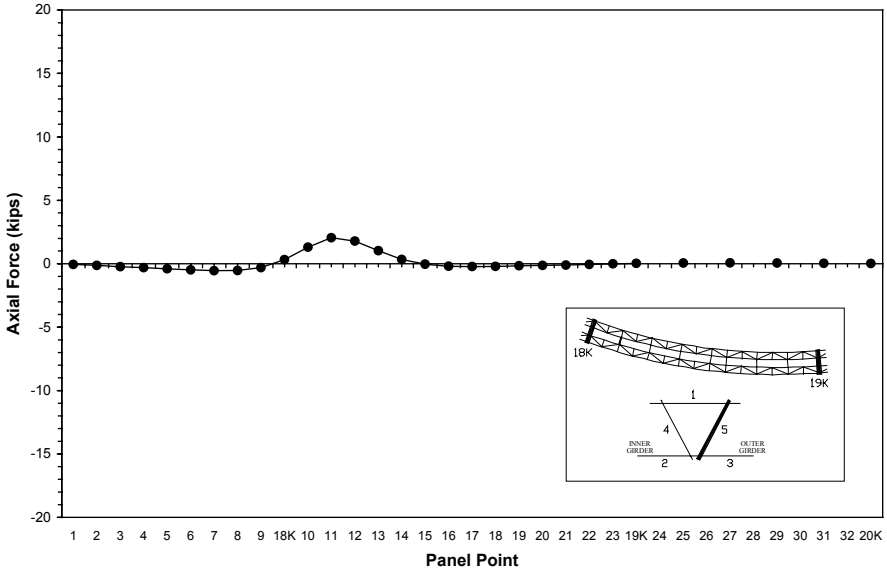

Figure C.15 Diaphragm #11-5 During K Live Load Test (Inner)

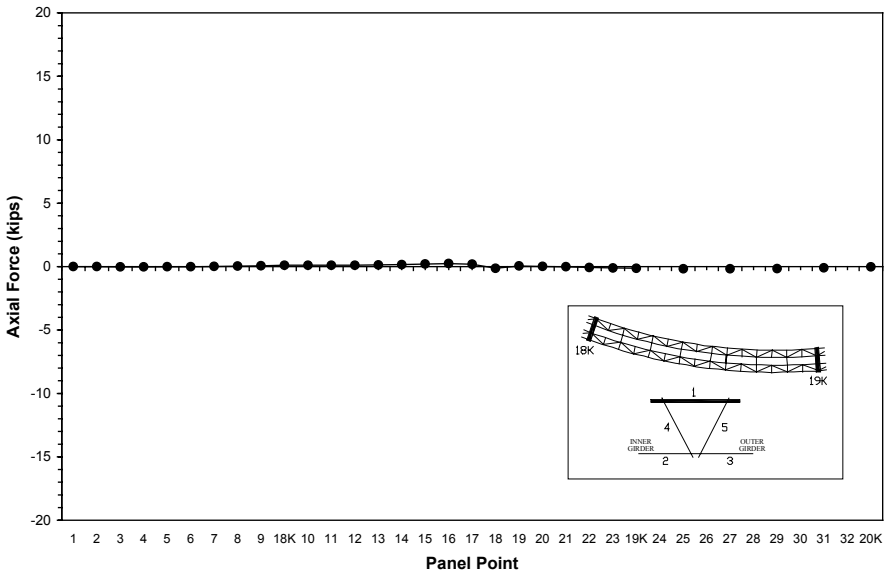

Figure C.16 Diaphragm #18-1 During K Live Load Test (Inner)

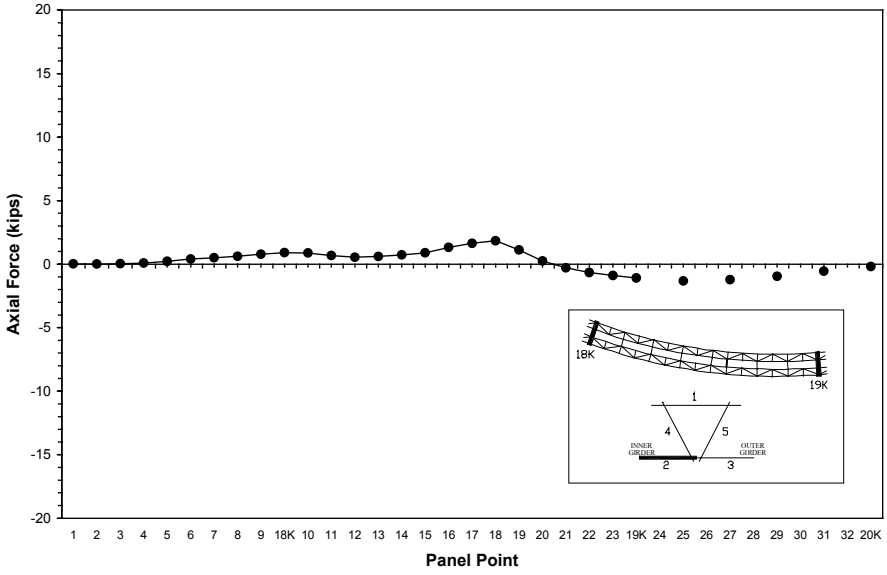

Figure C.17 Diaphragm #18-2 During K Live Load Test (Inner)

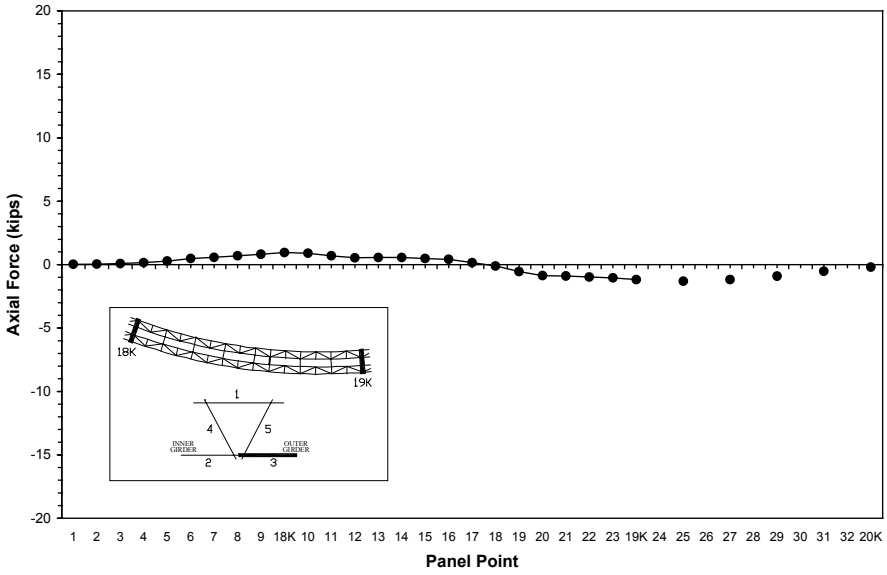

Figure C.18 Diaphragm #18-3 During K Live Load Test (Inner)

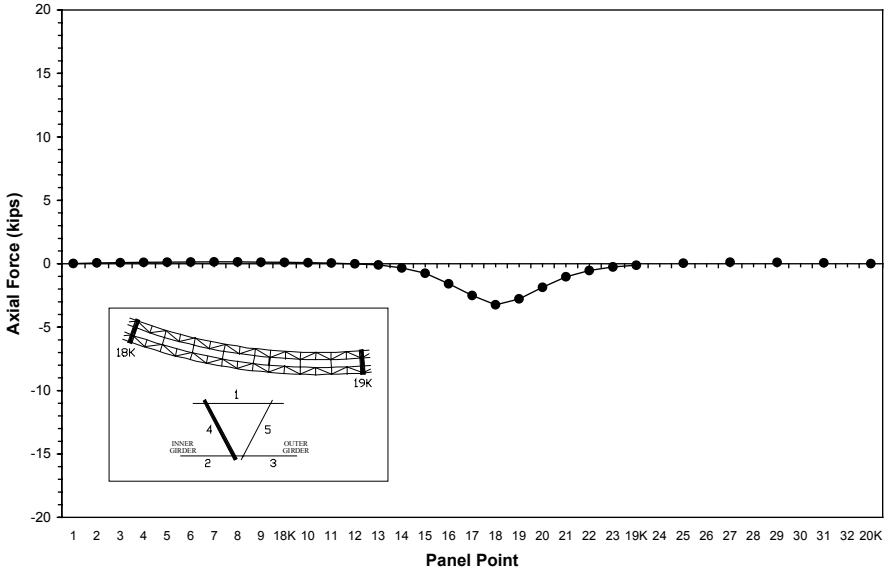

Figure C.19 Diaphragm #18-4 During K Live Load Test (Inner)

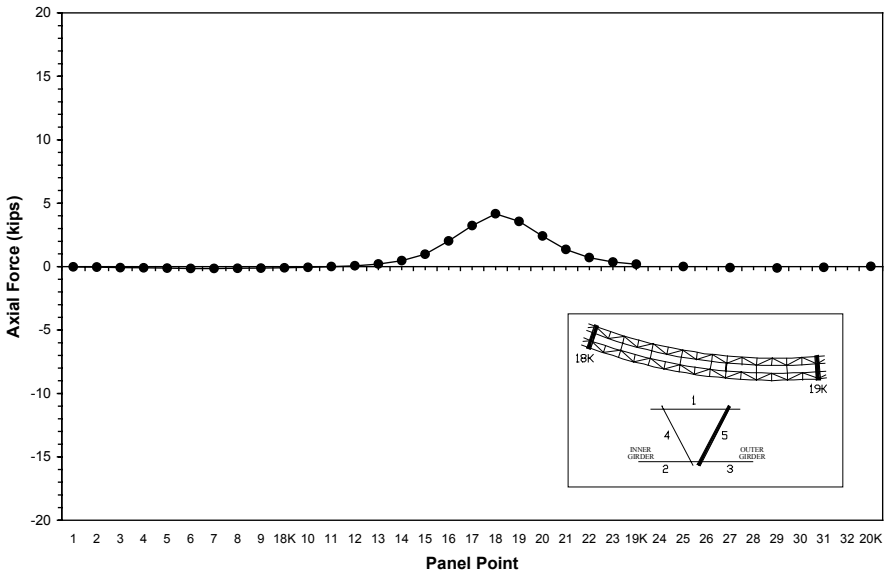

Figure C.20 Diaphragm #18-5 During K Live Load Test (Inner)

Table C.3 Axial Forces in Diaphragm #11 During K Live Load Test

(Trucks Over Inner Girder)

Panel Point	Position	#11-1	#11-2	#11-3	#11-4	#11-5
1	**1**	0.0	0.0	0.0	0.1	-0.1
2	**2**	0.0	-0.1	0.0	0.2	-0.1
3	**3**	-0.1	-0.2	0.0	0.3	-0.2
4	**4**	-0.1	-0.2	0.0	0.4	-0.3
5	**5**	-0.1	-0.2	0.1	0.4	-0.4
6	**6**	-0.1	-0.1	0.2	0.5	-0.5
7	**7**	-0.1	-0.2	0.2	0.6	-0.5
8	**8**	-0.1	-0.1	0.3	0.6	-0.5
9	**9**	0.0	0.1	0.4	0.3	-0.3
18K	**10**	0.1	0.6	0.4	-0.3	0.3
10	**11**	0.1	1.2	0.3	-1.3	1.3
11	**12**	-0.1	1.5	0.0	-2.0	2.1
12	**13**	0.1	1.2	-0.1	-1.8	1.8
13	**14**	0.1	0.8	0.0	-1.0	1.0
14	**15**	0.0	0.4	0.1	-0.3	0.3
15	**16**	0.0	0.1	0.1	0.1	0.0
16	**17**	0.0	0.0	0.1	0.3	-0.2
17	**18**	-0.1	-0.2	0.0	0.3	-0.2
18	**19**	0.0	-0.2	-0.1	0.3	-0.2
19	**20**	-0.1	-0.5	-0.3	0.3	-0.2
20	**21**	-0.1	-0.6	-0.5	0.2	-0.1
21	**22**	-0.1	-0.7	-0.6	0.2	-0.1
22	**23**	-0.1	-0.7	-0.6	0.1	-0.1
23	**24**	-0.1	-0.6	-0.6	0.1	0.0
19K	**25**	-0.1	-0.6	-0.6	0.0	0.0
24	**-----**	-----	-----	-----	-----	-----
25	**26**	-0.1	-0.6	-0.7	0.0	0.1
26	**-----**	-----	-----	-----	-----	-----
27	**27**	-0.1	-0.5	-0.6	0.0	0.1
28	**-----**	-----	-----	-----	-----	-----
29	**28**	-0.1	-0.4	-0.4	0.0	0.1
30	**-----**	-----	-----	-----	-----	-----
31	**29**	0.0	-0.2	-0.2	0.0	0.0
32	**-----**	-----	-----	-----	-----	-----
20K	**30**	0.0	-0.1	-0.1	0.0	0.0

Table C.4 Axial Forces in Diaphragm #18 During K Live Load Test

(Trucks Over Inner Girder)

Panel Point	Position	#11-1	#11-2	#11-3	#11-4	#11-5
1	**1**	0.0	0.0	0.0	0.0	0.0
2	**2**	0.0	0.0	0.0	0.1	0.0
3	**3**	0.0	0.0	0.1	0.1	-0.1
4	**4**	0.0	0.1	0.2	0.1	-0.1
5	**5**	0.0	0.2	0.3	0.1	-0.1
6	**6**	0.0	0.4	0.5	0.1	-0.1
7	**7**	0.0	0.5	0.6	0.1	-0.1
8	**8**	0.0	0.6	0.7	0.1	-0.1
9	**9**	0.1	0.8	0.8	0.1	-0.1
18K	**10**	0.1	0.9	0.9	0.1	-0.1
10	**11**	0.1	0.9	0.9	0.1	-0.1
11	**12**	0.1	0.7	0.7	0.1	0.0
12	**13**	0.1	0.5	0.5	0.0	0.1
13	**14**	0.1	0.6	0.6	-0.1	0.2
14	**15**	0.2	0.7	0.6	-0.3	0.5
15	**16**	0.2	0.9	0.5	-0.7	1.0
16	**17**	0.2	1.3	0.4	-1.6	2.0
17	**18**	0.2	1.6	0.2	-2.5	3.2
18	**19**	-0.1	1.8	-0.1	-3.2	4.2
19	**20**	0.1	1.1	-0.6	-2.8	3.6
20	**21**	0.0	0.2	-0.9	-1.9	2.4
21	**22**	0.0	-0.3	-0.9	-1.0	1.3
22	**23**	-0.1	-0.7	-1.0	-0.5	0.7
23	**24**	-0.1	-0.9	-1.0	-0.3	0.4
19K	**25**	-0.1	-1.1	-1.2	-0.1	0.2
24	**-----**	-----	-----	-----	-----	-----
25	**26**	-0.2	-1.3	-1.3	0.0	0.0
26	**-----**	-----	-----	-----	-----	-----
27	**27**	-0.2	-1.2	-1.2	0.1	-0.1
28	**-----**	-----	-----	-----	-----	-----
29	**28**	-0.2	-1.0	-0.9	0.1	-0.1
30	**-----**	-----	-----	-----	-----	-----
31	**29**	-0.1	-0.6	-0.5	0.1	-0.1
32	**-----**	-----	-----	-----	-----	-----
20K	**30**	0.0	-0.2	-0.2	0.0	0.0

References

AASHTO LRFD Bridge Design Specifications, American Association of State Highway and Transportation Officials, 1996.

Chen, Brian S. "Buckling of U-Shaped Girders with Top-Flange Lateral Bracing," M.S. thesis presented to The University of Texas at Austin, 1999.

Cheplak, Benjamin A. "Field Measures of Intermediate External Diaphragms on a Trapezoidal Steel Box Girder Bridge," M.S. thesis presented to The University of Texas at Austin, 2001.

Cheplak, Benjamin A., Karl H. Frank, Matthew A. Memberg, and Joseph A. Yura. "Field Studies of Steel Trapezoidal Box Girders," TxDOT Research Report to be published. The University of Texas at Austin, 2002.

Helwig, Todd and Zhanfei Fan. "Field and Computational Studies of Steel Trapezoidal Box Girder Bridges," TxDOT Research Report 1395-3. The University of Houston, August 2000.

Kolbrunner, C.F. and K. Basler. Torsion in Structures: An Engineering Approach. Springer-Verlag: Berlin, 1969. pp. 1-21, 47- 50.

"Preferred Practices For Steel Bridge Design Fabrication and Erection," Texas Steel Quality Council, November 2000. <http://www.steelbridge.org>

Seaburg, Paul A. and Charles J. Carter. Torsional Analysis of Structural Steel Members. *Steel Design Guide Series #9*. AISC: Chicago, 1997.

TxDOT Bridge Design Manual, Texas Department of Transportation, December 2001. <http://manuals.dot.state.tx.us/dynaweb/>

Timoshenko, Stephen. Theory of Elasticity. 1st ed. 5th impression. McGraw-Hill: New York, 1934.

Topkaya, Cem. "Behavior of Curved Trapezoidal Steel Box Girders During Construction," Ph.D. thesis in progress, to be presented to The University of Texas at Austin, 2002.

Tung, David H.H. and Richard S. Fountain. "Approximate Torsional Analysis of Curved Box Girders by the M/R-Method," *AISC Engineering Journal*. vol. 7, no. 3, July 1970. pp. 65-74.

Yura, Joseph A. "Fundamentals of Beam Bracing," *AISC Engineering Journal*. vol. 38, no. 1, First Quarter 2001. pp. 11-26.

Vita

Matthew Alex Memberg was born in Atlanta, Georgia, to Donald Memberg and the former Francine Zwirn on December 12, 1976. He grew up in the northern Atlanta suburb of Chamblee. After graduating from Chamblee High School in June 1995, he attended The Georgia Institute of Technology from September 1995 until August 2000, where he earned a Bachelor of Science in Civil Engineering with special recognitions for cooperative education and scholarship. He continued his studies in structural engineering at The University of Texas at Austin from August 2000 until summer 2002. While enrolled at UT-Austin, he was employed as a Graduate Research Assistant and worked with Drs. Joe Yura and Karl Frank.

Permanent Address: 3931 Granger Drive
Chamblee, GA 30341-1728

This thesis was typed by the author.